

## Highlights

### **A Statistical Introduction to Template Model Builder: A Flexible Tool for Spatial Modeling**

Aaron Osgood-Zimmerman, Jon Wakefield

- In-depth statistical review of Template Model Builder (TMB) methodology
- Large-scale continuous spatial simulation study assessing the Stochastic Partial Differential Equations representation of Gaussian Processes in TMB and R-INLA
- Discrete spatial simulation with conditionally constrained spatial distributions in TMB
- Novel nonlinear spatial model to jointly estimate cancer incidence and mortality in the European Union
- Provides example code for fitting popular continuous and discrete spatial models in TMB

# A Statistical Introduction to Template Model Builder: A Flexible Tool for Spatial Modeling

Aaron Osgood-Zimmerman<sup>a,\*</sup>, Jon Wakefield<sup>a,b</sup>

*University of Washington, Seattle*

<sup>a</sup>*Department of Statistics*

<sup>b</sup>*Department of Biostatistics*

---

## Abstract

The integrated nested Laplace approximation (INLA) is a well-known and popular technique for spatial modeling with a user-friendly interface in the R-INLA package. Unfortunately, only a certain class of latent Gaussian models are amenable to fitting with INLA. In this paper we describe Template Model Builder (TMB), an existing technique which is well-suited to fitting complex spatio-temporal models. TMB is relatively unknown to the spatial statistics community, but is a highly flexible random effects modeling tool which allows users to define complex random effects models through simple C++ templates. After contrasting the methodology behind TMB with INLA, we provide a large-scale simulation study assessing and comparing R-INLA and TMB for continuous spatial models, fitted via the Stochastic Partial Differential Equations (SPDE) approximation. The results show that the predictive fields from both methods are comparable in most situations even though TMB estimates for fixed or random effects may have slightly larger bias than R-INLA. We also present a smaller discrete spatial simulation study, in which both approaches perform well. We conclude with an analysis of breast cancer incidence and mortality data using a joint model which cannot be fit with INLA.

*Keywords:* Bayesian inference; Empirical Bayes; Laplace approximation; Stochastic Partial Differential Equations; Hierarchical models; Gaussian Markov random fields

---

\*Email: azimmer@uw.edu

## 1. Introduction

Inference for spatial random effects models is notoriously difficult, due to the dimensionality of the parameter space and the dependencies in the likelihood surface. Inference can proceed via either Markov chain Monte Carlo (Margossian et al., 2020) or analytic approximation methods, including variational methods (Blei et al., 2017) and those based on the Laplace approximation (LA). In this paper, we focus on the latter, since they are fast and are widely-used in practice. In particular, we consider the integrated nested Laplace approximation (INLA) method implemented in the R-INLA package (Rue et al. (2009), Martins et al. (2013)) and the LA within the Template Model Builder (TMB) package (Kristensen et al. (2016)).

Since its introduction, INLA has increasingly grown in popularity and is now the method of choice for many spatial and spatio-temporal analyses. The method is very well-documented (Rue et al. (2009), Blangiardo et al. (2013), Lindgren and Rue (2015), Rue et al. (2017), Martino and Riebler (2020)) and its popularity is evidenced by a number of book-length treatments specifically for spatial data (Blangiardo and Cameletti (2015), Krainski et al. (2018), Moraga (2019), Gomez-Rubio (2020)) along with numerous applications. However, the R implementation of INLA does not offer complete flexibility with respect to the likelihood specification.

In this paper, we discuss the utility of the existing random effects modeling tool TMB, developed by Kristensen et al. (2016). TMB is exceptionally flexible, allowing the user to define custom models within a C++ template, is computationally efficient, and is applicable to a wide class of sampling models. While base TMB, the focus of this paper, provides deterministic approximations to marginal densities, the release of `tmbstan` by Monnahan and Kristensen (2018) provides an approach to stochastically sample from target distributions defined with TMB templates using no U-turn sampling (NUTS) MCMC allowing for fully Bayesian inference. We focus on TMB since it is less well known to statisticians, though is popular in the ecological literature (Thorson and Kristensen (2016), Bolstad et al. (2017), Free et al. (2019)). We provide a detailed description of the methodology and source code to implement a variety of the most popular spatial models. The spatial simulation studies we use to assess TMB and R-INLA adds to a growing body of literature showing the strengths and limitations of these methods (Taylor and Diggle (2014), Ferkingstad et al. (2015), Auger-Méthé et al. (2017)). They also extend the limited number of studies validating the stochastic partial

differential equations (SPDE) approach to fitting continuous spatial models ([Teng et al. \(2017\)](#), [Righetto et al. \(2020\)](#)).

The structure of this paper is as follows. In Section 2 we describe the models that we are considering, along with an overview of inferential approaches. Sections 3 and 4 and 5 describe INLA and TMB and summarize their differences, respectively. Section 6 compares the two approaches, via extensive simulations, and Section 7 considers the modeling of European breast cancer data using an incidence/mortality model that can be fitted in TMB, but not in INLA. We conclude with a discussion in Section 8.

## 2. Inferential Overview

We will consider the model:

$$\mathbf{y}|\boldsymbol{\beta}, \mathbf{b}, \boldsymbol{\phi}_1 \sim p_1(\mathbf{y}|\boldsymbol{\beta}, \mathbf{b}, \boldsymbol{\phi}_1) \quad (1)$$

$$\mathbf{b}|\boldsymbol{\phi}_2 \sim p_2(\mathbf{b}|\boldsymbol{\phi}_2) \quad (2)$$

where  $\mathbf{y}$  represent data,  $p_1$  and  $p_2$  are the likelihood and random effects distributions, respectively,  $\boldsymbol{\beta}$  represent fixed effects,  $\mathbf{b}$  random effects and  $\boldsymbol{\phi} = [\boldsymbol{\phi}_1, \boldsymbol{\phi}_2]$  variance-covariance parameters, with  $\boldsymbol{\phi}_1$  appearing in the likelihood and  $\boldsymbol{\phi}_2$  in the prior. The random effects may be split into a set of spatial random effects  $\mathbf{u}$  and non-spatial random effects  $\mathbf{v}$  so that  $\mathbf{b} = [\mathbf{u}, \mathbf{v}]$ . We consider Gaussian spatial random effects so that  $\mathbf{b}|\boldsymbol{\phi}_2$  falls within the class of latent Gaussian models (LGMs).

A Bayesian approach to inference completes the model (1) and (2) by adding the hyperprior,  $p_3(\boldsymbol{\beta}, \boldsymbol{\phi}) = p_3(\boldsymbol{\beta})p_3(\boldsymbol{\phi})$ , with the prior for  $\boldsymbol{\beta}$  assumed to be Gaussian. INLA is generally used to carry out fully Bayesian inference. The automatic differentiation at the heart of TMB allows various inferential approaches. We let,

$$f(\boldsymbol{\beta}, \mathbf{b}, \boldsymbol{\phi}) = \log p_1(\mathbf{y}|\boldsymbol{\beta}, \mathbf{b}, \boldsymbol{\phi}_1) + \log p_2(\mathbf{b}|\boldsymbol{\phi}_2).$$

The simplest approach is maximum likelihood estimation (MLE) for the fixed effects and variance-covariance parameters (REML is also available for  $\boldsymbol{\phi}$ ). The MLEs maximize the marginal likelihood,

$$\mathcal{L}(\boldsymbol{\beta}, \boldsymbol{\phi}) = \int \exp [f(\boldsymbol{\beta}, \mathbf{b}, \boldsymbol{\phi})] \, d\mathbf{b}. \quad (3)$$

Inference may proceed via the asymptotic normal distribution of the MLE with uncertainty expressed via the observed information evaluated at the

MLE, as in TMB’s methodological ancestor, ADMB (Fournier et al. (2012)). Within TMB one may also maximize the marginal posterior,

$$p(\boldsymbol{\beta}, \boldsymbol{\phi} | \mathbf{y}) \propto \mathcal{L}(\boldsymbol{\beta}, \boldsymbol{\phi}) \times p_3(\boldsymbol{\beta}) \times p_3(\boldsymbol{\phi}), \quad (4)$$

to produce marginal maximum a posteriori (MMAP) estimates for the fixed effects and variance parameters, and where inference will be based on the asymptotic distribution of the posterior. In either setting, inference for the random effects then occurs through empirical Bayes by maximization of  $f(\hat{\boldsymbol{\beta}}, \mathbf{b}, \hat{\boldsymbol{\phi}})$  having conditioned on the parameter estimates,  $\hat{\boldsymbol{\beta}}$  and  $\hat{\boldsymbol{\phi}}$

### 3. Integrated Nested Laplace Approximation

INLA has been well described in a number of statistical venues including recently in Martino and Riebler (2020) and Rue et al. (2017). We provide a brief overview of its details here for comparison against the details of TMB presented in Section 4 and to aid in comparing the INLA and TMB simulation results presented in Section 6.

We first note that INLA does not use the “standard” Laplace approximation (which is used in TMB, as described in Section 4), but rather implements the Laplace ratio approximation (LRA) described in Tierney and Kadane (1986, Section 4.1) which benefits from some cancellation of approximation error.

INLA was introduced by Rue et al. (2009) to provide a quick option for Bayesian computation for the class of additive LGMs (ALGMs). In an ALGM, the general hierarchical model formulation described in (1) and (2) is restricted to models where the conditional expectation of the observations can be related to a linear combination of the fixed and random effects via a known link function  $g$ :

$$\text{E}[y_i | \boldsymbol{\beta}, \mathbf{b}] = g(\eta_i) = g\left(\beta_0 + \sum_{j=1}^J \beta_j z_{ij} + \sum_{k=1}^K b_i^{(k)}\right) \quad (5)$$

for observed covariates,  $z_{ij}$ , associated with the fixed effects,  $\beta_j, j = 1, \dots, J$ , random effects,  $\{b_i^{(k)}, k = 1, \dots, K\}$ , and with  $\eta_i$  the linear predictor for each observation  $i$ . All the parameters of the linear predictor are assumed to be Gaussian, completing the LGM definition.

We introduce a slight change of model formulation, to accommodate the consolidation of the like terms. Specifically, we collect together the Gaussian fixed and random effects, from (2), to write

$$p_2(\boldsymbol{\beta}, \mathbf{b}|\boldsymbol{\phi}_2) = p_2(\mathbf{b}|\boldsymbol{\phi}_2) \times p_3(\boldsymbol{\beta}).$$

Defining these terms to be  $\mathbf{B} = [\boldsymbol{\beta}, \mathbf{b}^{(1)}, \dots, \mathbf{b}^{(K)}]$ , in the LGM setting we then have

$$\mathbf{B}|\boldsymbol{\phi}_2 \sim N(\mathbf{0}, \mathbf{Q}^{-1}(\boldsymbol{\phi}_2)) \quad (6)$$

where  $\mathbf{Q}^{-1}(\boldsymbol{\phi}_2)$  is the precision matrix for the Gaussian field. This ensures that the linear predictor  $\boldsymbol{\eta}$  is Gaussian as well. To complete the Bayesian model specification, the hyperprior,  $p_3(\boldsymbol{\phi})$  is specified.

The primary targets of inference for the INLA algorithm are univariate posterior densities for the latent field parameters,  $p(B_i|\mathbf{y})$ , and the joint posterior of the hyperparameters,  $p(\boldsymbol{\phi}|\mathbf{y})$ . INLA approximates these in three steps:

1. Explore and discretize  $\boldsymbol{\phi}$ -space via an approximation,

$$\tilde{p}(\boldsymbol{\phi}|\mathbf{y}) \propto \frac{p_1(\mathbf{y}|\boldsymbol{\beta}, \mathbf{b}, \boldsymbol{\phi})p_2(\boldsymbol{\beta}, \mathbf{b}|\boldsymbol{\phi})p_3(\boldsymbol{\phi})}{\tilde{p}_G(\boldsymbol{\beta}, \mathbf{b}|\boldsymbol{\phi}, \mathbf{y})} \Big|_{\boldsymbol{\beta}=\boldsymbol{\beta}^*(\boldsymbol{\phi}), \mathbf{b}=\mathbf{b}^*(\boldsymbol{\phi})}, \quad (7)$$

where  $\tilde{p}_G(\boldsymbol{\beta}, \mathbf{b}|\boldsymbol{\phi}, \mathbf{y})$  is the Gaussian approximation to the conditional distribution obtained by numerically finding and matching the mode,  $\{\boldsymbol{\beta}^*(\boldsymbol{\phi}), \mathbf{b}^*(\boldsymbol{\phi})\}$ , and curvature at the mode, for given  $\boldsymbol{\phi}$ .

The approximation in (7) is equivalent to the Laplace Ratio Approximation (LRA) for the posterior marginal proposed by [Tierney and Kadane \(1986\)](#). As the hyperparameter space is explored, (7) is evaluated at  $L$  high-density points to generate an approximate discretization:  $\tilde{p}(\boldsymbol{\phi}^{(l)}|\mathbf{y})$  at points  $\{\boldsymbol{\phi}^{(1)}, \dots, \boldsymbol{\phi}^{(L)}\}$ . R-INLA has three available approaches for selecting  $\boldsymbol{\phi}^{(l)}$ : the empirical Bayes (EB) option uses only the modal value as a single integration point, the grid method develops a regular grid on the primary orthogonal axis of the hyperparameter space, and the central composite design (CCD) approach which efficiently selects the modal value and a group of ‘star points’ surrounding the center. The default within R-INLA selects the grid option for small numbers of hyperparameters and otherwise selects the CCD method

2. Approximate  $p(B_i|\boldsymbol{\phi}^{(l)}, \mathbf{y})$  for  $l = 1, \dots, L$  using one of three approximations: Gaussian, Laplace, or Simplified Laplace (SL).

In the Gaussian approximation,  $\tilde{p}_G(B_i|\boldsymbol{\phi}^{(l)}, \mathbf{y})$  is calculated directly as the marginal of  $\tilde{p}_G(\boldsymbol{\beta}, \mathbf{b}|\boldsymbol{\phi}, \mathbf{y})$ , from (7). While very fast, this approximation is often not particularly good (Blangiardo and Cameletti, 2015, Section 4.7.2). In the Laplace approximation, a computationally optimized version of the LRA of Tierney and Kadane (1986) is used,

$$\tilde{p}_L(B_i|\boldsymbol{\phi}^{(l)}, \mathbf{y}) \propto \frac{p_1(\mathbf{y}|\boldsymbol{\beta}, \mathbf{b}, \boldsymbol{\phi}^{(l)})p_2(\boldsymbol{\beta}, \mathbf{b}|\boldsymbol{\phi}^{(l)})p_3(\boldsymbol{\phi})}{\tilde{p}_G(\mathbf{B}_{-i}|B_i, \boldsymbol{\phi}^{(l)}, \mathbf{y})} \Big|_{\mathbf{B}_{-i}=\mathbf{B}_{-i}^*(B_i, \boldsymbol{\phi}^{(l)})}, \quad (8)$$

where  $\tilde{p}_G(\mathbf{B}_{-i}|B_i, \boldsymbol{\phi}, \mathbf{y})$  is the Gaussian Laplace approximation to  $p(\mathbf{B}_{-i}|B_i, \boldsymbol{\phi}, \mathbf{y})$  with mode  $\mathbf{B}_{-i}^*(B_i, \boldsymbol{\phi})$ . This approximation often works very well since the conditional distribution of the latent field parameters are generally close to Gaussian, but it is computationally expensive since it must be recomputed for all desired combinations of  $\mathbf{B}$  and  $\boldsymbol{\phi}$ . The SL approximation,  $\tilde{p}_{SL}(B_i|\boldsymbol{\phi}^{(l)}, \mathbf{y})$ , uses a Taylor-series approximation of  $\tilde{p}_L(B_i|\boldsymbol{\phi}^{(l)}, \mathbf{y})$ . This approximation is quick and accurate for many applications and is the default option within R-INLA. More details on this approximation can be found in (Rue et al., 2009, Section 3.2).

3. Approximate the marginal using numerical integration,

$$\tilde{p}(B_i|\mathbf{y}) = \sum_{l=1}^L \tilde{p}(B_i|\boldsymbol{\phi}^{(l)}, \mathbf{y}) \times \tilde{p}(\boldsymbol{\phi}^{(l)}|\mathbf{y}) \times \Delta_l, \quad (9)$$

over the integration points,  $\boldsymbol{\phi}^{(l)}$ , appropriately scaled by their associated weights,  $\Delta_l$ .

Although INLA returns the univariate marginals, in general we may be interested in functions of the parameters and R-INLA provides a method to sample from the approximate joint posterior, implemented in their sampling function, `inla.posterior.sample()`, using the mixture:

$$\tilde{p}(\boldsymbol{\beta}, \mathbf{b}, \boldsymbol{\phi}|\mathbf{y}) \approx \sum_{l=1}^L \tilde{p}_G(\boldsymbol{\beta}, \mathbf{b}, |\mathbf{y}, \boldsymbol{\phi}^{(l)}) \times \tilde{p}(\boldsymbol{\phi}^{(l)}|\mathbf{y}).$$

For each draw,  $d$ , first a sample,  $\boldsymbol{\phi}^{(d)}$  is drawn from the discretized hyperparameter posterior,  $\tilde{p}(\boldsymbol{\phi}^{(l)}|\mathbf{y})$ , and then a sample,  $\{\boldsymbol{\beta}^{(d)}, \mathbf{b}^{(d)}\}$ , is drawn

from a Gaussian approximation to the joint conditional latent distribution,  $\tilde{p}_G(\boldsymbol{\beta}, \mathbf{b}, |\mathbf{y}, \boldsymbol{\phi}^{(d)})$  which is found to match the mode and curvature at the mode conditional on the specific hyperparameter draw. While there is no guarantee that this joint approximation will lead to the same approximate univariate marginals from the full INLA algorithm, by default R-INLA corrects both the mean and the skew of the Gaussian marginals sampled from the joint posterior my mapping to a SkewNormal distribution using the better-approximated marginal posteriors (Wakefield et al. (2016)). We note that even when the EB method for the hyperparameter integration is chosen in INLA and there is only one ‘integration point’ for  $\boldsymbol{\phi}$ , this approximate joint distribution can still account for skew.

R-INLA only allows for a limited set of built-in likelihoods, and while INLA theoretically can be used on any ALGM, it does have some pragmatic suggestions to ensure reasonable computing times. In particular, a reasonably small dimension of  $\boldsymbol{\phi}$  is required (Rue et al. (2017) suggest 2-5 and not more than 20) to minimize the computational burden of the numerical integration in (9). Crucially, sparsity in the precision of the latent field parameters can be leveraged at numerous points in the algorithm by R-INLA to greatly reduce the computational cost and speed up the approximation. The class of ALGMs is the target of the INLA method because they often permit sparsity and because the posteriors can often be well approximated with the LRA. Spatial statistics applications commonly use Gaussian Markov Random Field (GMRF) model specifications which maintain high levels of sparsity in the precision. A multivariate Gaussian random variable is a GMRF on an undirected graph  $G = \{V, E\}$  with vertices,  $V$ , and edges  $E$  if non-zeros in the precision matrix correspond to the edges of  $G$ . GMRF models are used in the following simulations and in the cancer application.

#### 4. Template Model Builder

TMB, rooted in frequentist inference, requires the user to differentiate between random and non-random effects. We focus our description of TMB in the context of a frequentist treatment while noting the differences for Bayesian inference. In contrast to INLA, TMB uses a single LA to integrate out the random effects from the full joint distribution to obtain an approximation to the marginal likelihood in (3). Defining the conditional mode,

$$\hat{\mathbf{b}}(\boldsymbol{\beta}, \boldsymbol{\phi}) := \underset{\mathbf{b}}{\operatorname{argmin}} -f(\boldsymbol{\beta}, \boldsymbol{\phi}, \mathbf{b}), \quad (10)$$

TMB approximates (3) using the LA to marginalize over the random effects:

$$\mathcal{L}(\boldsymbol{\beta}, \boldsymbol{\phi}) \approx \tilde{\mathcal{L}}(\boldsymbol{\beta}, \boldsymbol{\phi}) = (2\pi)^{n/2} |\mathcal{H}(\boldsymbol{\beta}, \boldsymbol{\phi})|^{1/2} \exp[-f(\boldsymbol{\beta}, \hat{\mathbf{b}}(\boldsymbol{\beta}, \boldsymbol{\phi}), \boldsymbol{\phi})], \quad (11)$$

where  $\mathcal{H}(\boldsymbol{\beta}, \boldsymbol{\phi})$  is the Hessian of  $f(\boldsymbol{\beta}, \hat{\mathbf{b}}(\boldsymbol{\beta}, \boldsymbol{\phi}), \boldsymbol{\phi})$ , with  $(j, k)$ -th element

$$\frac{\partial^2}{\partial b_j \partial b_k} f(\boldsymbol{\beta}, \hat{\mathbf{b}}(\boldsymbol{\beta}, \boldsymbol{\phi}), \boldsymbol{\phi}). \quad (12)$$

Estimation in TMB is performed through a two-stage nested optimization procedure which searches for the vector  $(\hat{\boldsymbol{\beta}}, \hat{\boldsymbol{\phi}})$  maximizing  $\tilde{\mathcal{L}}(\boldsymbol{\beta}, \boldsymbol{\phi})$  as defined in (11). To evaluate  $\tilde{\mathcal{L}}(\boldsymbol{\beta}, \boldsymbol{\phi})$ , we need to evaluate both  $\hat{\mathbf{b}}$  in (10) and  $\mathcal{H}(\boldsymbol{\beta}, \boldsymbol{\phi})$  in (12), but neither are usually available in closed-form. While  $\hat{\mathbf{b}}(\boldsymbol{\beta}, \boldsymbol{\phi})$  may be evaluated through nonlinear optimization of  $f$ , the crux of the work is to evaluate  $\mathcal{H}(\boldsymbol{\beta}, \boldsymbol{\phi})$ . TMB computes gradients and the Hessian using automatic differentiation (Appendix A presents an overview) performed via CppAD (Bell, 2007) and at the same time can auto-detect sparsity in the model in order to leverage sparse matrix routines. TMB reuses the LA and the automatically generated Hessian to produce estimates of the joint covariance between the fixed effects estimates,  $\hat{\boldsymbol{\beta}}$  and  $\hat{\boldsymbol{\phi}}$ , and the random effects predictors,  $\hat{\mathbf{b}}$ , as described in Section 4.3. Inference then proceeds assuming asymptotic normality for the joint distribution of the estimated fixed effects and predicted random effects.

#### 4.1. The TMB Estimation Algorithm

TMB implements a two-step nested optimization routine to iteratively search for the fixed effects estimates with random effects predictions also being produced. Given initial starting values, the routine performs the following steps at each evaluation in the search:

1. Given current values of the fixed effects parameters,  $(\boldsymbol{\beta}^*, \boldsymbol{\phi}^*)$ , perform nonlinear optimization to find updated modal values of the random effects,  $\hat{\mathbf{b}}(\boldsymbol{\beta}^*, \boldsymbol{\phi}^*)$  as in (10) and set this to be the current value of the random effects,  $\mathbf{b}^*$ .
2. Given current values of the random effects parameters,  $\mathbf{b}^*$ , find the modal values of the Laplace approximation to the marginal likelihood,  $\tilde{\mathcal{L}}(\boldsymbol{\beta}, \boldsymbol{\phi})$ , shown in (11) and set them to the current value of the fixed effects,  $(\boldsymbol{\beta}^*, \boldsymbol{\phi}^*)$ . In addition, evaluate the gradient of the marginal likelihood to assess stopping conditions.

3. If the maximum gradient component (MGC) of the marginal likelihood is below a stopping threshold the routine stops, otherwise go to step 1.

If a stopping criteria was reached, then the final values of the fixed effect and random effects are returned as the fixed effects estimates,  $(\widehat{\boldsymbol{\beta}}, \widehat{\boldsymbol{\phi}}) = (\boldsymbol{\beta}^*, \boldsymbol{\phi}^*)$ , and the random effects predictions are updated one final time to yield  $\widehat{\mathbf{b}}(\widehat{\boldsymbol{\beta}}, \widehat{\boldsymbol{\phi}})$ .

#### 4.2. The TMB Estimators

In models without hyperpriors, TMB produces the marginal MLEs of the  $\boldsymbol{\beta}, \boldsymbol{\phi}$ , from the approximate marginal likelihood defined in (11). The random effects predictions in this setting, taken as the mode of their conditional distribution,  $p(\mathbf{b}|\widehat{\boldsymbol{\beta}}, \widehat{\boldsymbol{\phi}}_1, \mathbf{y})$ , using ‘plug-in’ estimates of the fixed effects MLEs, are empirical Bayes predictors ([De Valpine \(2009\)](#)).

In models with hyperpriors, TMB produces the marginal maximum a posteriori estimates of  $\boldsymbol{\beta}, \boldsymbol{\phi}$ , again using the Laplace approximation from (11) applied to the marginal posterior in (4). With priors, basing random effects inference on the estimated posterior,  $p(\mathbf{b}|\widehat{\boldsymbol{\beta}}, \widehat{\boldsymbol{\phi}}_1, \mathbf{y})$ , where the hyperparameters have been estimated using the data, TMB provides parameteric empirical Bayes (PEB) estimates ([Carlin and Louis, 2000](#), Chapter 3.3). In essence, this replaces the posterior,

$$p(\mathbf{b}|\mathbf{y}) = \int p(\mathbf{b}|\mathbf{y}, \boldsymbol{\beta}, \boldsymbol{\phi}) p(\boldsymbol{\beta}, \boldsymbol{\phi}|\mathbf{y}) \, d\boldsymbol{\beta} d\boldsymbol{\phi},$$

with  $p(\mathbf{b}|\widehat{\boldsymbol{\beta}}, \widehat{\boldsymbol{\phi}}_1, \mathbf{y})$  where  $\widehat{\boldsymbol{\beta}}$  and  $\widehat{\boldsymbol{\phi}}_1$  are MMAp estimates. The EB option for the numerical integration in (9) in the INLA algorithm makes the same tradeoff: skipping the computational complexity of the integration by not accounting for the uncertainty in the (hyper)parameters.

While the random effects predictors are fast to compute via optimization having conditioned on the fixed effects estimates, with the number of REs increasing proportionally to the number of data observations, EB predictions of random effects generally have no guarantees of consistency ([Thorson and Kristensen, 2016](#)). In order to improve the predictions for the random effects and differentiable functions of the mixed effects,  $\mathbf{d}(\boldsymbol{\beta}, \boldsymbol{\phi}, \mathbf{b})$ , TMB implements a generic bias-correction adjustment termed the “epsilon” method in [Thorson and Kristensen \(2016\)](#). The correction is applicable to quantities which depend on random effects,  $\mathbf{d}(\widehat{\boldsymbol{\beta}}, \widehat{\boldsymbol{\phi}}, \mathbf{b})$ , and has no effect on the fixed effects

estimates. This correction is based on an approximation to moment-generating functions, using  $M(\boldsymbol{\epsilon}) = E[\exp\{\boldsymbol{\epsilon} \cdot \mathbf{d}(\hat{\boldsymbol{\beta}}, \hat{\boldsymbol{\phi}}, \mathbf{b})\}]$ , with  $\cdot$  denoting the dot product, proposed by [Tierney et al. \(1989\)](#) (Section 3.1). Introducing an auxiliary parameter vector,  $\boldsymbol{\epsilon}$ , of dimension equal to the dimension of  $\mathbf{d}()$ , consider a new function with the auxiliary parameters:

$$e(\hat{\boldsymbol{\beta}}, \hat{\boldsymbol{\phi}}, \mathbf{b}, \boldsymbol{\epsilon} | \mathbf{y}) = \log \left( \int \exp(f(\hat{\boldsymbol{\beta}}, \hat{\boldsymbol{\phi}}, \mathbf{b}) + \boldsymbol{\epsilon} \cdot \mathbf{d}(\hat{\boldsymbol{\beta}}, \hat{\boldsymbol{\phi}}, \mathbf{b})) \, d\mathbf{b} \right). \quad (13)$$

Employing the namesake method of moment-generating functions, the form of the bias-corrected estimator is found by differentiating with respect to  $\boldsymbol{\epsilon}$  and then setting  $\boldsymbol{\epsilon} = \mathbf{0}$ :

$$\begin{aligned} \frac{\partial}{\partial \boldsymbol{\epsilon}} (e(\hat{\boldsymbol{\beta}}, \hat{\boldsymbol{\phi}}, \mathbf{b}, \boldsymbol{\epsilon} | \mathbf{y})) \Big|_{\boldsymbol{\epsilon}=\mathbf{0}} &= \frac{\int \exp(f(\hat{\boldsymbol{\beta}}, \hat{\boldsymbol{\phi}}, \mathbf{b}) + \boldsymbol{\epsilon} \cdot \mathbf{d}(\hat{\boldsymbol{\beta}}, \hat{\boldsymbol{\phi}}, \mathbf{b})) \, d(\hat{\boldsymbol{\beta}}, \hat{\boldsymbol{\phi}}, \mathbf{b}) \, d\mathbf{b}}{\int \exp(f(\hat{\boldsymbol{\beta}}, \hat{\boldsymbol{\phi}}, \mathbf{b}) + \boldsymbol{\epsilon} \cdot \mathbf{d}(\hat{\boldsymbol{\beta}}, \hat{\boldsymbol{\phi}}, \mathbf{b})) \, d\mathbf{b}} \Big|_{\boldsymbol{\epsilon}=\mathbf{0}} \\ &= \frac{\int \exp(f(\hat{\boldsymbol{\beta}}, \hat{\boldsymbol{\phi}}, \mathbf{b})) \, d(\hat{\boldsymbol{\beta}}, \hat{\boldsymbol{\phi}}, \mathbf{b}) \, d\mathbf{b}}{\int \exp(f(\hat{\boldsymbol{\beta}}, \hat{\boldsymbol{\phi}}, \mathbf{b})) \, d\mathbf{b}} \\ &= \mathbb{E}[\mathbf{d}(\hat{\boldsymbol{\beta}}, \hat{\boldsymbol{\phi}}, \mathbf{b}) | \mathbf{y}]. \end{aligned} \quad (14)$$

This identity allows TMB to improve the predictions for the random effects ( $\mathbf{d}(\cdot)$  is the identity) and nonlinear functions of the mixed effects using the gradient of the approximate marginal likelihood with respect to the auxiliary parameters,  $\boldsymbol{\epsilon}$ , leveraging its available tools: CppAD to automatically evaluate derivatives and the LA to approximate the integrals. [Thorson and Kristensen \(2016\)](#) note that this is only a bias correction algorithm because the LA used to evaluate both numerator and denominator in (14) will be inexact unless the likelihood, conditional on the fixed effects, is multivariate Gaussian.

#### 4.3. Variance of TMB Estimators

TMB approximates the covariance of the fixed effects using the inverse of the observed Hessian of the log-likelihood:

$$\boldsymbol{\Sigma}_{\hat{\boldsymbol{\beta}}, \hat{\boldsymbol{\phi}}} = \text{Cov}(\hat{\boldsymbol{\beta}}, \hat{\boldsymbol{\phi}}) = \left( -\nabla^2 \log \tilde{\mathcal{L}}(\hat{\boldsymbol{\beta}}, \hat{\boldsymbol{\phi}}) \right)^{-1}. \quad (15)$$

In models that include random effects, the joint covariance of the fixed and random effects is approximated using an application of the law of total

variance and a linearization:

$$\begin{aligned}\Sigma_{\hat{\beta}, \hat{\phi}, \hat{b}} &= \text{Cov} \left( \begin{pmatrix} \hat{\beta}, \hat{\phi} \\ \hat{b} \end{pmatrix} \right) = \text{E} \left[ \text{Cov} \left( \hat{\beta}, \hat{\phi}, \hat{b} \mid \hat{\beta}, \hat{\phi} \right) \right] + \text{Cov} \left[ \text{E} \left( \hat{\beta}, \hat{\phi}, \hat{b} \mid \hat{\beta}, \hat{\phi} \right) \right] \\ &\approx \begin{pmatrix} 0 & 0 \\ 0 & \mathcal{H}_{bb}^{-1}(\beta, b, \phi) \end{pmatrix} + \mathbf{J} \Sigma_{\hat{\beta}, \hat{\phi}} \mathbf{J}^T\end{aligned}\quad (16)$$

where  $\mathcal{H}_{bb}(\beta, b, \phi)$  is the random effects sub-matrix of the full joint Hessian of  $f(\beta, b, \phi)$ , and  $\mathbf{J}$  is the Jacobian of the vector  $(\theta, \hat{b}(\theta))^T$  with respect to  $\theta$ . The  $\delta$ -method is used to find the joint covariance of differentiable functions of the mixed effects:

$$\text{Cov} \left( \mathbf{d}(\hat{\beta}, \hat{\phi}, \hat{b}) \right) = \nabla \mathbf{d} \Sigma_{\hat{\beta}, \hat{\phi}, \hat{b}} \nabla \mathbf{d}^T, \quad (17)$$

where  $\nabla \mathbf{d}$  is the Jacobian of  $\mathbf{d}$ . For models with only fixed effects, this simplifies to

$$\text{Cov} \left( \mathbf{d}(\hat{\beta}, \hat{\phi}) \right) = \nabla \mathbf{d} \Sigma_{\hat{\beta}, \hat{\phi}} \nabla \mathbf{d}^T. \quad (18)$$

Much like the correction for the random effects predictions, TMB can improve the covariance estimator of the random effects prediction and functions of the mixed effects shown in (17) using the second derivative of  $e(\hat{\beta}, \hat{\phi}, u, \epsilon | y)$  from (13). The form of the improved variance estimator again uses the law of total variance:

$$\begin{aligned}\text{Cov} \left( \mathbf{d}(\hat{\beta}, \hat{\phi}, \hat{b}) \right) &= \left[ \frac{\partial^2}{\partial^2 \epsilon} \left( e(\hat{\beta}, \hat{\phi}, b, \epsilon | y) \right) + \right. \\ &\quad \left. \frac{\partial}{\partial \theta} \frac{\partial}{\partial \epsilon} \left( e(\hat{\beta}, \hat{\phi}, b, \epsilon | y) \right)^T \Sigma_{\hat{\beta}, \hat{\phi}} \frac{\partial}{\partial \theta} \frac{\partial}{\partial \epsilon} \left( e(\hat{\beta}, \hat{\phi}, b, \epsilon | y) \right) \right]_{\epsilon=0}\end{aligned}\quad (19)$$

where the first term on the right-hand side works out to be the standard variance estimator for random effects conditional on the fixed effects (demonstrated analogously to the derivation in (14)), and the second term accounts for having conditioned on the fixed effects estimators. This is an improvement over the naive EB variance estimators which ignore the conditioning on the fixed effects (Carlin and Louis, 2000, Chapter 3.5).

## 5. Contrasting TMB and INLA

For clarity, Table 1 provides a summary of the primary differences - and similarities - between TMB and INLA that were discussed in detail in the previous two sections.

TMB and INLA will yield the most similar results under the following conditions:

- TMB is coded to optimize the marginal posterior using the same priors and with the same internal parameter representations used by R-INLA,
- TMB uses both bias and variance corrections to functions of REs,
- R-INLA uses the Gaussian approximations and the empirical Bayes ‘integration’ strategy,
- R-INLA does not use the bias and skew corrections when drawing posterior samples.

## 6. Spatial Simulation Study

We performed two simulation studies on popular continuous and discrete spatial smoothing models to assess the ability of TMB and R-INLA to estimate the total spatial field effects, the parameters and hyperparameters, and how their computational performance scales as data volume and random effects dimension increase.

The second purpose of the continuous simulation study was to perform a thorough assessment the popular stochastic partial differential equations (SPDE) representation fitting GPs which uses a finite element method over a triangulation to solve a particular SPDE whose solution is known to have Matérn covariance ([Stein, 1999](#)). For details on the SPDE approximation, see [Lindgren et al. \(2010\)](#) and [Miller et al. \(2020\)](#). The discrete simulation study was included in part to assess and verify inference in TMB using hard constraints on the random effects parameters.

For each study, a grid of experiments, shown in Tables 2 and 3, was defined. Each level of each experiment was replicated 25 times to obtain Monte Carlo errors on the validation metrics. For each replicate within each experiment, completely new spatial fields, sampling locations, and observations were generated. For each of these, TMB and R-INLA algorithms were run,

	TMB	INLA
Inferential Method: FE	Frequentist: MLEs from marginal likelihood (or MMAP from marginal posterior)	Full Bayesian (or PEB)
Inferential Method: RE	Frequentist: EB (or PEB)	
Laplace approximation	Standard Gaussian approximation	LRA from <a href="#">Tierney and Kadane (1986)</a>
Bias Corrections	Yes, to functions of REs	Applied to align joint posterior samples with marginal distributions
Var. Corrections	Yes, to functions of REs	No
Skew Corrections	No	Applied to align joint posterior samples with marginal distributions
Hyperpar. Integration	No	Yes (no)
Inferential sampling	Gaussian centered at point estimates and covariance from observed information and linearization	Gaussian approximation to joint posterior with mean and skew corrections applied to marginals
Hessian Evaluation	Automatic Differentiation	Finite Differences
Sparse Matrices	Yes	Yes
Parallelization	Yes	Yes

Table 1: Summarization of primary differences between TMB and INLA. Entries in (parentheses) indicate outcomes from TMB for models that include priors and indicate outcomes from INLA under eb ‘numerical integration’ over the hyperparameters. The table is split into sections corresponding to methods, approximations, post-model sampling, and computation. FE=fixed effects, RE=random effects, MMAP=marginal maximum a posterior estimates, PEB = parametric Empirical Bayes, LRA = Laplace ratio approximation.

and inference and validation was performed using 500 joint samples drawn from each model, projected to  $5 \times 5 \text{ km}^2$  raster grids in the case of the continuous simulation, and compared against the truth. For both models, the internal representation of parameters in TMB were coded to align with those used by R-INLA. TMB was always run using its bias correction method and the improved variance estimates, and R-INLA joint estimates were gen-

erated using its available mean bias correction. All of the simulation analyses use the empirical distribution taken across the 25 replicates of each experimental level.

### 6.1. Continuous Spatial Simulation

This simulation was designed with respect to three governing motivations that dictated the choice of models, covariates, and true parameter ranges: (1) vetting TMB and INLA inference while (2) assessing the SPDE approximation in a variety of settings (3) using simulated risk fields and data akin to those commonly seen in public health settings. Although motivated by public health applications, the broad range the parameters, such as the maximum number of simulated data locations, greatly extend this study's applicability beyond any one applied domain.

We consider Gaussian process (GP) models with mean  $\mu(\mathbf{s})$  at location  $\mathbf{s}$ , and the Matérn function where the covariance between two spatial locations distance  $\|\mathbf{s}_i - \mathbf{s}_j\|$  from one another is:

$$C(u(\mathbf{s}_i), u(\mathbf{s}_j)) = \frac{\sigma_m^2}{2^{\nu-1}\Gamma(\nu)} (\kappa \|\mathbf{s}_i - \mathbf{s}_j\|)^\nu K_\nu(\kappa \|\mathbf{s}_i - \mathbf{s}_j\|), \quad (20)$$

where  $\sigma_m^2$  is the variance,  $\kappa > 0$  is a scaling parameter related to the range,  $r_m = \frac{\sqrt{8\nu}}{\kappa}$ , defined to be the distance at which the spatial correlation drops to 0.1,  $\nu > 0$  is related to the smoothness of the field, and  $K_\nu$  is the modified Bessel function of the second kind. For any finite collection of locations within the domain,  $\{\mathbf{s}_1, \dots, \mathbf{s}_n\} \in \mathcal{D}$ , the random vector  $\mathbf{u} = [u(\mathbf{s}_1), \dots, u(\mathbf{s}_n)]$  has multivariate Gaussian distribution with precision matrix  $\mathbf{Q}$ .

The simulated data, observed at locations  $\mathbf{s}_i$ ,  $i = 1, \dots, n_s$ , within Nigeria and selected using a stratified spatial sampling design, arise from the following hierarchical model:

$$\begin{aligned} \mathbf{y} | \boldsymbol{\beta}, \mathbf{b}, \boldsymbol{\phi}_1 &\sim p_1(\mathbf{y} | \boldsymbol{\beta}, \mathbf{b}, \boldsymbol{\phi}_1) \\ E[y_i | \boldsymbol{\beta}, u_i, v_i] &= g^{-1}(\alpha + \mathbf{z}_i^T \boldsymbol{\beta} + u_i + v_i) \\ \mathbf{u} &\sim N(\mathbf{0}, \mathbf{Q}(r_m, \sigma_m^2)) \\ \mathbf{v} &\sim N(\mathbf{0}, I_{n_s} \sigma_{\text{clust}}^2). \end{aligned}$$

where  $\alpha$  is the intercept and is fixed to  $-1$  across all simulations,  $I_{n_s}$  is the  $n_s \times n_s$  identity matrix and the last two lines correspond to  $p_2(\mathbf{b} | \boldsymbol{\phi}_2)$  with  $\mathbf{b} = [\mathbf{u}, \mathbf{v}]$  and  $\boldsymbol{\phi}_2 = [\sigma_m^2, r_m, \sigma_{\text{clust}}^2]$ . The precision for the spatial GP,

$\mathbf{Q}$  is Matérn with range  $r_m$  and standard deviation  $\sigma_m$ . In some models, two spatially varying covariates were included: access time to health care (Weiss et al. (2018)) and malaria incidence (Weiss et al. (2019)). While the SPDE representation is used to fit the spatial fields (using three different triangulation resolutions shown in Figure B.9), the true fields are simulated directly on a high resolution regular grid using the `RandomFields` R package (Schlather et al., 2015).

The domain, covariates and stratified sampling scheme were chosen to represent public health datasets, such as the Demographic and Health Surveys (DHS) and UNICEF Multiple Indicator Cluster Surveys, which are increasingly being used to predict continuous spatial(-temporal) maps of health outcomes. Our stratified cluster sampling design mimics the one used by DHS which stratifies by regions (administrative level 1 units) and urban/rural status and usually collects observations at 250-750 clusters, with typically 25-35 households sampled within each cluster. The covariates, access (travel time) to health care and malaria incidence, are both reasonable choices to be correlated with health risks and were further chosen for their different spatial characteristics, and the magnitude of the GP and total field were selected to yield moderately rare outcomes. Both Binomial and Gaussian data are commonly collected in a variety of applications (Poisson likelihoods are examined in the discrete simulation), and the binary data provide an extra challenge for both TMB and INLA. The Matérn range was selected to represent medium-small and medium-large spatial ranges over the approximate  $10 \times 10$  (degrees latitude-longitude) domain. The Matérn variance takes two values representing small- and large-scale spatial effects relative to the covariate effects and the small, medium, and large values of the *iid* cluster variance and Gaussian observation variance. The number of vertices in the SPDE triangulation were selected to represent medium, fine, and very fine meshes, relative to the domain and resolution of the  $5 \times 5$ km raster representation, and to assess the computational scaling of TMB and R-INLA. While the INLA method with empirical Bayes integration and Gaussian approximations are closest to the methods in TMB, we also evaluate some of the more accurate options in order to asses the default (and better) approximations available in R-INLA.

The (nearly) full combinatorial grid of simulation parameters shown in Table 2 comprised the set of 16128 experiments (R-INLA with 8000 clusters and the full Laplace approximation was excluded due to computational time constraints and the Gaussian variances were not varied for Binomial observations). We note that the internal representation of parameters in TMB

were coded to align with those used by R-INLA. Additional details including prior specification, the stratified spatial sampling scheme, and SPDE mesh generation may be found in [Appendix B](#).

Parameter	Simulation Values
Data Observations	Binomial, Gaussian
Gaussian Observation Variance, $\sigma_{obs}^2$	$0.1^2, 0.2^2, 0.4^2$
Covariates	None, $(-.25 \times \text{access} + .25 \times \text{Malaria Incid.})$
Number of Clusters, $n_s$	250, 500, 750, 1000, 2000, 4000, 8000
Expected Samples per Cluster, $E[n_i]$	35
Spatial Range (lat-lon degrees)	$1, \sqrt{8}$
Spatial Variance	$0.25^2, 0.5^2$
Cluster Variance, $\sigma_{clust}^2$	$0, 0.1^2, 0.2^2, 0.4^2$
Num. Nodes in SPDE Mesh	3631, 7922, 13869 (low, medium, high resolution)
R-INLA Integration Strategy	Empirical Bayes (EB), Central Composite Design (CCD)
R-INLA Approximation Strategy	Gaussian, Simplified Laplace, Laplace

Table 2: Parameters varied across the continuous simulation experiments. The total number of experiments was 16128 (Gaussian variance was not varied for Binomial experiments), each replicated 25 times.

### *Selected Continuous Simulation Results*

The simulation comparisons presented in this section compare results from TMB against those from R-INLA using the default options: the simplified Laplace approximation and the CCD numerical integration scheme with mean and skew corrections to the marginals of the joint posterior sampling distribution (see [Section 3](#)). While using the grid numerical integration scheme and the full Laplace approximations could offer an overall better approximation, and the empirical Bayes integration with Gaussian approximations would be closest to the approximations in TMB, the default INLA options provide a nice balance between computation and accuracy and are what many users explicitly or implicitly choose to use. For these reasons we felt this setting to be a useful and fair benchmark for which to contrast TMB. The extended online results also include comparisons with other combinations of INLA approximations and a number of additional selections are included in [Appendix B](#).

Additional continuous simulation results for all experiments in Table 2

can be explored via an interactive R-Shiny web application by visiting [faculty.washington.edu/jonno/software.html](http://faculty.washington.edu/jonno/software.html).

The following four figures display:

- Figure 1: Binomial scenarios' parameter bias for the intercept, access and malarian incidence coefficients, cluster variance, and the Matérn standard deviation and range.
- Figure 2: Binomial, medium-resolution mesh, scenarios' mean pixel coverage, stratified by the value of the true GP, and faceted by cluster variance and number of spatial observations.
- Figure 3: Normal  $\sigma_{obs}^2 = 0.04$ , medium-resolution mesh, scenarios' mean pixel coverage, stratified by the value of the true GP, and faceted by cluster variance and number of spatial observations.

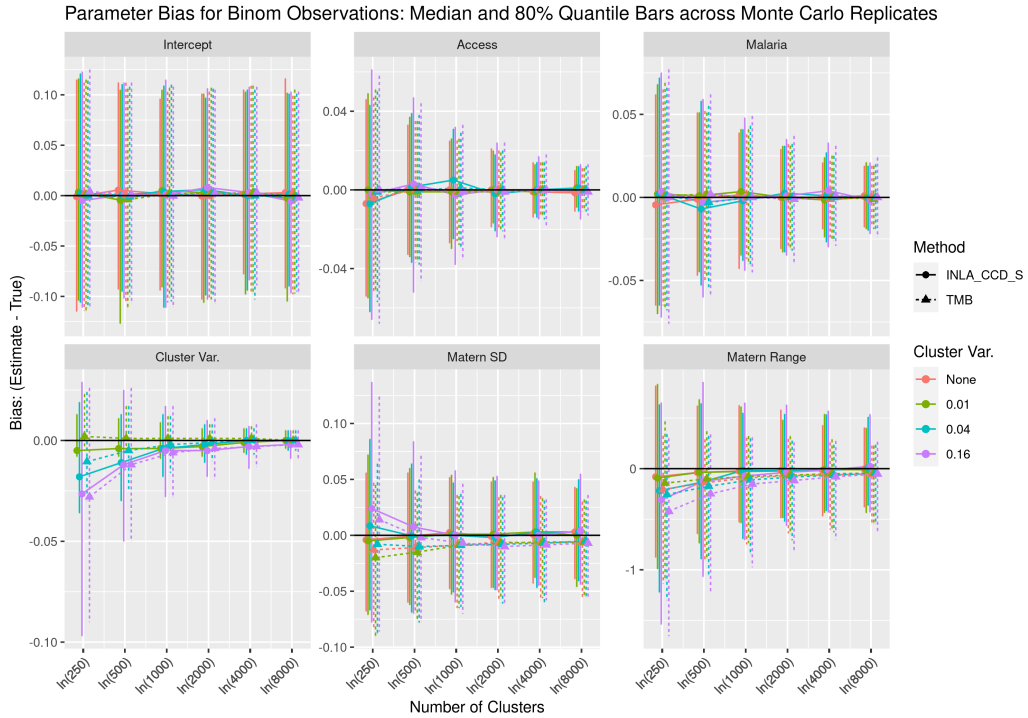


Figure 1: Comparison of the estimated parameter bias from TMB (dashed lines) and R-INLA using CCD hyperparameter integration and simplified Laplace approximations (solid lines) plotted against the number of cluster observations for Binomial observation experiments. Colors represent different cluster (i.i.d nugget) variances used in an experiment. Each point is the median bias of 3 experiments (coarse, medium, and fine SPDE triangulation), calculated across 75 replicates, and the bars represent the middle 80% quantile range of the bias across replicates.

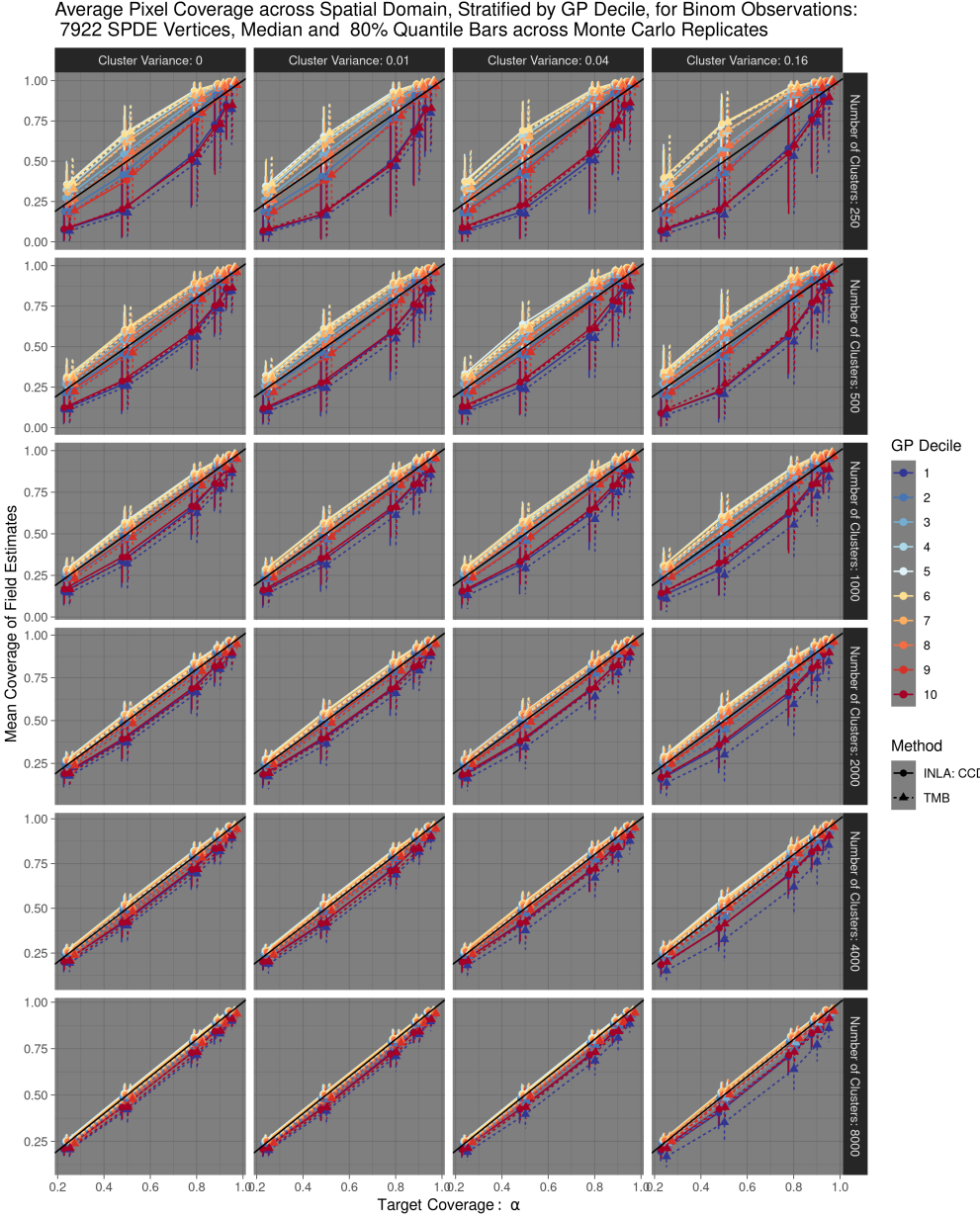


Figure 2: Comparison of the average estimated field coverage of the simulated truth, faceted by cluster (i.i.d. nugget) variance and the number of clusters, from TMB (dashed lines) and R-INLA using CCD hyperparameter integration and simplified Laplace approximations (solid lines) plotted against the target nominal coverage,  $\alpha$ , for Binomial observation experiments with the medium resolution SPDE triangulation. Colors stratify pixels included in the average coverage calculation by the decile of the true GP for the experiment replicate. Each point is the median average coverage of an experiment, calculated across 25 replicates, and the bars represent the middle 80% quantile range of the average coverage across replicates.

Average Pixel Coverage across Spatial Domain, Stratified by GP Decile, for Normal Observations with Var = 0.040:  
7922 SPDE Vertices, Median and 80% Quantile Bars across Monte Carlo Replicates

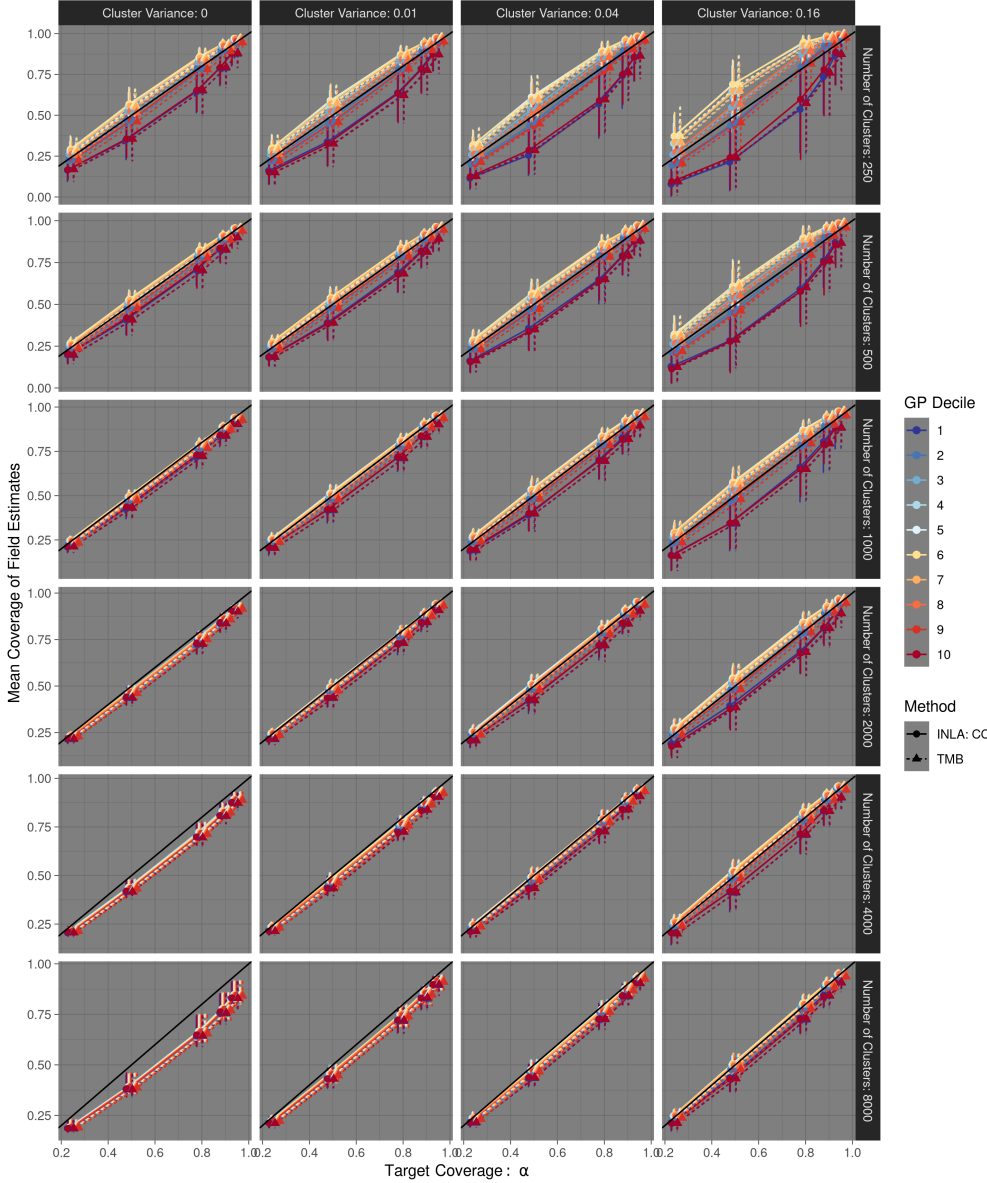


Figure 3: Comparison of the average estimated field coverage of the simulated truth, faceted by cluster (i.i.d. nugget) variance and the number of clusters, from TMB (dashed lines) and R-INLA using CCD hyperparameter integration and simplified Laplace approximations (solid lines) plotted against the target nominal coverage,  $\alpha$ , for Gaussian observation experiments with  $\sigma^2 = 0.04$  and the medium resolution SPDE triangulation. Colors stratify pixels included in the average coverage calculation by the decile of the true GP for the experiment replicate. Each point is the median average coverage of an experiment, calculated across 25 replicates, and the bars represent the middle 80% quantile range of the average coverage across replicates.

While the overall results are quite similar, TMB generally has larger bias in the fixed effects estimators, particularly hyperparameters which may deviate further from Gaussianity, as shown in the continuous Binomial experiments, Figures 1, and the continuous Gaussian experiments, Figure B.10. This trend appears consistently across a variety of INLA options, Figures B.13-B.18.

In spatial statistics settings, the hyperparameters (and sometimes all parameters) may not be of inferential interest. Figures 2 and 3 demonstrate that TMB consistently yields results very similar to those from R-INLA at the spatial field level, and that the results are similar across all ranges of the spatial effect. Figures B.11 and B.12 show these results collapsed across the GP magnitude. In contrast to R-INLA, TMB seems to consistently have slightly lower coverage which could be attributed to the lack of integration over the hyperparameters even though the covariance estimator in (19) attempts to account for this.

In the Binomial experiment, we saw no notable differences in the spatial field coverage across the different resolutions of the SDDE triangulation suggesting that the approximation was appropriately resolved. In the Gaussian data setting, we observed that the coarser meshes undercovered the field estimates in experiments with small  $\sigma_{clust}^2$  and large sample sizes - but this was mostly remedied at the finer triangulation resolution. Interestingly, we saw more severe field undercoverage for larger numbers of spatial observations. These patterns were observed in results from both TMB and INLA. See the lower left plots of Figures B.19-B.21.

## 6.2. Discrete Spatial Simulation

For the discrete simulation study, we considered the BYM2 model (a modern formulation of the classic Besag-York-Mollie model developed by [Riebler et al. \(2016\)](#)). This model requires a sum-to-zero constraint a hard constraint, using appropriate conditional densities ([Gelfand et al., 2010](#), Section 12.1.7.4), was implemented in TMB to match the linear constraint used in the R-INLA BYM2 model formulation.

The discrete model was implemented over the 37 regions (first-level administrative units) of Nigeria, and neighbors were defined by to be regions with shared boundaries. Within each region, the population,  $n_s$ , for that area was first sampled from iid Poisson distributions. Conditional on the population, poisson observations were simulated from the following hierarchical model:

$$\begin{aligned}
 y_i | n_s, \eta_i &\sim \text{Poisson}(n_s \times \eta_i) \\
 \eta_i &= \exp(\alpha + \mathbf{b}_i) \\
 \mathbf{b} &= \frac{1}{\sqrt{\tau}} (\sqrt{1-\varphi} \mathbf{v} + \sqrt{\varphi} \mathbf{u}_*) \\
 \mathbf{v} &\sim N(\mathbf{0}, \mathbf{I}) \\
 \mathbf{u}_* &\sim N(\mathbf{0}, \mathbf{Q}_*^{-1}), \text{s.t. } \sum_{i=1}^{37} u_{*i} = 0,
 \end{aligned} \tag{21}$$

with  $\alpha$  the GMRF intercept, fixed at -3 across simulations, BYM2 field  $\mathbf{b}$  with total variance  $\tau^{-1}$ , mixing parameter  $\varphi$  controlling the contribution of  $\mathbf{v}$ , the unstructured i.i.d. portion of the BYM2 field, and  $\mathbf{u}_*$ , the scaled spatially structured component of the BYM2. The structured portion of the BYM2 is specified with precision  $\mathbf{Q}_*$ , a scaled version of the precision from the classic BYM ICAR model, and is constrained to sum to zero.

The full combinatorial grid of simulation parameters is shown in Table 3 consisted of a set of 20 experiments, with each experiment replicated 25 times to obtain Monte Carlo errors on the validation metrics. Additional details including prior specification and the constrained random effects density may be found in [Appendix C](#).

### Discrete Simulation Results

The results from the discrete simulations, summarized in term of parameter bias in Figure 4 and in terms of spatial field coverage in Figure 5, share

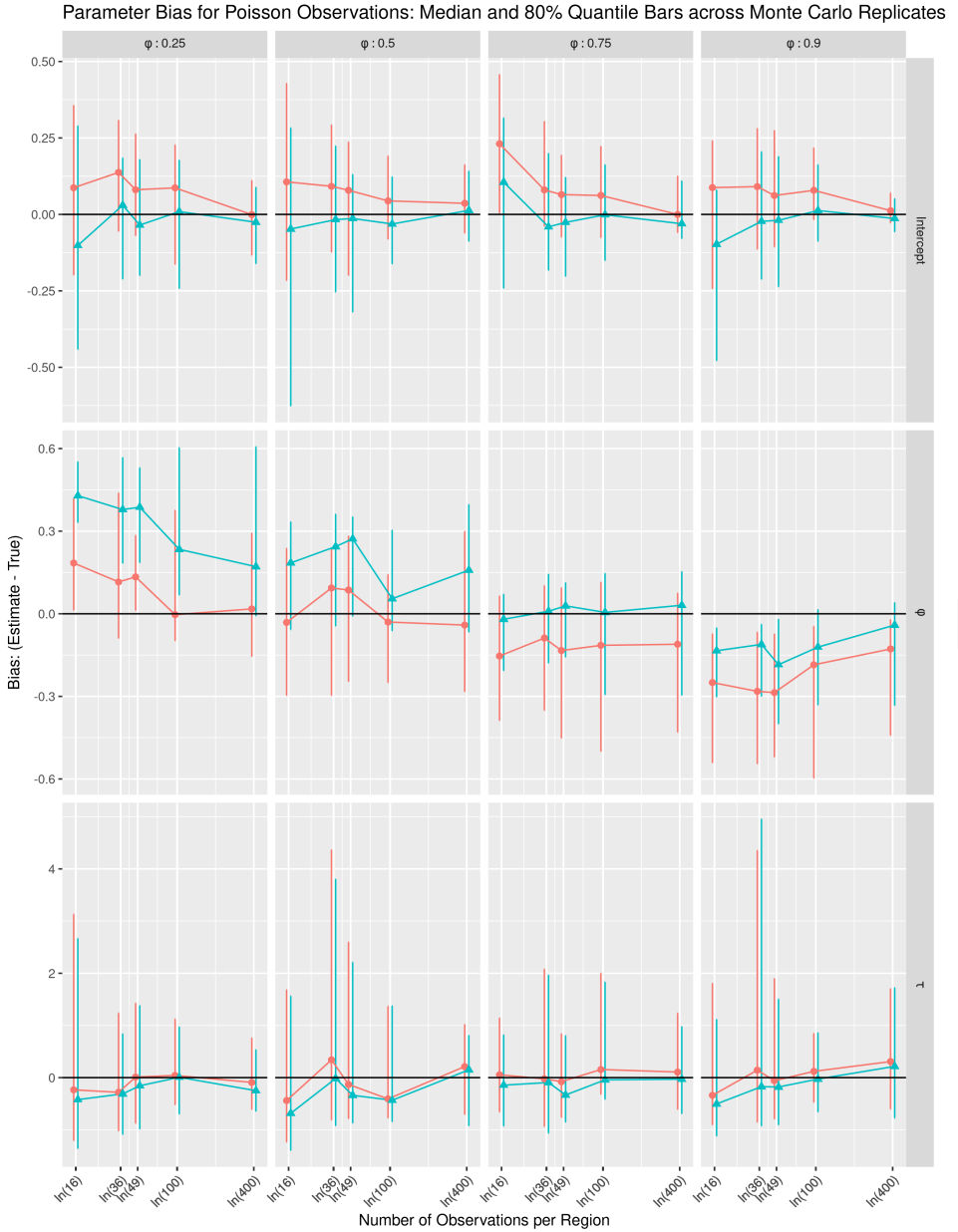


Figure 4: Comparison of the estimated parameter bias from TMB (red) and R-INLA (blue) plotted against the number of observations per region for Poisson data experiments with varying values of the true BYM2  $\varphi$ . Each point is the median bias of 1 experiments, calculated across 25 replicates, and the bars represent the middle 80% quantile range of the bias across replicates.

Average Field Coverage across Spatial Regions for Poisson Observations:  
Median and 80% Quantile Bars across Monte Carlo Replicates

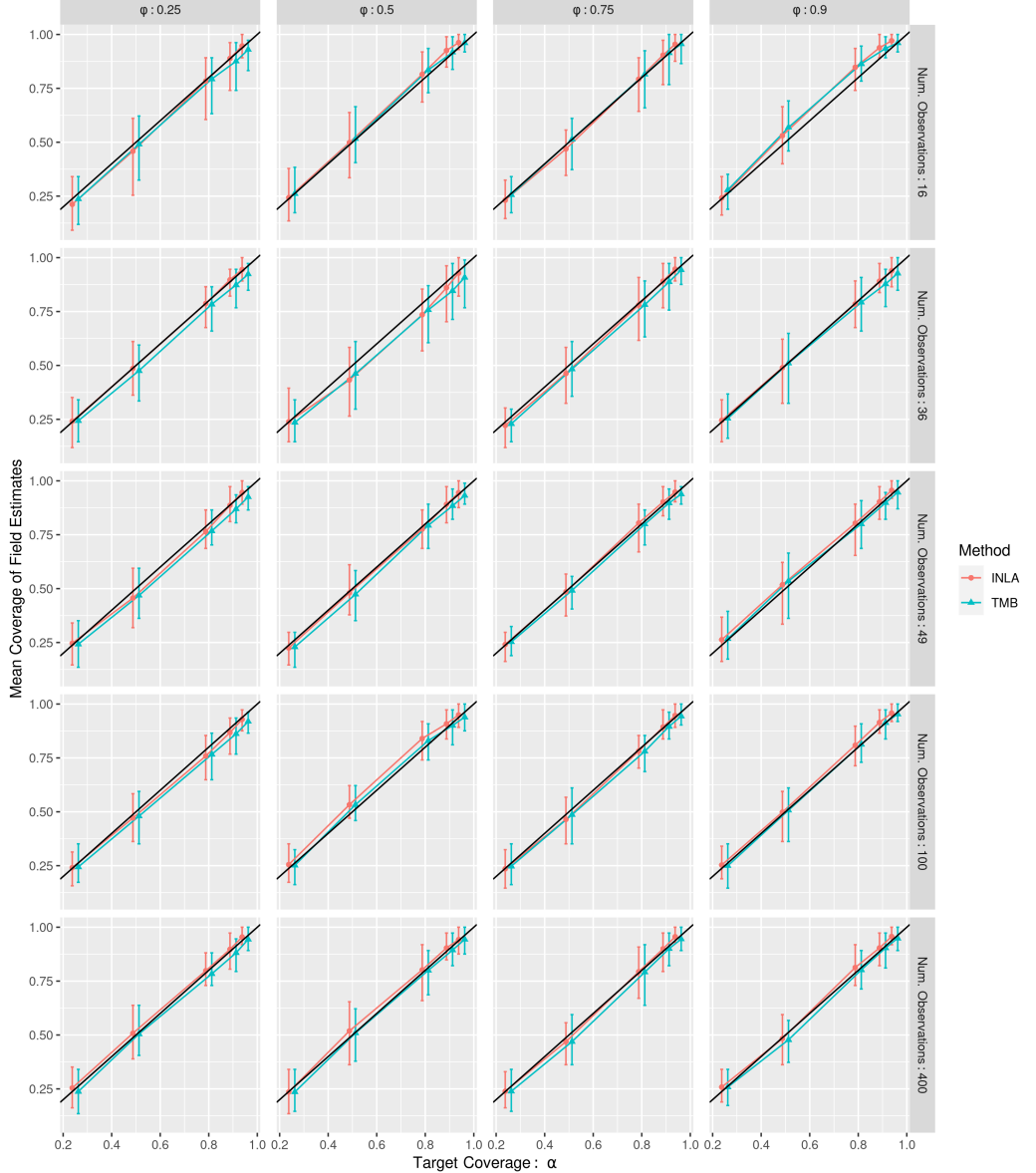


Figure 5: Comparison of the average estimated region coverage of the simulated truth, faceted by values of the true BYM2  $\varphi$  and number of observations per region, from TMB (red) and R-INLA (blue), plotted against the target nominal coverage,  $\alpha$ , for Poisson observation experiments. Each point is the median average coverage of an experiment, calculated across 25 replicates, and the bars represent the middle 80% quantile range of the average coverage across replicates.

Parameter	Simulation Values
Data Observations	Poisson
Mean Observations per Region, $E[n_s]$	16, 36, 49, 100, 400
BYM2 $\varphi$	1, 0.25, 0.5, 0.75, 0.9
BYM2 Variance, $(\tau^{-1})$	0.5
GMRF Intercept	-3
R-INLA Integration Strategy	Central Composite Design (CCD)
R-INLA Approximation Strategy	Simplified Laplace

Table 3: Parameters varied across the discrete simulation experiments. The total number of experiments was 20, and each was replicated 25 times.

many similarities to those observed in the continuous simulations of Section 6.1. Both methods produce very similar spatial field estimates though TMB appears more likely to have larger bias for some parameters.

## 7. European Breast Cancer Application

Data quality for cancer monitoring vary significantly across the European Union (EU) and range from complete registry coverage and high quality mortality estimates from vital registration to countries with no data. We use TMB to fit a similar model to one previously detailed by [Mercer \(2016\)](#) and fitted with user-written MCMC code. We describe a two-level nonlinear model which first assumes a Poisson model for cancer incidence and then, conditional on cancer counts, models deaths as a binomial outcome. This model appropriately handles the variety of cancer data present in the EU in part because the conditional two-level Poison-Binomial form induces a Poisson model for unconditional mortality to account for countries without incidence data from registries. Using data provided by the International Agency for Research on Cancer (IARC), we implement a Bayesian spatial smoothing model to borrow strength between countries to provide estimates of national incidence and mortality, along with measures of uncertainty.

The approach directly models mortality (which is more universally available) and the mortality-incidence (MI) ratio, to estimate both incidence and mortality for all countries. The model synthesizes four types of country data: type I countries with national incidence and mortality data, type II countries with sub-national incidence and mortality data (from registries) in addition to national mortality, type III countries with only national mortality, and type IV countries with no available data. While there is reason to think cancer incidence may be spatially correlated across countries, for example due to environmental and lifestyle risks, different preventions and screening strategies may result in large variability between nearby countries. For this reason, the BYM2 model presented in Section 6.2 was used to model a combination of spatial and iid country effects. We would also expect some smoothness in mortality over space due to similarities in GDP, and therefore healthcare, in close by countries.

For countries,  $c$ , that have both national mortality and incidence data (type I) we assume a Poisson process with rate  $p_c$  for cancer incidence, where  $Y_c$  is the number of reported individuals with breast cancer from a population of  $N_c$ . Conditional on having cancer, we model total mortality,  $Z_c$ , as a binomial outcome with probability of death  $r_c$  for each of the  $Y_c$  individuals with cancer. This induces a Poisson process for mortality when incidence is unobserved with rate  $p_c \times r_c$ . For illustration, we work with only with data

from 2008 in women aged 50-54. Our base model for type I countries is:

$$Y_c|N_c, p_c \sim \text{Poisson}(N_c \times p_c), \quad p_c = \exp(\alpha_c^I) \quad (22)$$

$$Z_c|Y_c, r_c \sim \text{Binomial}(Y_c, r_c), \quad r_c = \frac{\exp(\alpha_c^{MI})}{1 + \exp(\alpha_c^{MI})} \quad (23)$$

which implies the unconditional mortality model:

$$Z_c|N_c, p_c \sim \text{Poisson}(N_c q_c), \quad q_c = p_c \times r_c. \quad (24)$$

We assume a log- and logit-linear model for incidence and conditional mortality and we assign the following forms:

$$\alpha_c^I = \alpha^I + b_c^I \quad (25)$$

$$\alpha_c^{MI} = \alpha^{MI} + b_c^{MI} \quad (26)$$

where  $p_c$  is the reported incidence,  $r_c$  is the reported mortality,  $\alpha^I$  and  $\alpha^{MI}$  are global intercepts, and  $b_c^I$  and  $b_c^{MI}$  are country random effects that are assumed to have BYM-2 structure comprising of a spatially correlated term as well as an unstructured (iid) country specific term. Additional details on the data and the model may be found in [Appendix D](#). Maps of  $\hat{b}_c^I$ ,  $\hat{b}_c^{MI}$ ,  $\hat{p}_c$ , and  $\hat{r}_c$ , with measures of uncertainty, are presented in [Figure 6](#).

The nonlinear unconditional mortality rate,  $q_c = p_c \times r_c$ , is necessary to include countries with incomplete or missing mortality data and prohibits this model from being fit within INLA. A similar model that used country-level fixed effects without the spatial random effect would be possible in INLA ([Meehan et al., 2020](#)) but without complete data in each country this is not feasible.

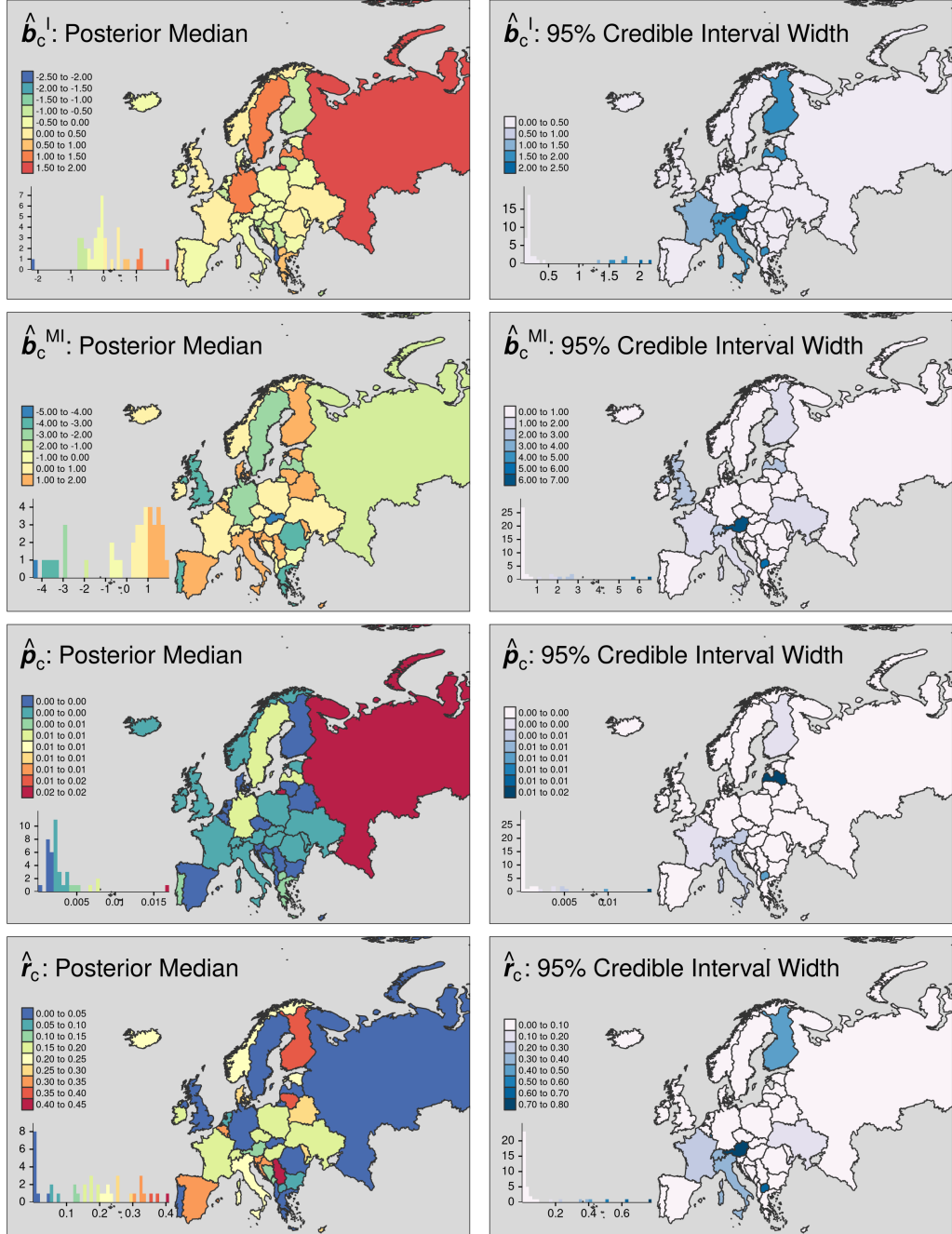


Figure 6: Each row consists of a pair of posterior median and 95% credible interval widths for the estimated quantity. Row 1: the BYM2 country random effects for incidence, row 2: the BYM2 country random effects for MI ratio, row 3: estimates country incidence rates, and row 4: estimated country mortality—incidence probabilities.

## 8. Discussion

We were pleasantly surprised to find near concurrence in spatial field estimator distributions in TMB and R-INLA – in both continuous and linearly constrained discrete model settings – across a wide range of simulation parameters. The generally smaller parameter bias in INLA results may be due to the integration over the fixed effects, similar to restricted maximum likelihood (REML) inference which is known to reduce bias, in contrast to the ML inference performed in TMB. One possible remedy for this could be to effectively enable REML in TMB by adding all linear fixed effects parameters to the list of ‘random’ parameters input by the modeler.

The field coverage figures clearly demonstrate that random effects coverage is a function of the magnitude of the effect ([Yu and Hoff \(2018\)](#)) and should serve as a warning for those trying to interpret coverage of specific portions of estimated spatial fields. The discrete Poisson experiment showed excellent recovery of the BYM2 field and the continuous models, with the SPDE approximation to the GP performed nearly as well. We see that the SPDE approximation in the binomial scenarios appears more robust than in the Gaussian and the undercoverage under extremely large data volumes warrants further investigation. Even so, the SPDE approximation performs very well across a wide range of experiments and by increasing the density of the mesh until the results no longer change the user should be able to confidently determine when the approximation is resolved. We believe these to be the largest-scale simulation studies on the SPDE approach to fitting GPs in TMB or in R-INLA and we hope that the demonstrated success encourages continued use of this convenient approach.

The simulations also provided an opportunity to assess the relative computational burdens of TMB and R-INLA. [Appendix B.3.3](#) describes both the serial (one CPU thread) and parallelized timing experiments. Figures [B.22](#) and [B.23](#) demonstrate that TMB scales extremely well, even in comparison to R-INLA which was designed, in part, to be a computationally efficient and quick alternative to MCMC sampling. We note that timing tests attempting to replicate ‘real world’ experience are quite difficult and these timing results only provide some crude measures of computational cost. Nonetheless, TMB appears to perform quite favorably and, at minimum, it could be used to quickly test and iterate models before final inference is performed using the modeler’s method of choice.

One of the main limitations of this study is the lack of tuning of any par-

ticular simulation and inference. Due to the sheer number of experiments, a set of default model parameters (for example, the starting values) were used across simulations. The simulation code was built to catch and relaunch convergence issues in both TMB and R-INLA that may, with human interaction, have been remedied. While sensible tuning decisions were attempted, this also implies a lack of sensitivity analysis on the prior selection for any one simulated dataset or experiment. Furthermore, these simulation studies use correctly specified models and do not attempt to study either tool under model misspecification.

The novel incidence-mortality model from Section 7 demonstrates the utility of the flexibility TMB provides. Simulation results for this model shown in Figure D.26 indicate that TMB is capable of recovering parameter estimates from nonlinear mixed effects models that cannot be fit within R-INLA. One of the main tradeoffs in return for this flexibility is relative difficulty of constructing the C++ templates. There has already been efforts, such as the `glmmTMB` R-package (Brooks et al. (2017)) which allows users to run TMB from within R using standard R notation for mixed effects models, to streamline the use of TMB, but none will likely be able to offer the freedom of directly coding within the C++ templates. We note that there are numerous tutorial documents and examples available on the TMB github page and the TMB authors have worked to make it easier for R coders to use. Example code for fitting spatial GPs via the SPDE approach is available in Appendix E to provide a sense of modeling in TMB and R-INLA, and the full code used in this study is available online to serve as starting points for those interested in spatial modeling in TMB. Furthermore, others have previously used TMB in spatial settings, such as classic spatial models (for example, Dwyer-Lindgren et al. (2016)), and more recent work to account for missing spatial information (Wilson and Wakefield (2020), Wilson and Wakefield (2021) and Marquez and Wakefield (2021)), and their code is available too.

The primary restriction of TMB’s applicability lies in the assumptions underlying the LA. Although many models may be fit within the TMB framework, it is clear that the LA will not perform equally well on all of them - though intelligently chosen reparameterization, like those used for the hyperparameters in both simulations, can help significantly. While the quality of the LA may be difficult to assess, the recent availability of the `tmbstan` package permits MCMC sampling from TMB models - with or without the integration of the random effects performed by LA. By comparing results run with TMB and the LA against those run with MCMC without the LA,

it is possible to assess the quality of the LA in particular applications. The speed of TMB makes it a useful option for iterating through models during exploration phases of research and it may provide opportunities to fit models that could not otherwise be fit in reasonable amounts of time or at all.

After conducting these extensive simulations, we have found TMB to perform more than adequately in comparison to existing well-trusted tools. We hope that this unified and detailed explanation of TMB and the additional new model demonstrations will improve understanding, instill confidence, and generate further interest and use in a compelling and generally unknown statistical computational tool.

## Acknowledgments

We thank the International Agency for Research on Cancer (IARC) for access to the cancer data used in this study. This work was partially supported by the Institute for Health Metrics and Evaluation (IHME), and we thank them for use of the computing cluster needed to run the continuous spatial simulations and for their support.

## References

- Alappat, C., A. Basermann, A. R. Bishop, H. Fehske, G. Hager, O. Schenk, J. Thies, and G. Wellein (2020, June). A recursive algebraic coloring technique for hardware-efficient symmetric sparse matrix-vector multiplication. *ACM Trans. Parallel Comput.* 7(3).
- Auger-Méthé, M., C. M. Albertsen, I. D. Jonsen, A. E. Derocher, D. C. Lidgard, K. R. Studholme, W. D. Bowen, G. T. Crossin, and J. M. Flemming (2017). Spatiotemporal modelling of marine movement data using Template Model Builder (TMB). *Marine Ecology Progress Series* 565, 237–249.
- Bell, B. (2007). CppAD: a package for C++ algorithmic differentiation. <http://www.coin-or.org/CppAD>. Accessed: 2021-01-19.
- Blangiardo, M. and M. Cameletti (2015). *Spatial and Spatio-Temporal Bayesian Models with R-INLA*. John Wiley & Sons.

- Blangiardo, M., M. Cameletti, G. Baio, and H. Rue (2013). Spatial and spatio-temporal models with R-INLA. *Spatial and Spatio-temporal Epidemiology* 4, 39–55.
- Blei, D. M., A. Kucukelbir, and J. D. McAuliffe (2017). Variational inference: A review for statisticians. *Journal of the American Statistical Association* 112(518), 859–877.
- Bollhöfer, M., O. Schenk, R. Janalik, S. Hamm, and K. Gullapalli (2020). State-of-the-art sparse direct solvers. pp. 3–33.
- Bolstad, G. H., K. Hindar, G. Robertsen, B. Jonsson, H. Sægrov, O. H. Diserud, P. Fiske, A. J. Jensen, K. Urdal, T. F. Næsje, et al. (2017). Gene flow from domesticated escapes alters the life history of wild atlantic salmon. *Nature Ecology & Evolution* 1(5), 1–5.
- Brooks, M. E., K. Kristensen, K. J. van Bentham, A. Magnusson, C. W. Berg, A. Nielsen, H. J. Skaug, M. Maechler, and B. M. Bolker (2017). glmmTMB balances speed and flexibility among packages for zero-inflated generalized linear mixed modeling. *The R Journal* 9(2), 378–400.
- Carlin, B. P. and T. A. Louis (2000). *Bayes and Empirical Bayes Methods for Data Analysis*. Chapman & Hall/CRC.,
- De Valpine, P. (2009). Shared challenges and common ground for Bayesian and classical analysis of hierarchical statistical models. *Ecological Applications* 19(3), 584–588.
- Dwyer-Lindgren, L., A. Bertozzi-Villa, R. W. Stubbs, C. Morozoff, M. J. Kutz, C. Huynh, R. M. Barber, K. A. Shackelford, J. P. Mackenbach, F. J. van Lenthe, et al. (2016). US county-level trends in mortality rates for major causes of death, 1980–2014. *The Journal of the American Medical Association* 316(22), 2385–2401.
- Ferkingstad, E., H. Rue, et al. (2015). Improving the INLA approach for approximate Bayesian inference for latent Gaussian models. *Electronic Journal of Statistics* 9(2), 2706–2731.
- Fournier, D. A., H. J. Skaug, J. Ancheta, J. Ianelli, A. Magnusson, M. N. Maunder, A. Nielsen, and J. Sibert (2012). AD Model Builder: using automatic differentiation for statistical inference of highly parameterized

- complex nonlinear models. *Optimization Methods and Software* 27(2), 233–249.
- Free, C. M., J. T. Thorson, M. L. Pinsky, K. L. Oken, J. Wiedenmann, and O. P. Jensen (2019). Impacts of historical warming on marine fisheries production. *Science* 363(6430), 979–983.
- Fuglstad, G.-A., D. Simpson, F. Lindgren, and H. Rue (2019). Constructing Priors that Penalize the Complexity of Gaussian Random Fields. *Journal of the American Statistical Association* 114(525), 445–452.
- Gelfand, A. E., P. Diggle, P. Guttorp, and M. Fuentes (2010). *Handbook of Spatial Statistics*. CRC press.
- Gómez-Rubio, V. (2020). *Bayesian Inference with INLA*. CRC Press.
- Griewank, A. and A. Walther (2008). *Evaluating derivatives: principles and techniques of algorithmic differentiation* (2 ed.). Society for Industrial and Applied Mathematics.
- Kraainski, E. T. E. T., V. Gómez-Rubio, H. Bakka, A. Lenzi, D. Castro-Camilo, D. Simpson, F. Lindgren, and H. Rue (2018). *Advanced Spatial Modeling with Stochastic Partial Differential Equations using R and INLA*. Chapman & Hall/CRC.
- Kristensen, K., A. Nielsen, C. W. Berg, H. Skaug, and B. M. Bell (2016). TMB : Automatic Differentiation and Laplace Approximation. *Journal of Statistical Software* 70(5), 1–21.
- Lindgren, F., J. Lindström, and H. Rue (2010). *An explicit link between Gaussian fields and Gaussian Markov random fields: The SPDE approach*. Mathematical Statistics, Centre for Mathematical Sciences, Faculty of Engineering, Lund University.
- Lindgren, F. and H. Rue (2015). Bayesian Spatial Modelling with R-INLA. *Journal of Statistical Software* 63(19), 1–25.
- Margossian, C., A. Vehtari, D. Simpson, and R. Agrawal (2020). Hamiltonian Monte Carlo using an adjoint-differentiated Laplace approximation: Bayesian inference for latent Gaussian models and beyond. *Advances in Neural Information Processing Systems* 33, 1–12.

- Marquez, N. and J. Wakefield (2021). Harmonizing binomial outcome health data at disparate geographic levels. *Statistical Methods in Medical Research*. To appear.
- Martino, S. and A. Riebler (2020). Integrated Nested Laplace Approximations (INLA). In *Wiley StatsRef: Statistics Reference Online*, pp. 1–19. American Cancer Society.
- Martins, T. G., D. Simpson, F. Lindgren, and H. Rue (2013). Bayesian computing with INLA: New features. *Computational Statistics & Data Analysis* 67, 68–83.
- Meehan, T. D., N. L. Michel, and H. Rue (2020). Estimating animal abundance with n-mixture models using the r-inla package for r. *Journal of Statistical Software, Articles* 95(2), 1–26.
- Mercer, L. (2016). *Space-Time Smoothing Models for Surveillance and Complex Survey Data*. Ph. D. thesis, University of Washington.
- Miller, D. L., R. Glennie, and A. E. Seaton (2020). Understanding the stochastic partial differential equation approach to smoothing. *Journal of Agricultural, Biological and Environmental Statistics* 25(1), 1–16.
- Monnahan, C. C. and K. Kristensen (2018). No-U-turn sampling for fast Bayesian inference in ADMB and TMB: Introducing the adnuts and tmbstan R packages. *PloS ONE* 13(5), e0197954.
- Moraga, P. (2019). *Geospatial Health Data: Modeling and Visualization with R-INLA and Shiny*. CRC Press.
- Riebler, A., S. H. Sørbye, D. Simpson, and H. Rue (2016). An intuitive Bayesian spatial model for disease mapping that accounts for scaling. *Statistical Methods in Medical Research* 25(4), 1145–1165.
- Righetto, A. J., C. Faes, Y. Vandendijck, and P. J. Ribeiro Jr (2020). On the choice of the mesh for the analysis of geostatistical data using R-INLA. *Communications in Statistics-Theory and Methods* 49(1), 203–220.
- Rue, H., S. Martino, and N. Chopin (2009). Approximate Bayesian inference for latent Gaussian models by using integrated nested Laplace approximations (with discussion). *Journal of the Royal Statistical Society: Series B (Statistical Methodology)* 71(2), 319–392.

- Rue, H., A. Riebler, S. H. Sørbye, J. B. Illian, D. P. Simpson, and F. K. Lindgren (2017). Bayesian computing with INLA: A review. *Annual Review of Statistics and Its Application* 4(1), 395–421.
- Schlather, M., A. Malinowski, P. Menck, M. Oesting, and K. Strokorb (2015). Analysis, simulation and prediction of multivariate random fields with package RandomFields. *Journal of Statistical Software* 63(8), 1–25.
- Simpson, D., H. Rue, A. Riebler, T. G. Martins, and S. H. Sørbye (2017). Penalising model component complexity: A principled, practical approach to constructing priors. *Statistical Science* 32(1), 1–28.
- Stein, M. (1999). *Interpolation of Spatial Data: Some Theory for Kriging*. Springer.
- Taylor, B. M. and P. J. Diggle (2014). INLA or MCMC? A tutorial and comparative evaluation for spatial prediction in log-Gaussian Cox processes. *Journal of Statistical Computation and Simulation* 84(10), 2266–2284.
- Teng, M., F. Nathoo, and T. D. Johnson (2017). Bayesian computation for log-Gaussian Cox processes: A comparative analysis of methods. *Journal of Statistical Computation and Simulation* 87(11), 2227–2252.
- Thorson, J. T. and K. Kristensen (2016). Implementing a generic method for bias correction in statistical models using random effects, with spatial and population dynamics examples. *Fisheries Research* 175, 66–74.
- Tierney, L. and J. B. Kadane (1986). Accurate approximations for posterior moments and marginal densities. *Journal of the American Statistical Association* 81(393), 82–86.
- Tierney, L., R. E. Kass, and J. B. Kadane (1989). Fully exponential laplace approximations to expectations and variances of nonpositive functions. *Journal of the American Statistical Association* 84(407), 710–716.
- Wakefield, J., D. Simpson, and J. Godwin (2016). Comment: Getting into space with a weight problem. *Journal of the American Statistical Association* 111(515), 1111–1118.
- Weiss, D. J., T. C. Lucas, M. Nguyen, A. K. Nandi, D. Bisanzio, K. E. Battle, E. Cameron, K. A. Twohig, D. A. Pfeffer, J. A. Rozier, et al.

- (2019). Mapping the global prevalence, incidence, and mortality of plasmodium falciparum, 2000–17: a spatial and temporal modelling study. *The Lancet* 394(10195), 322–331.
- Weiss, D. J., A. Nelson, H. Gibson, W. Temperley, S. Peedell, A. Lieber, M. Hancher, E. Poyart, S. Belchior, N. Fullman, et al. (2018). A global map of travel time to cities to assess inequalities in accessibility in 2015. *Nature* 553(7688), 333–336.
- Whittle, P. (1954). On Stationary Processes in the Plane. *Biometrika* 41(3/4), 434–449.
- Wilson, K. and J. Wakefield (2020). Pointless spatial modeling. *Biostatistics* 21, e17–e32.
- Wilson, K. and J. Wakefield (2021). Estimation of health and demographic indicators with incomplete geographic information. *Spatial and Spatio-temporal Epidemiology*. To appear.
- Yu, C. and P. D. Hoff (2018). Adaptive multigroup confidence intervals with constant coverage. *Biometrika* 105(2), 319–335.

## Appendix A. Automatic Differentiation

This appendix is provided as a brief introduction and overview for those unfamiliar with automatic differentiation (AD), also known as algorithmic differentiation. AD comprises a set of computational techniques used to evaluate the derivative of functions within a computer framework. The methods generally work by noting that computers must break down even the most complicated functions into elementary or unary arithmetic operations in order to evaluate them, and that by (repeatedly) applying the chain rule to these operations, derivatives of different orders may also be numerically evaluated. Furthermore, it is well-established that the computational cost to evaluate the derivatives will be no more than a small multiplicative factor above the cost to evaluate the original function. To help provide some intuition with AD, we will use simple linear regression to provide an example of the fundamental AD process.

For  $i \in \{1, \dots, n\}$ , assume a simple linear regression model:

$$\begin{aligned} y_i &= a + b \cdot x_i + \epsilon_i \\ \epsilon_i &\sim N(0, \sigma^2) \end{aligned}$$

where the common least squares the values for  $a$  and  $b$  are determined by minimizing the objective function:

$$RSS = \sum_{i=1}^n \left( y_i - (a + b \cdot x_i) \right)^2. \quad (\text{A.1})$$

As a minimization problem, the solution may be determined by symbolically differentiating the function in (A.1) with respect to both  $a$  and  $b$ , setting both equations to zero and simultaneously solving for the two unknowns:

$$\begin{aligned} \frac{\partial RSS}{\partial a} &= \sum_{i=1}^n -2(y_i - (a + b \cdot x_i)) = 0 \\ \frac{\partial RSS}{\partial b} &= \sum_{i=1}^n -2x_i \cdot (y_i - (a + b \cdot x_i)) = 0. \end{aligned} \quad (\text{A.2})$$

For a computer to compute these derivatives through AD, it would generate a list of all the unary operations needed to evaluate (A.1), as well as the derivatives for each unary operation, which can then be combined using

Unary Evaluation	Unary Operation	Symbolic Value	Partials
1	$u_1 = b \cdot x_i$	$b \cdot x_i$	$\frac{\partial u_1}{\partial b} = x_i$ $\frac{\partial u_1}{\partial u_1} = b$ $\frac{\partial u_1}{\partial x_i} = 1$
2	$u_2 = a + u_1$	$a + b \cdot x_i$	$\frac{\partial u_2}{\partial a} = 1$ $\frac{\partial u_2}{\partial u_1} = 1$ $\frac{\partial u_2}{\partial x_i} = 0$
3	$u_3 = y_i - u_2$	$y_i - (a + b \cdot x_i)$	$\frac{\partial u_3}{\partial y_i} = 1$ $\frac{\partial u_3}{\partial u_2} = -1$ $\frac{\partial u_3}{\partial a} = 0$ $\frac{\partial u_3}{\partial b} = 0$
4	$u_4 = u_3^2$	$(y_i - (a + b \cdot x_i))^2$	$\frac{\partial u_4}{\partial u_3} = 2u_3$ $\frac{\partial u_4}{\partial a} = 0$ $\frac{\partial u_4}{\partial b} = 0$
5	$RSS_i = u_4$	$(y_i - (a + b \cdot x_i))^2$	$\frac{\partial RSS_i}{\partial u_4} = 1$ $\frac{\partial RSS_i}{\partial a} = 0$ $\frac{\partial RSS_i}{\partial b} = 0$

Table A.4: Unary operations taken to evaluate the objective function defined in (A.1) as well as the numeric evaluation of the first partial derivatives shown in (A.2).

the chain rule to arrive at the forms of the partial derivatives shown in (A.2). The elementary steps taken to do this are shown in Table A.4 and (A.3).

Once the function has been broken into its elementary operations and the partials have been derived for each of the basic elementary operations, the partials of the complete function can be quickly evaluated through the chain rule:

$$\begin{aligned}
 \frac{\partial RSS}{\partial a} &= \sum_{i=1}^n \frac{\partial RSS_i}{\partial a} = \sum_{i=1}^n \frac{\partial RSS_i}{\partial u_4} \frac{\partial u_4}{\partial u_3} \frac{\partial u_3}{\partial u_2} \frac{\partial u_2}{\partial a} \\
 &= \sum_{i=1}^n 1 \cdot 2u_3 \cdot -1 \cdot 1 = \sum_{i=1}^n -2 \left( y_i - (a + b \cdot x_i) \right) \\
 \frac{\partial RSS}{\partial b} &= \sum_{i=1}^n \frac{\partial RSS_i}{\partial b} = \sum_{i=1}^n \frac{\partial RSS_i}{\partial u_4} \frac{\partial u_4}{\partial u_3} \frac{\partial u_3}{\partial u_2} \frac{\partial u_2}{\partial u_1} \frac{\partial u_1}{\partial b} \\
 &= \sum_{i=1}^n 1 \cdot 2u_3 \cdot -1 \cdot 1 \cdot x_i = \sum_{i=1}^n -2x_i \left( y_i - (a + b \cdot x_i) \right). \quad (\text{A.3})
 \end{aligned}$$

Once this formulation of the derivative has been built, the derivative may be quickly evaluated for different values of the parameters,  $a$ , and  $b$ , conditional on the data,  $\mathbf{y}$  and  $\mathbf{x}$ . Of course, higher order derivatives may then be calculated by iteratively applying AD.

When TMB compiles a function to quickly evaluate a function, often a likelihood, that has been coded up in a C++ template, it also returns a

function, generated through AD, that can quickly evaluate the gradient of the function, as well as the Hessian. The gradient can then be used to more efficiently find the minimum of the function, or it could be used to sample directly from the posterior in, e.g., a Hamiltonian MCMC. The Hessian, as in (12), can thus be quickly calculated with AD without the need for human generated symbolic differentiation and explicit coding - which can be tedious and error prone - and can then be used in TMB's Laplace approximation shown in (11).

See [Fournier et al. \(2012\)](#) and [Kristensen et al. \(2016\)](#) for further details about the AD methods used in TMB and [Griewank and Walther \(2008\)](#) for more general AD theory.

## Appendix B. Continuous Spatial Simulation Study

An overview of the continuous simulation details is provided in Section 6.1. Here we provide an in-depth version with all remaining details and an additional selection of results.

### Appendix B.1. Continuous Spatial Simulation Details

We consider Gaussian process (GP) models with mean  $\mu(\mathbf{s})$  at location  $\mathbf{s}$ , and the Matérn function (Stein, 1999) where the covariance between two spatial locations distance  $\|\mathbf{s}_i - \mathbf{s}_j\|$  from one another is:

$$C(u(\mathbf{s}_i), u(\mathbf{s}_j)) = \frac{\sigma_m^2}{2^{\nu-1}\Gamma(\nu)} (\kappa\|\mathbf{s}_i - \mathbf{s}_j\|)^\nu K_\nu(\kappa\|\mathbf{s}_i - \mathbf{s}_j\|), \quad (\text{B.1})$$

where  $\sigma_m^2$  is the variance,  $\kappa > 0$  is a scaling parameter related to the range,  $r_m = \frac{\sqrt{8\nu}}{\kappa}$ , defined to be the distance at which the spatial correlation drops to 0.1,  $\nu > 0$  is related to the smoothness of the field, and  $K_\nu$  is the modified Bessel function of the second kind. For any finite collection of locations within the domain,  $\{\mathbf{s}_1, \dots, \mathbf{s}_n\} \in \mathcal{D}$ , the random vector  $\mathbf{u} = [u(\mathbf{s}_1), \dots, u(\mathbf{s}_n)]$  has multivariate Gaussian distribution with precision matrix  $\mathbf{Q}$ .

The simulated data, sampled at locations  $\mathbf{s}_i$ ,  $i = 1, \dots, n_s$ , arise from the following hierarchical model:

$$\begin{aligned} \mathbf{y} | \boldsymbol{\beta}, \mathbf{b}, \boldsymbol{\phi}_1 &\sim p_1(\mathbf{y} | \boldsymbol{\beta}, \mathbf{b}, \boldsymbol{\phi}_1) \\ \mathbb{E}[y_i | \boldsymbol{\beta}, u_i, v_i] &= g^{-1}(\mathbf{z}_i^T \boldsymbol{\beta} + u_i + v_i) \\ \mathbf{u} &\sim \text{N}(\mathbf{0}, \mathbf{Q}(r_m, \sigma_m^2)) \\ \mathbf{v} &\sim \text{N}(\mathbf{0}, \mathbf{I}_{n_s} \sigma_{\text{clust}}^2). \end{aligned}$$

where  $\mathbf{I}_{n_s}$  is the  $n_s \times n_s$  identity matrix and the last two lines correspond to  $p_2(\mathbf{b} | \boldsymbol{\phi}_2)$  with  $\mathbf{b} = [\mathbf{u}, \mathbf{v}]$  and  $\boldsymbol{\phi}_2 = [\sigma_m^2, r_m, \sigma_{\text{clust}}^2]$ . The precision for the spatial GP,  $\mathbf{Q}$  is Matérn with range  $r_m$  and standard deviation  $\sigma_m$ . In some models, two spatially varying covariates, shown in Figure B.7, were included: access time to health care (Weiss et al. (2018)) and malaria incidence (Weiss et al. (2019)). While the SPDE representation is used to fit the spatial fields (using three different triangulation resolutions shown in Figure B.9, the true fields are simulated directly on a high resolution regular grid using the `RandomFields` R package (Schlather et al., 2015)).

To complete the model specification, the following priors are specified:

$$\begin{aligned}\boldsymbol{\beta} &\sim N(0, 5^2) \\ r_m, \sigma_m &\sim PCspde(u_r = 10, \alpha_r = .95, u_\sigma = 1, \alpha_\sigma = .05) \\ \tau_{\text{clust}} = \sigma_{\text{clust}}^{-2} &\sim PCprec(u = .5, \alpha = .05)\end{aligned}$$

The penalized complexity (PC) priors ([Simpson et al., 2017](#); [Fuglstad et al., 2019](#)) shrink towards a base model and are set such that  $\text{Prob}(r_m < 10^\circ) = .95$ ,  $\text{Prob}(\sigma_m > 1) = .05$  and  $\text{Prob}(\sigma_{\text{clust}} > .5) = .05$ .

Internally, TMB was coded to use the same internal representations of parameters used in R-INLA:  $\log(\kappa)$ , and  $\log(\tau_*)$ .

Simulations are performed with  $n_i$  observations taken at each spatial location  $\mathbf{s}_i$ ,  $i = 1, \dots, n_s$ . Experiments are run on Gaussian data with  $\text{Var}(y_i) = \sigma_{\text{obs}}^2/n_i$ , using an identity link function, and with the same PCprec prior on the observation variance,  $\sigma_{\text{obs}}^2 \in \phi_1$ , as is used for  $\sigma_{\text{clust}}^2$ . Experiments run on binomial data have no  $\sigma_{\text{obs}}^2$  and use a logit link function.

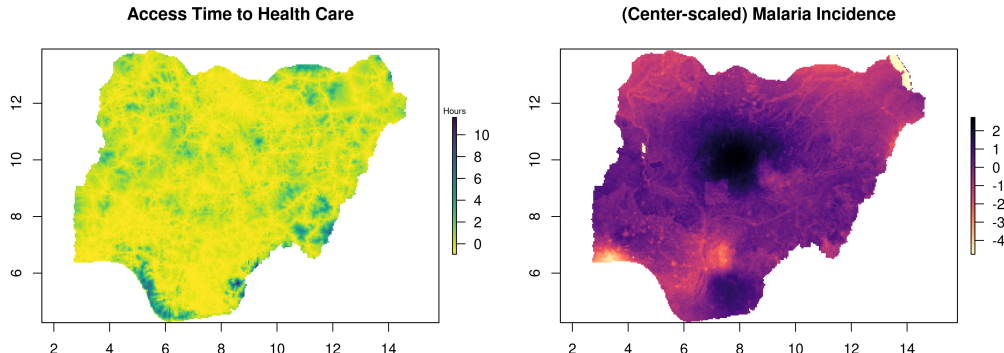


Figure B.7: Covariates used in the continuous simulation studies: access (time in hours) to healthcare ([Weiss et al. \(2018\)](#)) and malaria incidence ([Weiss et al. \(2018\)](#)) in Nigeria.

### Appendix B.2. SPDE Details

Spatial models can be notoriously difficult to fit at scale and in this study we use the SPDE finite element method representation to approximate the GPs. [Lindgren et al. \(2010\)](#) prove that specific discretely indexed GMRF models defined on triangulations can approximate continuous spatial GPs

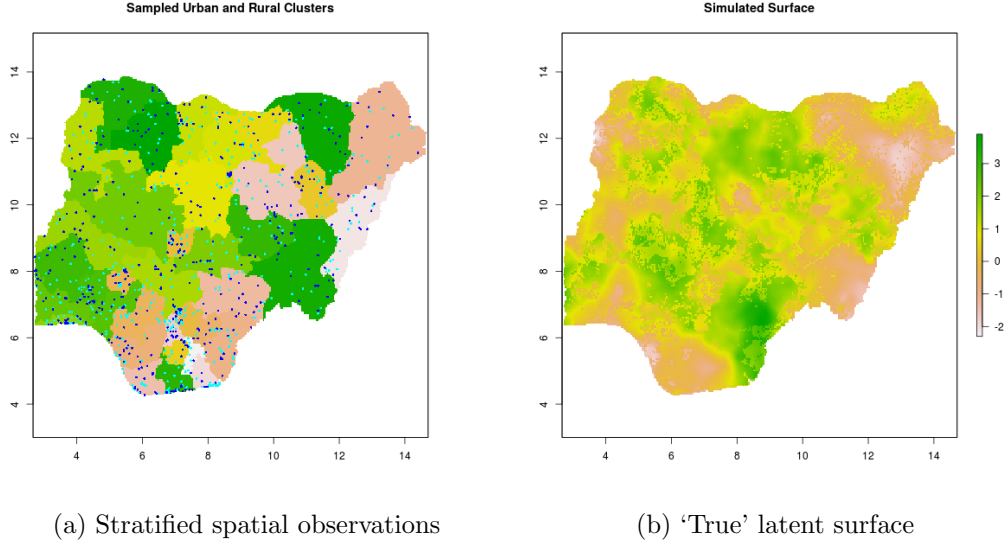


Figure B.8: Examples of (a) simulated cluster locations and (b) a simulated latent surface comprised of covariates and GP.

with Matérn covariance (B.1). This relationship relies on the fact that solutions to a specific SPDE class have the Matérn covariance and that their GMRF models are approximate solutions to the SPDE and allows the use of fast and efficient sparse matrix operations permitted on GMRFs to applied to GP models. The specific SPDE of interest takes the form:

$$(\kappa^2 - \Delta)^{\alpha/2}(\tau x(\mathbf{s})) = \mathcal{W}(\mathbf{s}), \quad (\text{B.2})$$

where  $\Delta$  is the Laplacian,  $\alpha$  controls the smoothness,  $\kappa > 0$  the scale,  $\tau$  the variance, and  $\mathcal{W}(\mathbf{s})$  is a Gaussian spatial white noise process. Whittle (1954) showed that the exact stationary solution to this SPDE is the stationary Gaussian field  $x(\mathbf{s})$ . There is a well-defined relationship between the parameters in (B.2) and (B.1) (Blangiardo and Cameletti, 2015, Section 6.5). The GMRF approximation uses a finite element method basis function representation defined on a triangulation over the domain:

$$x(\mathbf{s}) \approx \sum_{i=1}^V \psi(\mathbf{s}) w_i$$

with compact deterministic basis functions  $\psi(\mathbf{s})$  with weights  $w_i$  summed over  $V$  vertices in the triangulation. For specific basis functions, the vector

of weights,  $\mathbf{w}$ , are Gaussian with mean zero and sparse precision matrix that depends on the parameters in (B.2). See [Lindgren et al. \(2010\)](#) for details.

One of the key aspects of this approximation, as demonstrated by [Righetto et al. \(2020\)](#), is the choice of triangulation. Unlike their work, we have chosen to generate the triangulations to be constant density over the domain without using any of the data locations. The reason for this choice was two-fold. First, it allowed us to fix the mesh across the experiments and replications, removing one source of known variability. This allows us to more readily study the effect of the mesh density which has been shown to be a driver of oversmoothing ([Teng et al. \(2017\)](#)). Secondly, the discretization error varies by size of the triangles and triangulations with pronounced variability in resolution may lead to different effects of the spatial field parameters across the domain.

In the continuous spatial simulation we used three different mesh resolutions characterized by the largest allowed triangle edge length: 0.15, 0.2, and 0.3 degrees which corresponded to 3616, 7933, and 13866 vertices, respectively. The triangulations were generated using the `inla.mesh.2d` function from the R-INLA package. The centroid of every 5x5km pixel within Nigeria, the modeling domain, were used supplied `loc.domain` argument to define the extent, and the maximum allowed edge length outside the extent was set to 5 degrees. All other arguments were left as the defaults. Plots of the three triangulation meshes are shown in Figure B.9.

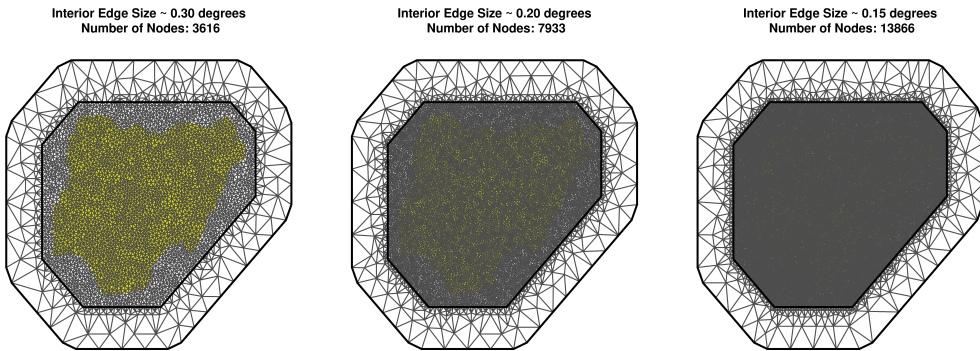


Figure B.9: Coarse, medium, and fine resolution Delauney triangulations used in the SPDE approximation to the GP. The outline of the spatial domain, Nigeria, is shown beneath the mesh for reference.

### *Appendix B.3. Additional Continuous Spatial Simulation Results*

We provide a few additional plots, extending those show in Section 6.1, contrasting TMB against the default INLA option results. Figure B.10 shows the parameter bias from these experiments analogous to Figure 1 in the main text. Figures B.11 and B.12 show collapsed versions of Figures 2 and 3 where averaging has been performed over the entire spatial field (as opposed to stratifying by the magnitude of the true GP).

Appendix B.3.1 includes parameter bias figures from the Binomial data setting for all combinations of INLA numerical integration and marginal approximations implemented in this study.

Appendix B.3.2 contains three figures showing severe undercoverage of the spatial field estimates in certain Gaussian data experiments that (mostly) disappears as the resolution of the mesh is increased. This pattern is reflected across all combinations of INLA options, but the figures presented here plot the highest quality options we evaluated, CCD integration and full Laplace approximations, demonstrating that the issue is pervasive across both TMB and INLA results.

Appendix B.3.3 describes two different timing experiments, one using serial computation and one with parallelization, used to compare the computational burden of TMB and R-INLA and includes figures summarizing the timing results.

Interactive online plots allow the interested reader to study versions of these figures for all levels of the experiment defined in Table 2. A link to the interactive web app may be found at:

<https://faculty.washington.edu/jonno/software.html>.

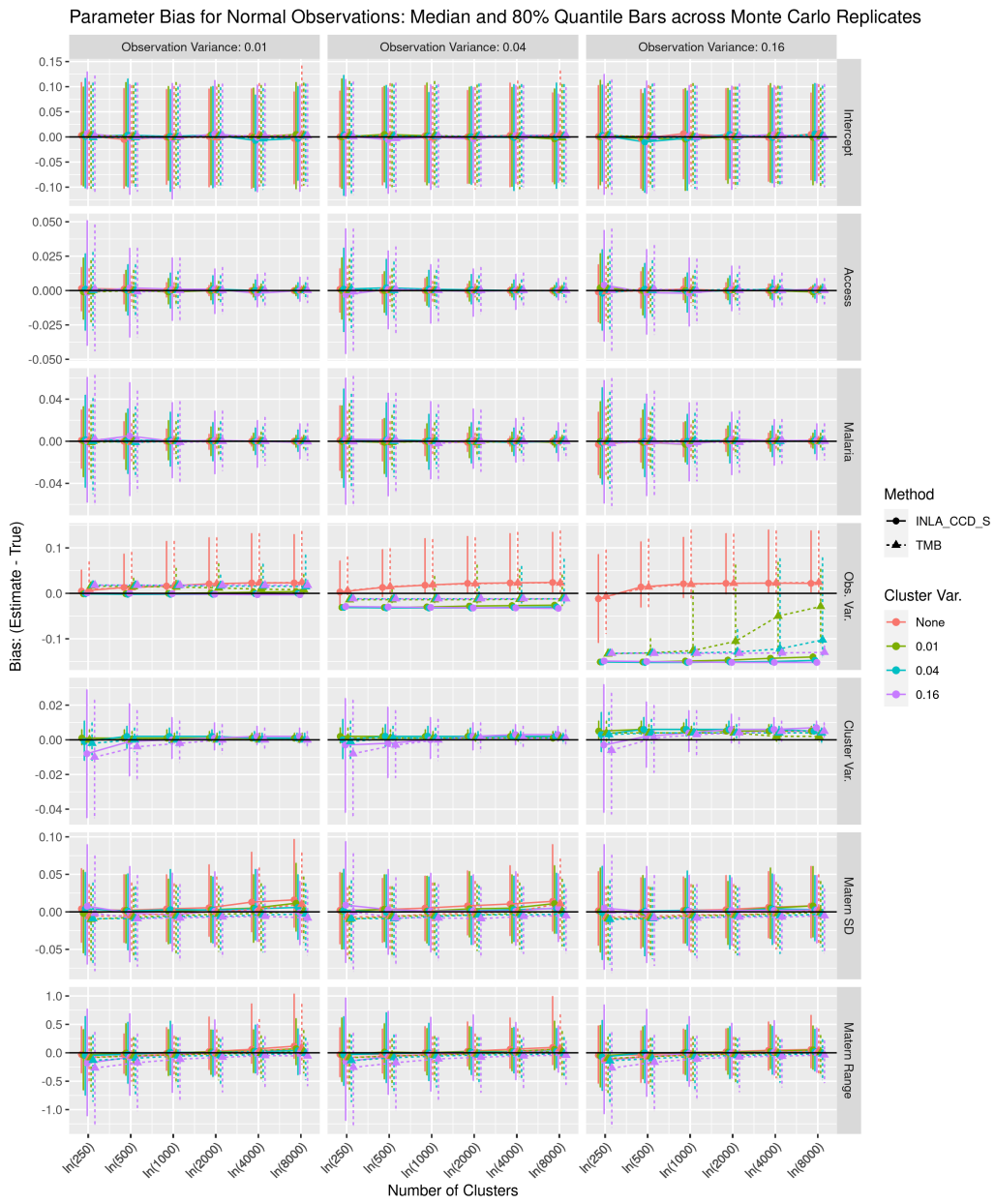


Figure B.10: Comparison of the estimated parameter bias from TMB (dashed lines) and R-INLA using CCD hyperparameter integration and simplified Laplace approximations (solid lines) plotted against the number of cluster observations for the Gaussian data experiments with varying observation variances. Colors represent different cluster (i.i.d nugget) variances used in an experiment. Each point is the median bias of 3 experiments (coarse, medium, and fine SPDE triangulation), calculated across 75 replicates, and the bars represent the middle 80% quantile range of the bias across replicates.

Average Pixel Coverage across Spatial Domain for Binom Observations:  
Median and 80% Quantile Bars across Monte Carlo Replicates

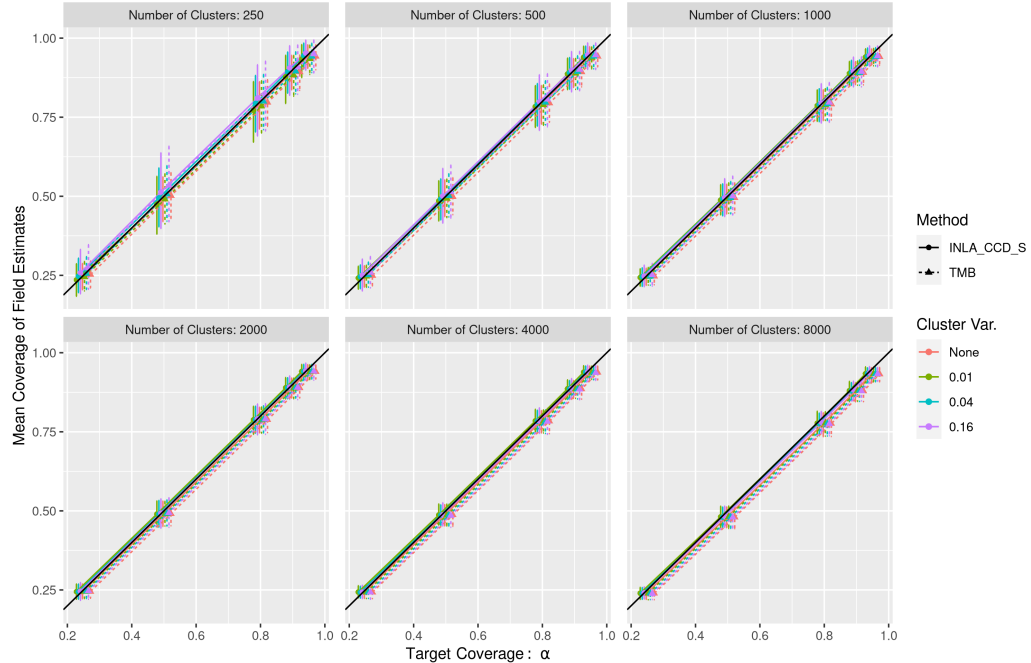


Figure B.11: Comparison of the average estimated field coverage of the simulated truth from TMB (dashed lines) and R-INLA using CCD hyperparameter integration and simplified Laplace approximations (solid lines) plotted against the target nominal coverage,  $\alpha$ , for Binomial observation experiments. Colors represent different cluster (i.i.d nugget) variances used in an experiment. Each point is the median average coverage of 3 experiments (coarse, medium, and fine SPDE triangulation), calculated across 75 replicates, and the bars represent the middle 80% quantile range of the average coverage across replicates.

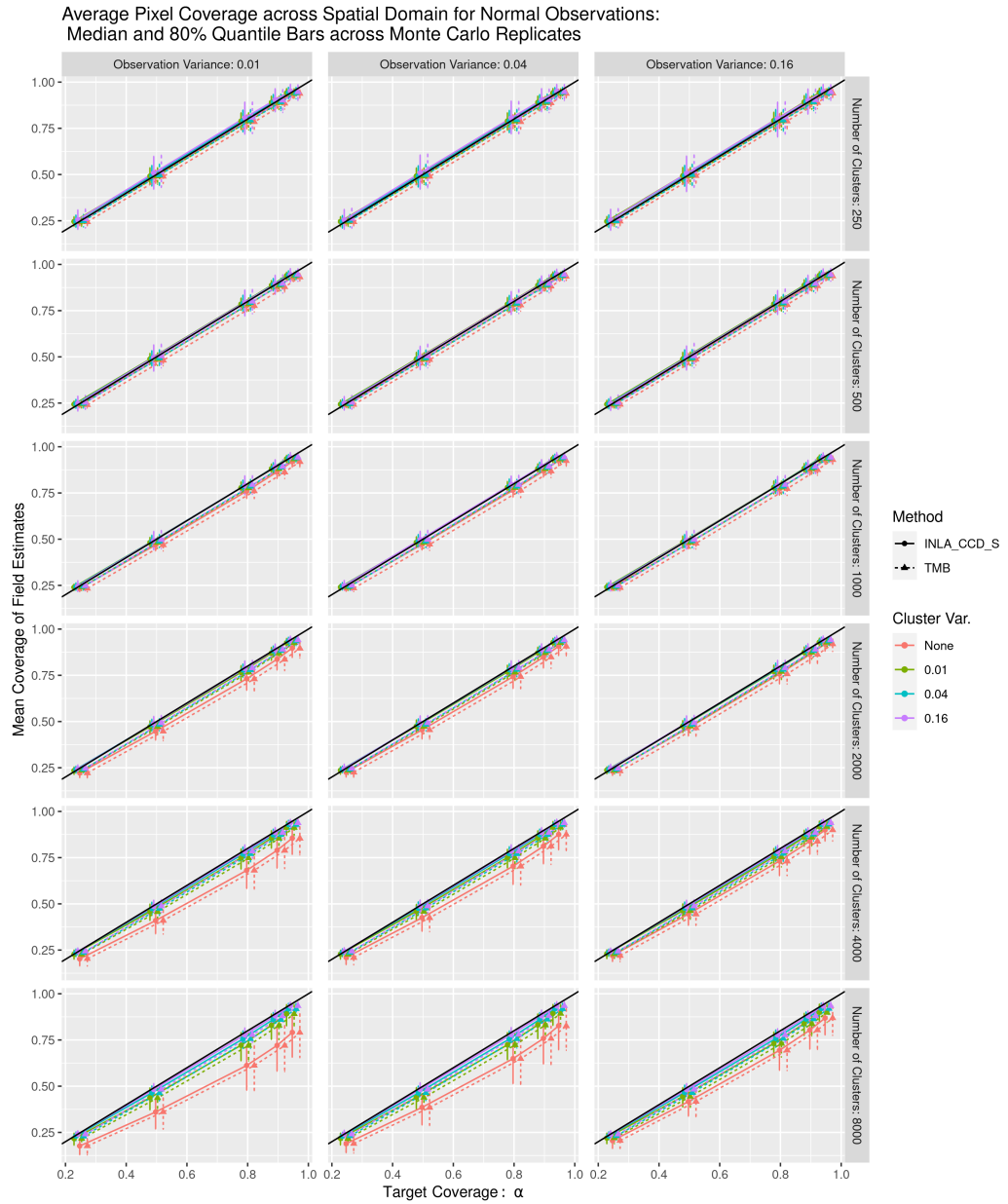


Figure B.12: Comparison of the average estimated field coverage of the simulated truth from TMB (dashed lines) and R-INLA using CCD hyperparameter integration and simplified Laplace approximations (solid lines) plotted against the target nominal coverage,  $\alpha$ , for Gaussian observation experiments with varying observation variances. Colors represent different cluster (i.i.d nugget) variances used in an experiment. Each point is the median average coverage of 3 experiments (coarse, medium, and fine SPDE triangulation), calculated across 75 replicates, and the bars represent the middle 80% quantile range of the average coverage across replicates.

### Appendix B.3.1. Various INLA options

All figures shown in this section compare bias results from Binomial data experiments. Bias from TMB (dashed lines) and INLA results (solid lines), under a variety of approximation options, are plotted against the number of cluster observations for Binomial observation experiments. Colors represent different cluster (i.i.d nugget) variances used in an experiment. Each point is the median bias of 3 experiments (coarse, medium, and fine SPDE triangulation), calculated across 75 replicates, and the bars represent the middle 80% quantile range of the bias across replicates.

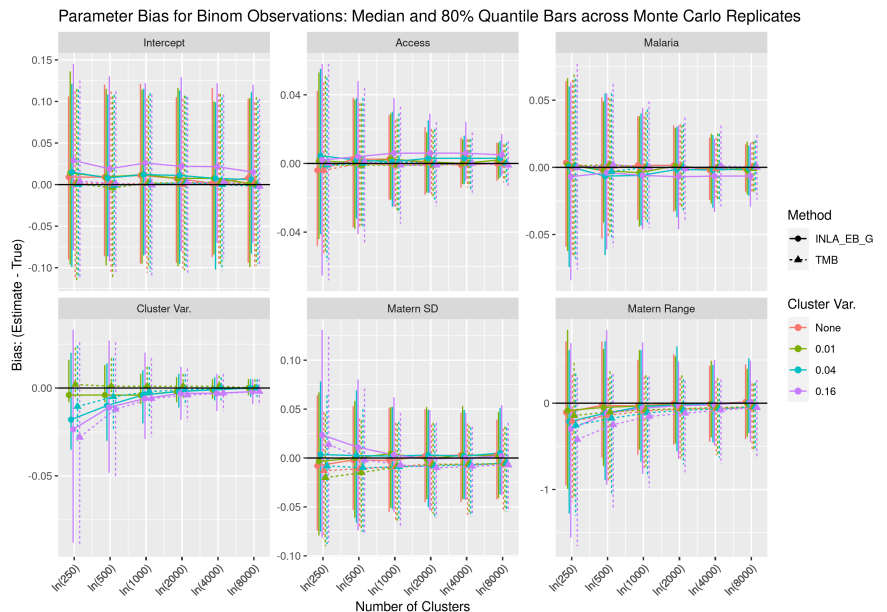


Figure B.13: Comparison of the estimated parameter bias from TMB (dashed lines) and R-INLA using EB ‘integration’ and Gaussian approximations (solid lines).

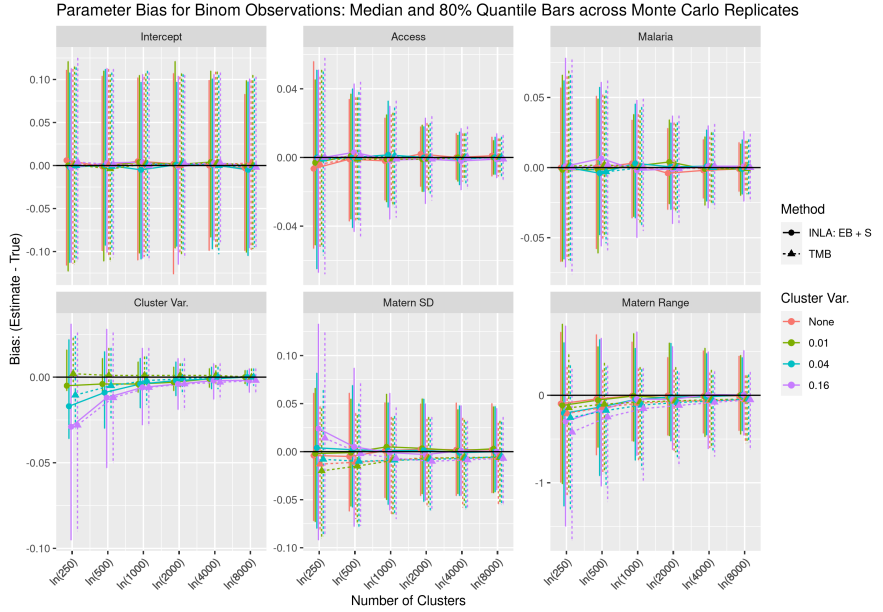


Figure B.14: Comparison of the estimated parameter bias from TMB (dashed) and R-INLA using EB ‘integration’ and simplified Laplace approximations (solid).

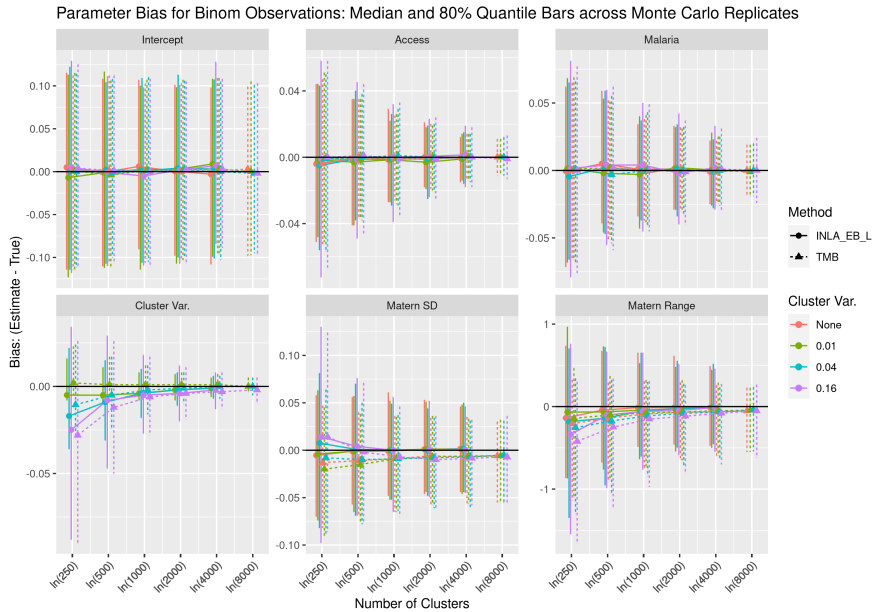


Figure B.15: Comparison of the estimated parameter bias from TMB (dashed) and R-INLA using EB ‘integration’ and full Laplace approximations (solid).

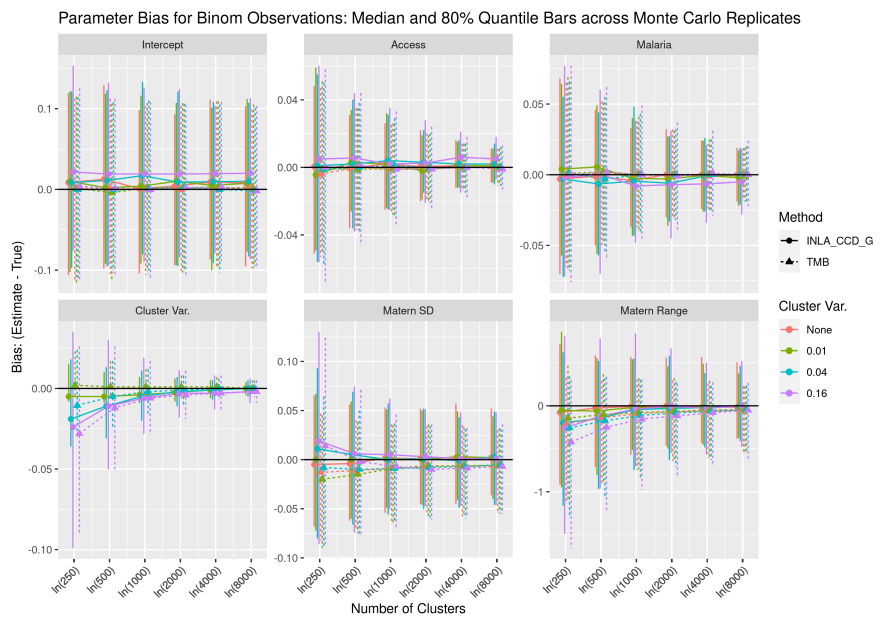


Figure B.16: Comparison of the estimated parameter bias from TMB (dashed) and R-INLA using CCD integration and Gaussian approximations (solid).

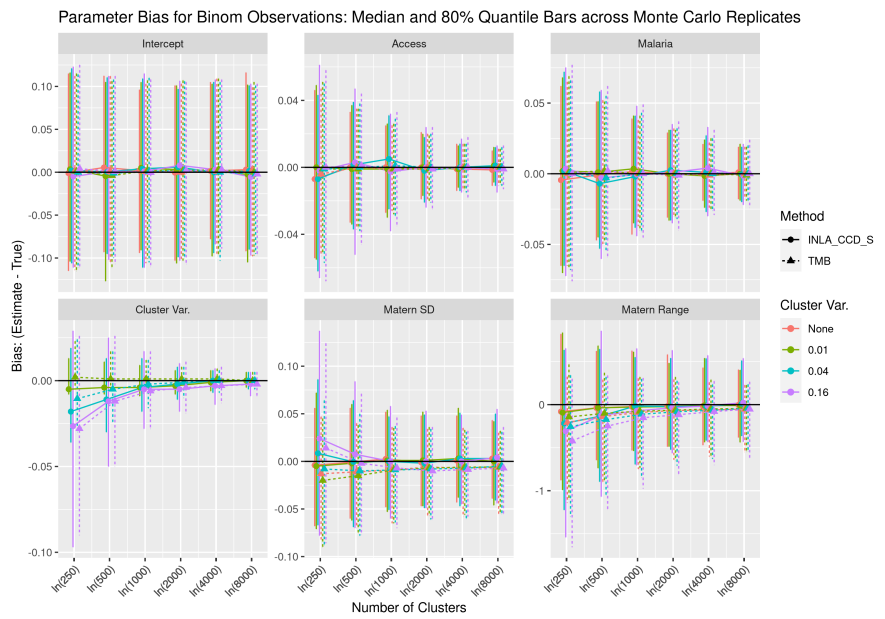


Figure B.17: Comparison of the estimated parameter bias from TMB (dashed) and R-INLA using CCD integration and simplified Laplace approx. (solid). Same as Figure 1.

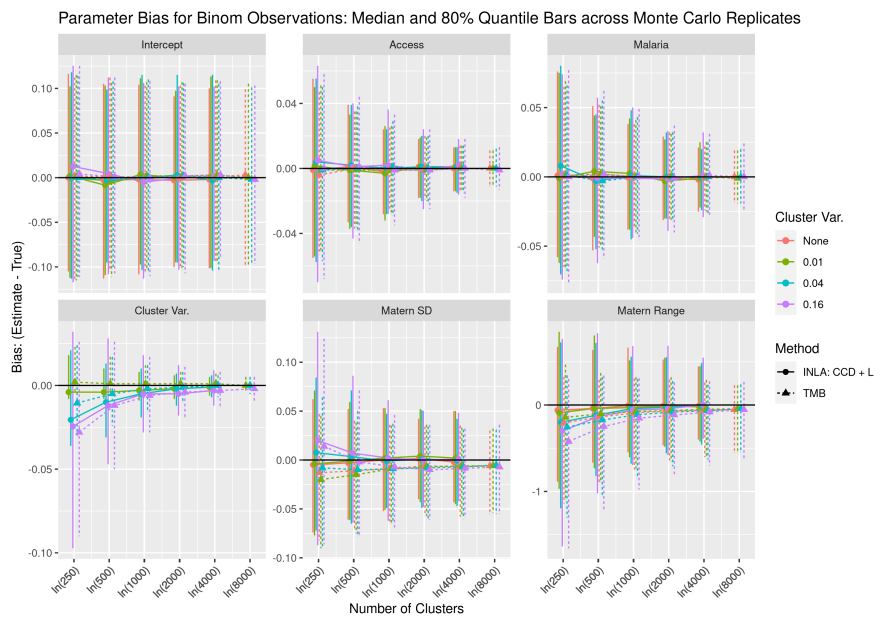


Figure B.18: Comparison of the estimated parameter bias from TMB (dashed) and R-INLA using CCD integration and full Laplace approximations (solid).

### *Appendix B.3.2. Differences due to SPDE triangulation resolution*

Plots in this section show decreasing undercoverage of the spatial field of the true spatial field by the estimated field as the resolution of the triangulation mesh size increases (as the mesh becomes more dense with more vertices). The figures contrast results from TMB against those from INLA using the CCD integration and full Laplace approximations as the mesh density increases. These are the results from the best INLA approximations we evaluated, even though this pattern persists across all other INLA options evaluated, to demonstrate that this pattern is a functions of the SPDE approximation and not the INLA options or TMB algorithm.

Average Pixel Coverage across Spatial Domain, Stratified by GP Decile, for Normal Observations with Var = 0.040:  
3631 SPDE Vertices, Median and 80% Quantile Bars across Monte Carlo Replicates

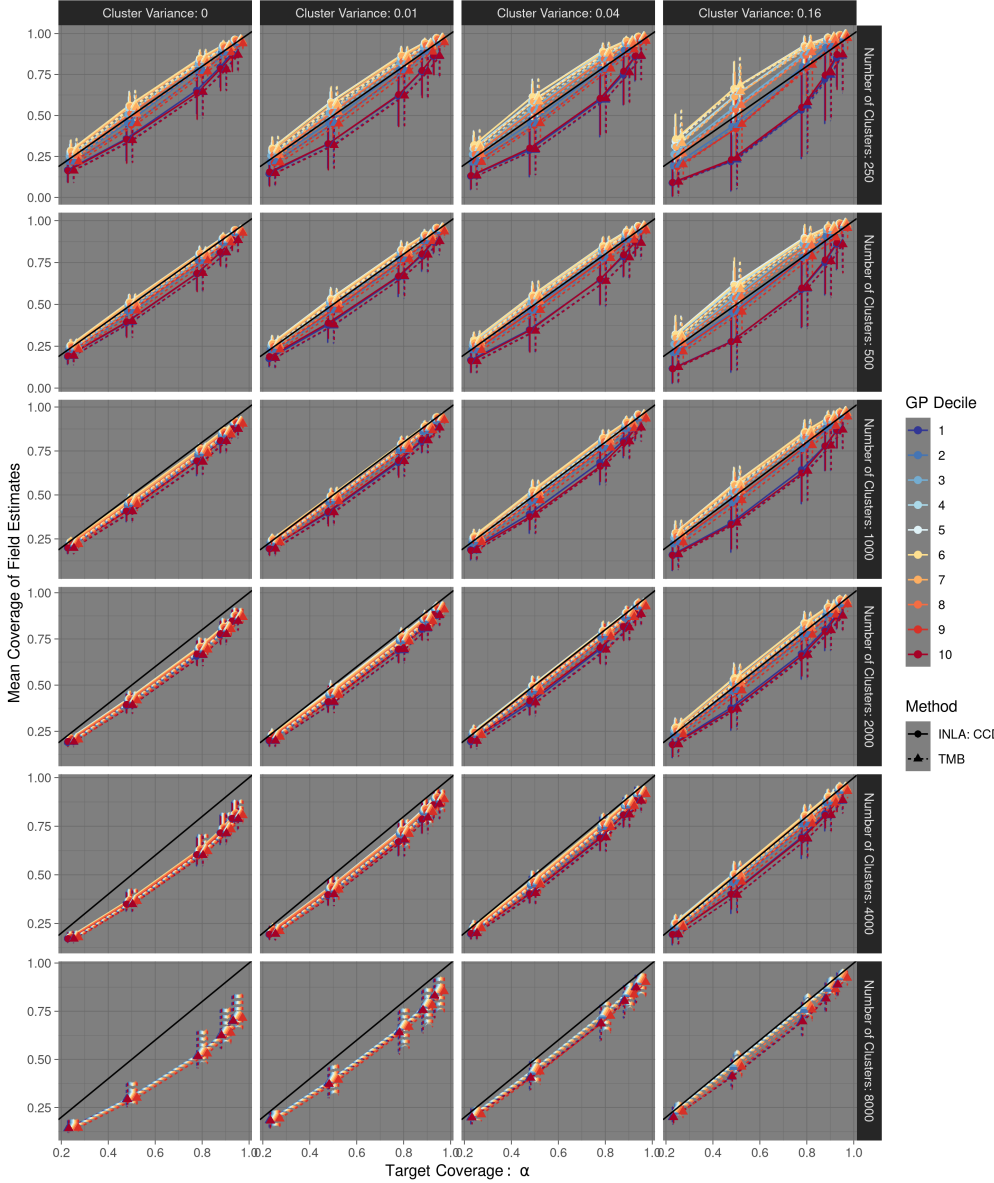


Figure B.19: Comparison of the average estimated field coverage of the simulated truth, faceted by cluster (i.i.d. nugget) variance and the number of clusters, from TMB (dashed lines) and R-INLA using CCD hyperparameter integration and full Laplace approximations (solid lines) plotted against the target nominal coverage,  $\alpha$ , for Gaussian observation experiments with  $\sigma^2 = 0.04$  and the coarse resolution SPDE triangulation. Colors stratify pixels included in the average coverage calculation by the decile of the true GP for the experiment replicate. Each point is the median average coverage of an experiment, calculated across 25 replicates, and the bars represent the middle 80% quantile range of the average coverage across replicates.

Average Pixel Coverage across Spatial Domain, Stratified by GP Decile, for Normal Observations with Var = 0.040:  
7922 SPDE Vertices, Median and 80% Quantile Bars across Monte Carlo Replicates

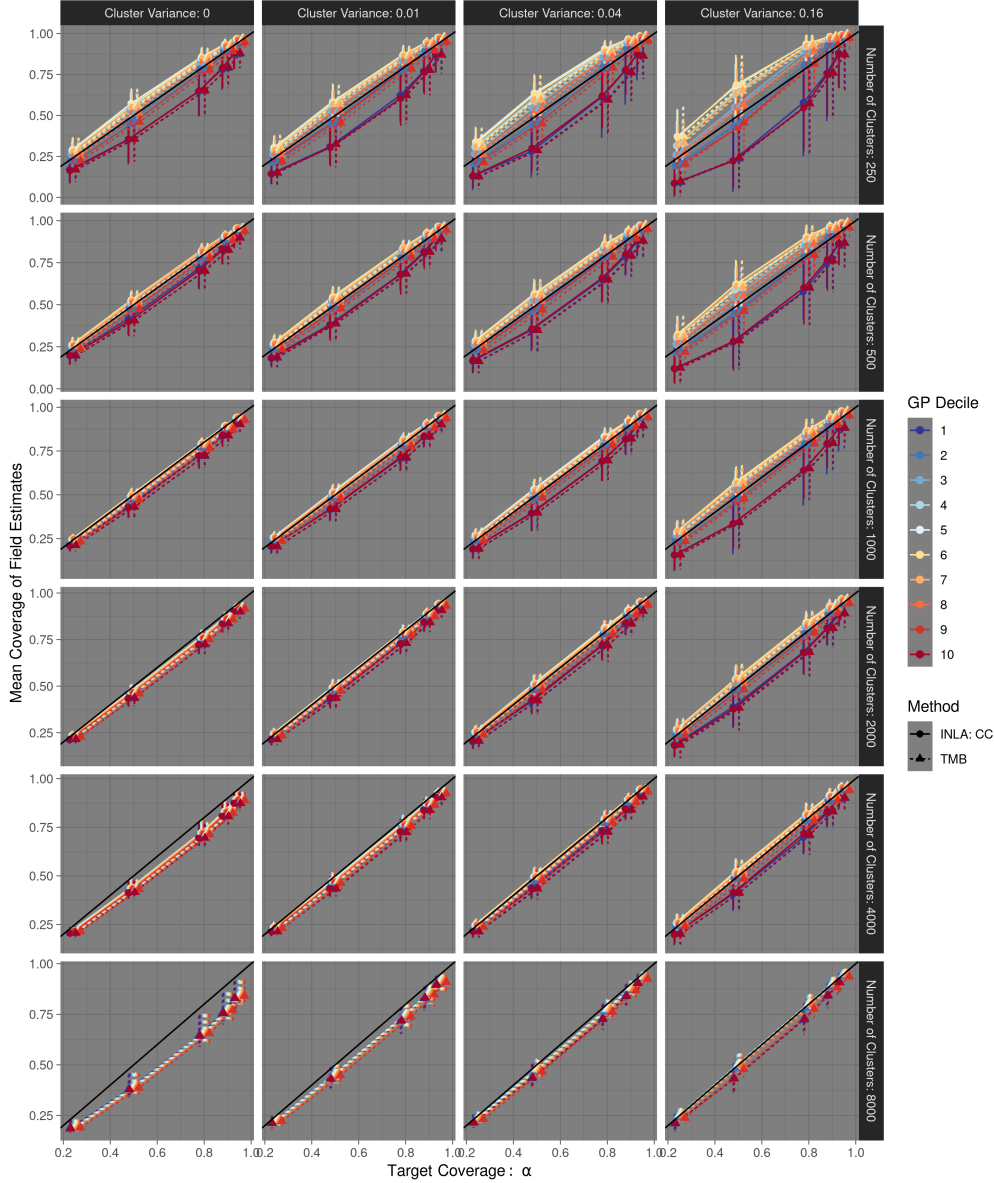


Figure B.20: Comparison of the average estimated field coverage of the simulated truth, faceted by cluster (i.i.d. nugget) variance and the number of clusters, from TMB (dashed lines) and R-INLA using CCD hyperparameter integration and full Laplace approximations (solid lines) plotted against the target nominal coverage,  $\alpha$ , for Gaussian observation experiments with  $\sigma^2 = 0.04$  and the medium resolution SPDE triangulation. Colors stratify pixels included in the average coverage calculation by the decile of the true GP for the experiment replicate. Each point is the median average coverage of an experiment, calculated across 25 replicates, and the bars represent the middle 80% quantile range of the average coverage across replicates. This figure is shown in the main results section, but is replicated here for easy comparison against the other supplemental plots.

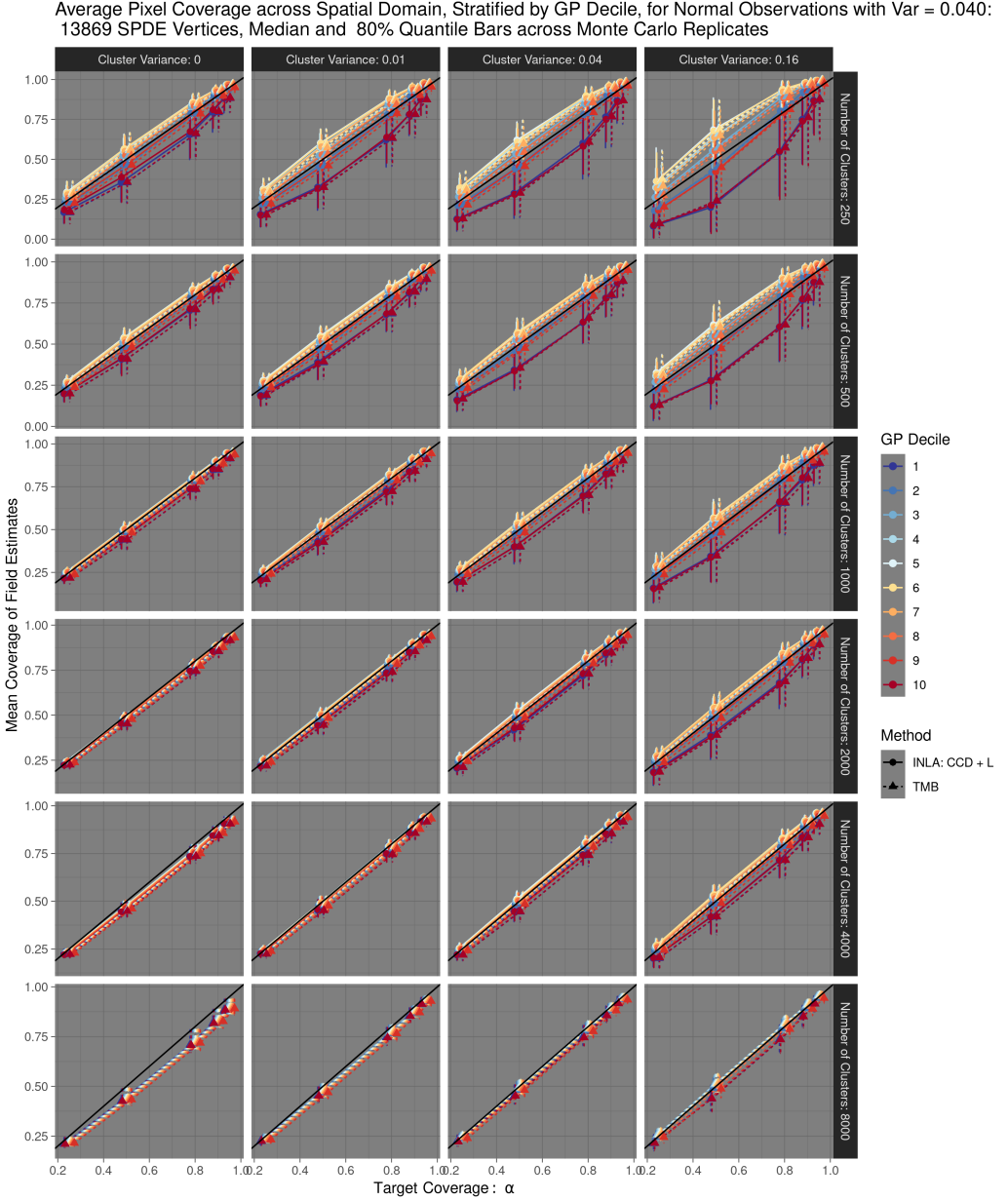


Figure B.21: Comparison of the average estimated field coverage of the simulated truth, faceted by cluster (i.i.d. nugget) variance and the number of clusters, from TMB (dashed lines) and R-INLA using CCD hyperparameter integration and full Laplace approximations (solid lines) plotted against the target nominal coverage,  $\alpha$ , for Gaussian observation experiments with  $\sigma^2 = 0.04$  and the fine resolution SPDE triangulation. Colors stratify pixels included in the average coverage calculation by the decile of the true GP for the experiment replicate. Each point is the median average coverage of an experiment, calculated across 25 replicates, and the bars represent the middle 80% quantile range of the average coverage across replicates.

### *Appendix B.3.3. Timing comparisons*

The main set of continuous simulation experiments, shown in Table 2, were run restricting both TMB and R-INLA to use a single CPU thread. This was done in order to better leverage the particulars of the computing cluster which was used. The median and 80% percent timing quantiles, taken across the 25 replicates of each experimental level, are shown in Figure B.22. The plot breaks down the timing by the number the method, the number of cluster observations and whether the observed data were Binomial or Gaussian, and the dimension of the spatial random effects. While it would be unusual for people under normal circumstances to restrict either method to use a single core, this plot nonetheless gives some indication of the total computational burden of each of the methods.

In addition, a small experiment to give a sense of the timing under more usual, parallelized, scenarios was run. The design of this experiment was very similar to those of the Binomial data continuous GP experiments but only the number of clusters (250, 2500, 10000), the number of spatial random effects (low, medium, and high resolution SPDE triangulations with 3616, 7933, and 13866 vertices, respectively), and the number of CPU threads (1, 2, 4) were varied. This created 27 experimental levels, each which was replicated 5 times. The mean of the fit, prediction, and total times are summarized in Figure B.23. R-INLA was run using the PARDISO library ([Alappat et al. \(2020\)](#), [Bollhöfer et al. \(2020\)](#), [?? \(par\)](#)), and it was forced to use the requested number of threads (it has built-in logic that, by default, is capable of using fewer than the max threads if it believes that will be more efficient). TMB was run using METIS to create fill reducing orderings of sparse matrices and parallelization was enabled by setting the available OpenMP threads.

Details on the software versions and hardware used in this study can be found in .

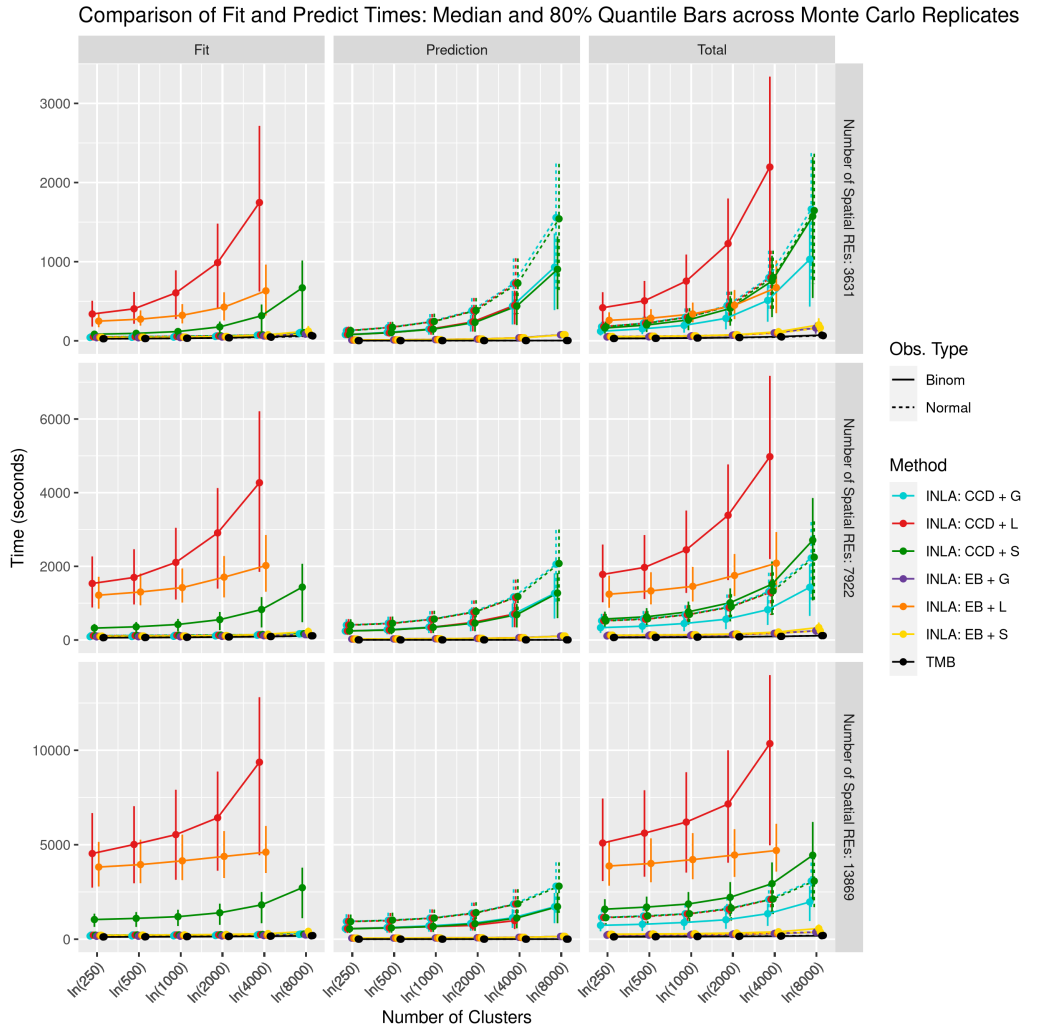


Figure B.22: Comparison of the average fit, predict, and total times from TMB and R-INLA, faceted by the number of spatial random effects, plotted against the number of clusters. Each point is the median time of an experiment, calculated across 25 replicates, and the bars represent the middle 80% quantile range of the bias across replicates.

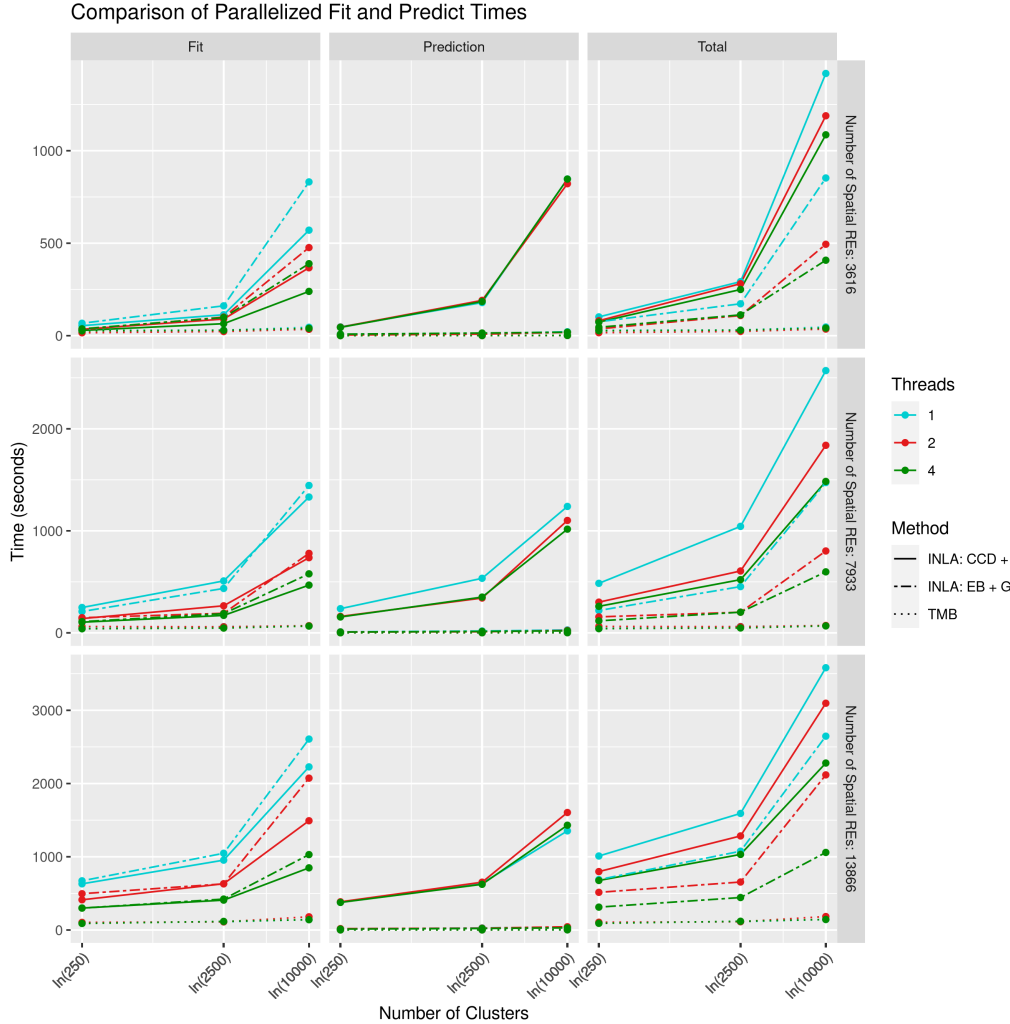


Figure B.23: Comparison of the average fit, predict, and total times from TMB and R-INLA, faceted by the number of spatial random effects, plotted against the number of clusters. Each point is the mean time across 5 replicates of a Binomial data experiment. The colors represent the number of threads available for parallelization within each method.

## Appendix C. Discrete Spatial Simulation Study

An overview of the discrete simulation details is provided in Section 6.2. Here we provide an in-depth version with all remaining details.

### Appendix C.1. Discrete Spatial Simulation Details

In addition to the continuous simulations, this study also assessed discrete spatial models simulations using TMB and R-INLA. In order to correctly implement the BYM2 discrete spatial model (a modern formulation of the classic Besag-York-Mollie model developed by [Riebler et al. \(2016\)](#)), a sum-to-zero constraint was implemented in TMB using appropriate conditional densities ([Gelfand et al., 2010](#), Section 12.1.7.4).

The discrete model was implemented over the 37 regions (first-level administrative units) of Nigeria, and neighbors were defined by immediate adjacency. Within each region, Poisson observations were simulated from a population of size  $n_s$ , arising from the following hierarchical model:

$$\begin{aligned}
 y_i | n_s, \eta_i &\sim \text{Poisson}(n_s \times \eta_i) \\
 \eta_i &= \exp(\alpha + \mathbf{b}_i) \\
 \mathbf{b} &= \frac{1}{\sqrt{\tau}} (\sqrt{1-\varphi} \mathbf{v} + \sqrt{\varphi} \mathbf{u}_*) \\
 \mathbf{v} &\sim N(\mathbf{0}, \mathbf{I}) \\
 \mathbf{u}_* &\sim N(\mathbf{0}, \mathbf{Q}_*^{-1}), \text{s.t. } \sum_{i=1}^{37} u_{*i} = 0,
 \end{aligned} \tag{C.1}$$

with  $\alpha$  the GMRF intercept, fixed at -3 across simulations, BYM2 field  $\mathbf{b}$  with total variance  $\tau^{-1}$ , mixing parameter  $\varphi$  controlling the contribution of  $\mathbf{v}$ , the unstructured i.i.d. portion of the BYM2 field, and  $\mathbf{u}_*$ , the scaled spatially structured component of the BYM2. The structured portion of the BYM2 is specified with precision  $\mathbf{Q}_*$ , a scaled version of the precision from the classic BYM ICAR model, and is constrained to sum to zero. The effect of the constraint was correctly included in TMB by conditioning on the constraint:

$$p(\mathbf{u}_* | \mathbf{A}\mathbf{u}_*) = \frac{p(\mathbf{A}\mathbf{u}_* | \mathbf{u}_*) p(\mathbf{u}_*)}{p(\mathbf{A}\mathbf{u}_*)} \tag{C.2}$$

where, generally,  $\mathbf{A}\mathbf{u}_* = \mathbf{e}$  encodes the linear constraints and specific to this example,  $\mathbf{A}\mathbf{u}_* = \sum \mathbf{u}_* = 0$ .

To complete the model specification, the following priors are included:

$$\begin{aligned}\alpha &\sim N(0, 5^2) \\ \varphi &\sim \text{Beta}(.5, .5) \\ 1/\sqrt{\tau} = \sigma &\sim N(0, 5^2) \mathbb{1}_{\sigma>0}.\end{aligned}$$

Internally, TMB was coded to use the same internal representations of parameters for the optimization step:  $\text{logit}(\varphi)$  and  $\log(\tau)$ .

The full combinatorial grid of simulation parameters shown in Table 3 comprised the set of 20 experiments and each experiment was replicated 25 times to obtain Monte Carlo errors on the validation metrics. For each replicate within each experiment, constrained BYM2 fields are generated, new observations are simulated, models are fit in both TMB and in R-INLA, and 500 joint estimator samples are drawn from each model to compare the estimates against the truth. The results shown in the following section use the empirical distribution taken across all replicates for each level of the experiment.

## Appendix D. European Breast Cancer Application Details

### Appendix D.1. Data

We work with breast cancer incidence and mortality data from IARC for this report. The current implementation of the methods described in this paper rely on an aggregated version of the IARC scores and are limited to countries within Europe. We will refer to countries as having one of four types of data:

- (I) national incidence and mortality
- (II) sub-national incidence and mortality (from registries) and national mortality,
- (III) only national mortality, and
- (IV) no available data.

Figure D.24 shows the data type available for the 40 countries from 1990-2010.

Although the data is available across age groups and time, this current project will focus on ages 50-54 (age group 11). While we will use data

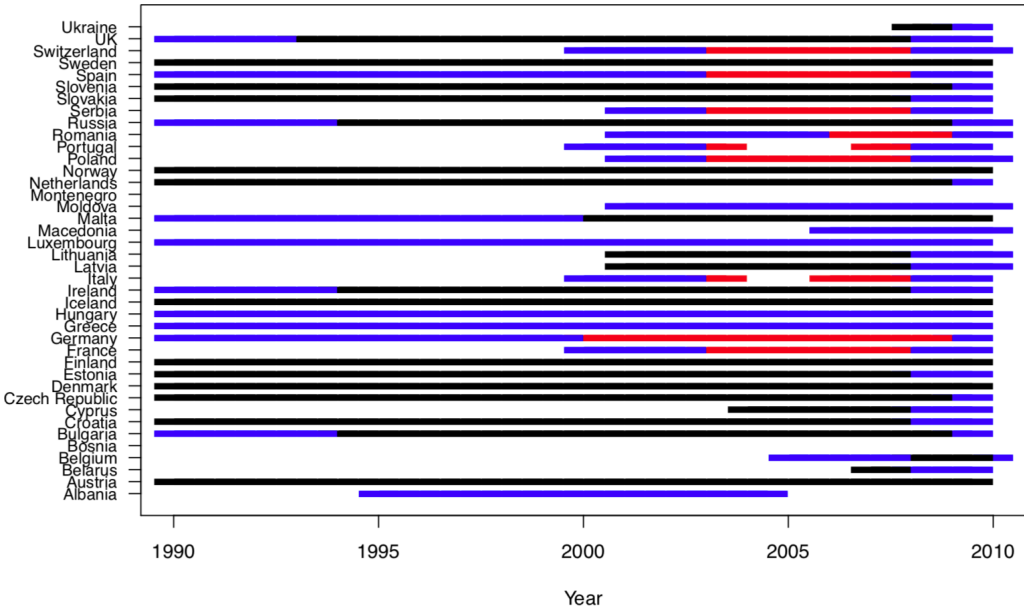


Figure D.24: Data type by country from 1990–2010. Type IV (Montenegro) is blank.

from all time periods, allowing the country type to vary in time, we assume that the underlying parameters are fixed in time and only estimate spatial variability.

#### *Appendix D.2. Model*

We assume a probabilistic models for incidence, mortality, and mortality given incidence. For most countries an alternative would be to rely only on unconditional models for just incidence and mortality. The MI modeling approach facilitates estimating national incidence in countries without out national or without local incidence data by providing an explicit link between mortality and incidence.

First, notation is defined. For a country,  $c$ , an age group,  $a$ , and a time period (year),  $t$ , we use  $L$  to denote local registry data and  $R$  to denote the remainder of the data. In countries with no local registry data ( $L$ ), all the data will fall into the remainder category ( $R$ ). With terms, we define:

- $N_{act}^L$  = Population for age group  $a$  in country  $c$  at time  $t$  covered by the available registry,

- $Y_{act}^L$  = Total incident reported cases from all registries for age group  $a$ , country  $c$ , and time  $t$ ,
- $Z_{act}^L$  = Total reported deaths (mortality) from all registries for age group  $a$  in country  $c$  at time  $t$ ,
- $N_{act}^R$  = Population for age group  $a$  in country  $c$  at time  $t$  not covered by the available registry,
- $Y_{act}^R$  = Total incident reported cases not covered by registries for age group  $a$  in country  $c$  at time  $t$ ,
- $Z_{act}^R$  = Total reported deaths (mortality) not covered by registries for age group  $a$  in country  $c$  at time  $t$ ,
- $N_{act} = N_{act}^L + N_{act}^R$  is the total population for age group  $a$  in country  $c$  at time  $t$ ,
- $Y_{act} = Y_{act}^L + Y_{act}^R$  is all reported cases for age group  $a$  in country  $c$  at time  $t$ ,
- $Z_{act} = Z_{act}^L + Z_{act}^R$  is all reported deaths for age group  $a$  in country  $c$  at time  $t$ ,
- $p_{act} = P(\text{ Reported incidence } | a, c, t)$ ,
- $r_{act} = P(\text{ Reported mortality } | a, c, t)$ ,
- $q_{act} = P(\text{ Reported mortality } | \text{ Reported incidence }, a, c, t)$ .

For countries that have both national mortality and incidence data (type I) we can assume a Poisson process for cancer incidence, and then conditional on having cancer, we model mortality as a binomial outcome. This also induces a Poisson process for mortality when incidence is unobserved. We suppress age and time notation. Our base model for type I countries is:

$$Y_c | N_c, p_c \sim \text{Poisson}(N_c p_c), \quad p_c = \exp(\alpha_c^I) \quad (\text{D.1})$$

$$Z_c | Y_c, r_c \sim \text{Binomial}(Y_c r_c), \quad r_c = \frac{\exp(\alpha_c^{MI})}{1 + \exp(\alpha_c^{MI})} \quad (\text{D.2})$$

which implies the unconditional mortality model:

$$Z_c | N_c, p_c \sim \text{Poisson}(N_c q_c), \quad q_c = p_c \cdot r_c. \quad (\text{D.3})$$

We assume a log- and logit-linear model for incidence and conditional mortality and we assume the following forms:

$$\alpha_c^I = \alpha^I + b_c^I \quad (\text{D.4})$$

$$\alpha_c^{MI} = \alpha^{MI} + b_c^{MI} \quad (\text{D.5})$$

where  $\alpha^*$  are global intercepts, and  $b_c^*$  are country random effects that are assumed to have BYM-2 structure comprising of a spatially correlated term as well as an unstructured (iid) country specific term. Specifically, each vector of the country random effects are assumed to independent from one another take the form of the BYM2 effects defined in (C.1) and (C.2).

The  $\alpha^I$ ,  $\alpha^{MI}$ ,  $\mathbf{b}^I$ , and  $\mathbf{b}^{MI}$  parameters are used for across all the country types, but the way that these parameters learn and leverage the information depend on the country data type and thus the way the data enter into the joint likelihood.

For type II countries, those with local incidence and mortality data and national mortality data, we assume the same model used for type I countries for the local registry data and the implied mortality Poisson process for the remaining national mortality data.

That is, for the local data we assume:

$$Y_c^L | N_c^L, p_c \sim \text{Poisson}(N_c^L p_c), \quad p_c = \exp(\alpha_c^I) \quad (\text{D.6})$$

$$Z_c^L | Y_c^L, r_c \sim \text{Binomial}(Y_c r_c), \quad r_c = \frac{\exp(\alpha_c^{MI})}{1 + \exp(\alpha_c^{MI})} \quad (\text{D.7})$$

where the intercept parameters are of the form shown in D.4 and D.5.

Furthermore, for the remaining non-registry mortality data, we assume that the MI ratio is the same in the local registry and national remainder data and we model it as the implied (unconditional) Poisson process:

$$Z_c^R | N_c^R, q_c \sim \text{Poisson}(N_c^R q_c), \quad q_c = \exp(\alpha_c^I) \cdot \frac{\exp(\alpha_c^{MI})}{1 + \exp(\alpha_c^{MI})}. \quad (\text{D.8})$$

For type III countries, those with only national level mortality, we use the induced unconditional Poisson model as written in (D.3).

Finally, for type IV countries, those with no data, we rely on the global intercept and the country random effect (both the iid and the spatially correlated and smoothed random components from the BYM-2) from the posterior distribution to estimate their incidence and mortality rates.

To complete the Bayesian specification, we assign the following prior distributions:

- $aI, aMI \sim (iid) N(0, \sigma^2 = 100)$
- $\varphi_* \sim (iid) \text{Beta}(.5, .5)$
- $1/\sqrt{\tau_*} = \sigma_* \sim (iid) N(0, 5^2) \mathbb{1}_{\sigma > 0}$ .

The model is fit in R using *Template Model Builder* and the nonlinear optimizer, *nlinminb*.

#### *Appendix D.3. Simulation*

To assess the feasibility of this model, we first consider a small simulation restricting ourselves to a single year and age group. We set  $\alpha^I = -6.5$ ,  $\alpha^{MI} = -1.0$  and the standard deviation of the spatial random effects to be 0.5 (with no iid country effect - effectively setting the mixing term for the BYM-2 to be 1.0). We use the form of the data (country types and populations) from 2008 and age-group 50-54. This resulted in 14, 2, 21, and 3 type I, II, III, and IV countries respectively. Conditional on these true parameters, country data types, and the observed populations, data was simulated from the model outlined in Section [Appendix D.2](#). Results for the fits are summarized in the appendix in Figure [D.26](#) and indicate that overall the model is performing well, even in the challenging situation with over half of the countries set to type III or IV. Notably, the precision for the MI country random effects has been estimated to be too high and this has resulted in some over-shrinkage of the MI estimates.

#### *Appendix D.4. Results*

The model can be run quite quickly in R and once it has finished fitting, 1000 multivariate normal draws are taken from the joint posterior of all parameters. These draws are then summarized and some relevant quantities are shown in Figures [6](#) and [D.25](#).

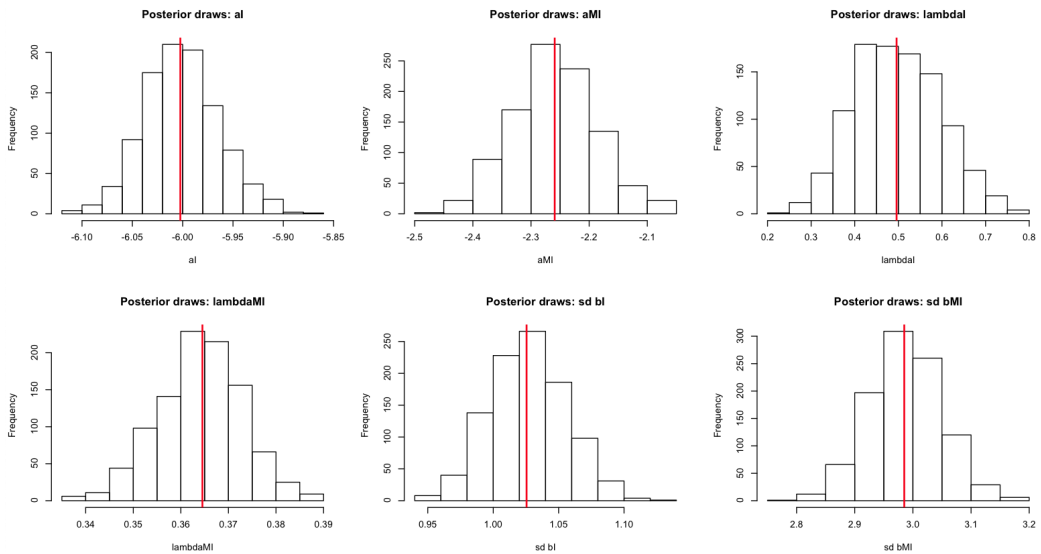


Figure D.25: Top row: histograms of the incidence rate intercept  $aI$ , mortality-incidence ratio intercept  $aMI$ , and the BYM2 incidence mixture parameter  $\lambda_I$ . Top row: histograms of the BYM2 mortality-incidence mixture parameter  $\lambda_{MI}$ , and the standard deviations ( $\tau_*^{-1/2}$ ) of the two BYM2 processes.

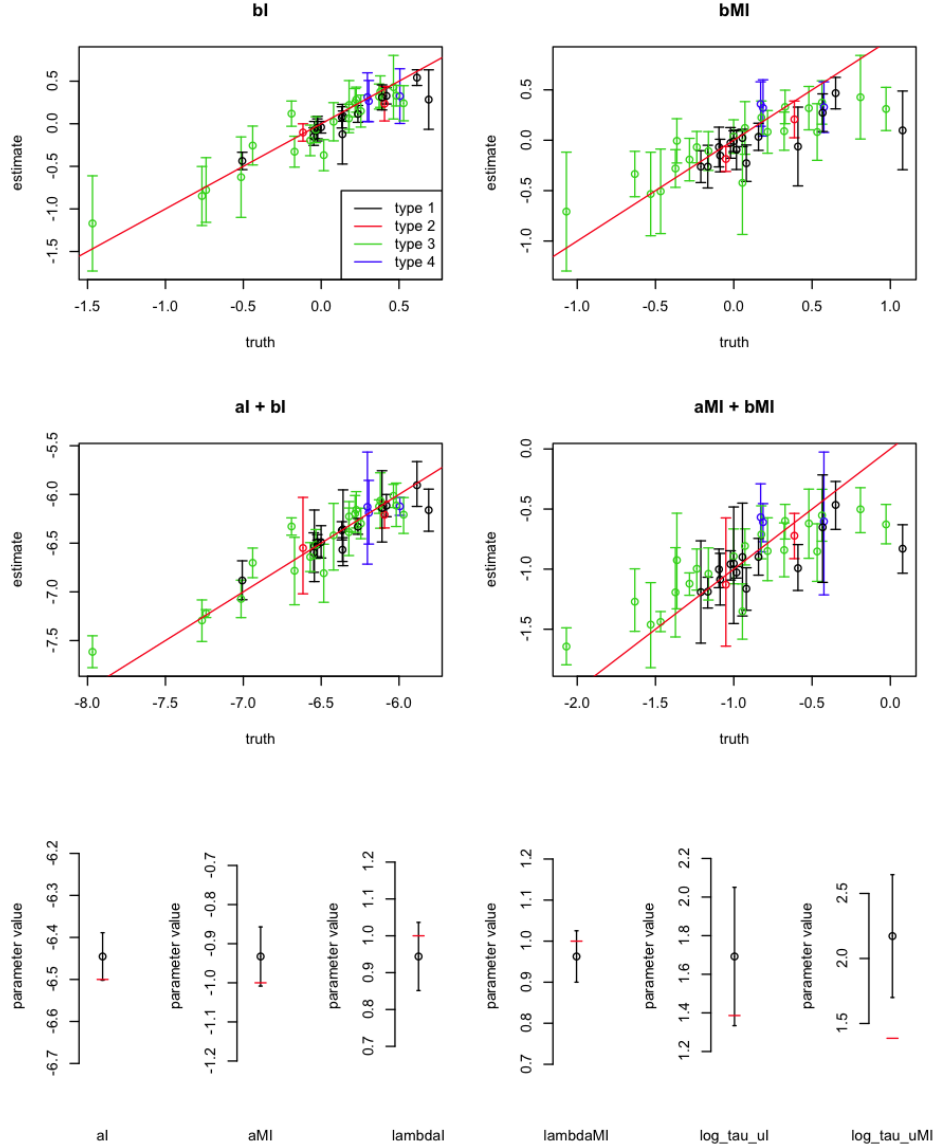


Figure D.26: Fitted results from one run of the simulation study. The top row shows the simulated country random effects from the BYM2 specification plotted against the associated fitted median and 95% credible intervals. The second row shows the simulated overall country effect (intercept plus country random effects) plotted against the associated fitted median and 95% credible intervals. In the third row we have the true values for each of the fixed and hyperparameters (shown with the red line) plotted against the associated fitted median and 95% credible intervals.

## Appendix E. Example spatial model code

The complete code used in this study is available online at: <https://faculty.washington.edu/jonno/software.html>. The following two sections provide succinct yet complete examples of continuous and discrete spatial model inference in both TMB and R-INLA. We start by simulating data on the unit square, and then use R-INLA functions to make the SPDE objects for fitting, some of which are re-used by TMB.

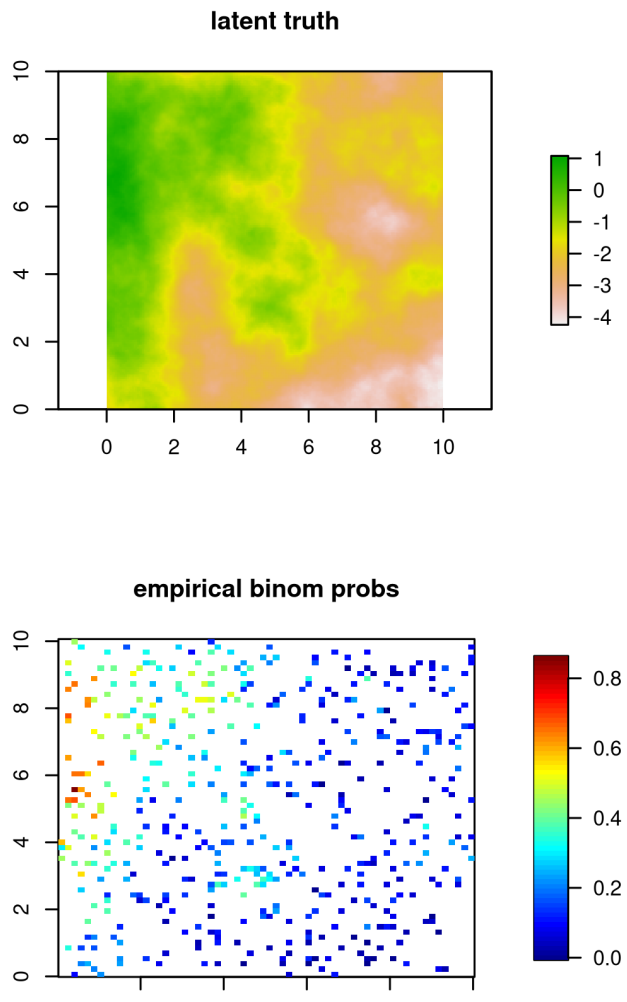
### Appendix E.1. Simulating data and generating SPDE objects

```
1 ## install missing packages
2 pkgs <- c('data.table', 'ggplot2', 'RColorBrewer', 'RandomFields',
3         'raster', 'TMB', 'viridis')
4 new.packages <- pkgs[!(pkgs %in% installed.packages()[, "Package"])]
5 if(length(new.packages)) install.packages(new.packages)
6 if(!(INLA %in% installed.packages()[, 'Package'])){
7   ## INLA is not on CRAN
8   install.packages("INLA",
9     repos=cgetOption("repos"),
10    INLA="https://inla.r-inla-download.org/R/stable"),
11    dep=TRUE)
12 }
13 # load packages
14 invisible(lapply(c(pkgs, 'INLA'), library, character.only = TRUE))
15
16 ## setup continuous domain
17 set.seed(413206)
18 x <- seq(0, 10, length = 200)
19 grid.pts <- expand.grid(x, x)
20
21 ## set up matern params, also set param priors to be used in modeling
22 sp.alpha <- 2
23 sp.kappa <- 0.5
24 sp.var <- 0.5
25 gp.int <- -2
26 # prior on spde parameters: c(a, b, c, d), where
27 # P(sp.range < a) = b
28 # P(sp.sigma > c) = d
29 matern.pri <- c(10, .95, 1., .05) ## a, b, c, d
30 # mean and sd for normal prior on fixed effects (alpha and betas)
31 alpha.pri <- c(0, 3) ## N(mean, sd)
32
33 ## sample from matern RF on our grid
34 model <- RMmatern(nu      = sp.alpha - 1, ## from INLA book
35                     scale = sqrt(2 * (sp.alpha - 1)) / sp.kappa,
36                     var   = 1)
37 true.gp <- RFsimulate(model, x = x, y = x, n = 1, spConform = FALSE)
38
39 ## insert into a raster
40 gp.rast <- raster(nrows=length(x), ncols=length(x),
41                    xmn=0, xmx=10, ymn=0, ymx=10,
```

```

43             vals=(true.gp + gp.int))
44
45 ## define cluster locations and sample size at each
46 n.clust <- 500
47 clust.mean.ss <- 35
48 dat <- data.table(x = runif(n.clust, min = min(x), max = max(x)),
49                     y = runif(n.clust, min = min(x), max = max(x)),
50                     n = rpois(n.clust, clust.mean.ss)
51 )
52
53 ## extract value of raster at cluster locs and logit transform
54 ## to binom probs
55 dat[, latent.truth := raster::extract(x = gp.rast, y = cbind(x, y))]
56 dat[, p.truth := plogis(latent.truth)]
57
58 ## sample binomial data
59 dat[, obs := rbinom(n = .N, size = n, p = p.truth)]
60
61 ## make SPDE triangulation mesh over our domain
62 mesh.s <- inla.mesh.2d(loc.domain = grid.pts,
63                         max.e = c(0.25, 5))
64 ## check number of vertices
65 mesh.s[['n']]
66
67 ## plot true latent field, the observed/empirical binom probs at
68 ## cluster locs, and the mesh
69 par(mfrow = c(3, 1))
70 plot(gp.rast, maxpixels = length(x) ^ 2,
71       xlim = range(x), ylim = range(x), main = 'latent truth')
72 fields::quilt.plot(dat[, x], dat[, y], dat[, obs] / dat[, n],
73                      main = 'empirical binom probs')
74 plot(mesh.s)
75 polygon(x = c(0, 0, 10, 10, 0), y = c(0, 10, 10, 0, 0),
76 col = NA, border = 2, lwd = 5)
77
78 ## make the SPDE objects (including prec components)
79 spde <- inla.spde2.pcmatern(mesh = mesh.s, alpha = 2,
80                               prior.range = matern.pri[1:2],
81                               prior.sigma = matern.pri[3:4])
82
83 ## make projector matrices to:
84 ## 1) project data to mesh
85 ## 2) project mesh to raster grid
86 A.proj <- inla.spde.make.A(mesh = mesh.s,
87                             loc = dat[, as.matrix(x, y)])
88 A.pred <- inla.spde.make.A(mesh = mesh.s,
89                            loc = as.matrix(grid.pts),
90                            group = 1)

```



**Constrained refined Delaunay triangulation**

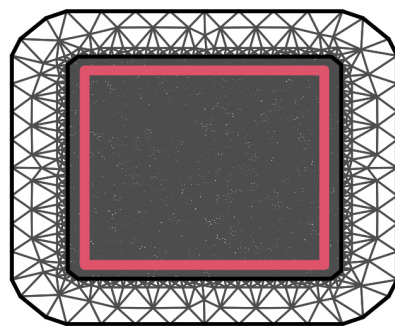


Figure E.27: Simulated GP on  $10 \times 10$  grid, simulated data locations and empirical probabilities, and SPDE mesh from the preparation portion of the code example.

## Appendix E.2. Continuous GP modeling with SPDE in R-INLA

```

1 ## prep inputs for INLA
2 design_matrix <- data.frame(int = rep(1, nrow(dat)))
3 stack.obs <- inla.stack(tag='est',
4                           data=list(Y = dat$obs, ## response
5                                     N = dat$n), ## binom trials
6                           A=list(A.proj, ## A.proj for space
7                                 1), ## 1 for design.mat
8                           effects=list(
9                             space = 1:mesh.s[['n']],
10                            design_matrix))
11
12 ## define the INLA model
13 formula <- formula(Y ~ -1 + int + f(space, model = spde))
14
15 ## run INLA
16 i.fit <- inla(formula,
17                 data = inla.stack.data(stack.obs),
18                 control.predictor = list(A = inla.stack.A(stack.obs),
19                                           compute = FALSE),
20                 control.fixed = list(expand.factor.strategy = 'inla',
21                                       prec = list(default = 1 / alpha.pri[2] ^ 2)),
22                 control.inla = list(strategy = 'simplified.laplace',
23                                       int.strategy = 'ccd'),
24                 control.compute=list(config = TRUE),
25                 family = 'binomial',
26                 Ntrials = N,
27                 verbose = FALSE,
28                 keep = FALSE)
29
30 ## take draws from inla
31 i.draws <- inla.posterior.sample(n = 500, i.fit,
32                                   use.improved.mean = TRUE,
33                                   skew.corr = TRUE)
34
35 ## summarize the draws
36 par_names <- rownames(i.draws[[1]][['latent']])
37 s_idx <- grep('^space.*', par_names)
38 a_idx <- which(!c(1:length(par_names)) %in%
39                grep('`^space.*|Predictor|clust.id', par_names))
40
41 # project from mesh to raster, add intercept
42 pred_s <- sapply(i.draws, function (x) x[['latent']][s_idx])
43 pred_inla <- as.matrix(A.pred %*% pred_s)
44 alpha_inla_draws <- sapply(i.draws, function (x) x[['latent']][a_idx])
45 pred_inla <- sweep(pred_inla, 2, alpha_inla_draws, '+')
46
47
48 ## find the median and sd across draws, as well as 90% intervals
49 summ_inla <- cbind(median = (apply(pred_inla, 1, median)),
50                      sd = (apply(pred_inla, 1, sd)),
51                      lower = (apply(pred_inla, 1, quantile, .05)),
52                      upper = (apply(pred_inla, 1, quantile, .95)))
53
54 ## make summary rasters
55 ras_med_inla <- ras_sdv_inla <- ras_lower_inla <-

```

```

56 ras_upper_inla <- ras_inInt_inla <- gp.rast
57 values(ras_med_inla) <- summ_inla[, 1]
58 values(ras_sdv_inla) <- summ_inla[, 2]
59 values(ras_lower_inla) <- summ_inla[, 3]
60 values(ras_upper_inla) <- summ_inla[, 4]
61 values(ras_inInt_inla) <- 0
62 ras_inInt_inla[gp.rast < ras_lower_inla | ras_upper_inla < gp.rast] <- 1
63
64 ## plot truth, pixels falling within/without the 90% interval,
65 ## post. median, and post sd
66
67 # set the range for the truth and median
68 rast.zrange <- range(c(values(gp.rast), values(ras_med_inla)), na.rm = T)
69
70 # plot
71 par(mfrow = c(2, 2))
72 plot(gp.rast, main = 'Truth', zlim = rast.zrange, col = (viridis(100)))
73 points(dat[, .(x, y)])
74 plot(ras_inInt_inla, main = 'Pixels where 90% CIs did not cover Truth')
75 points(dat[, .(x, y)])
76 plot(ras_med_inla, main = 'INLA Posterior Median',
77       zlim = rast.zrange, col = (viridis(100)))
78 points(dat[, .(x, y)])
79 plot(ras_sdv_inla, main = 'INLA Posterior Standard Deviation')
80 points(dat[, .(x, y)])

```

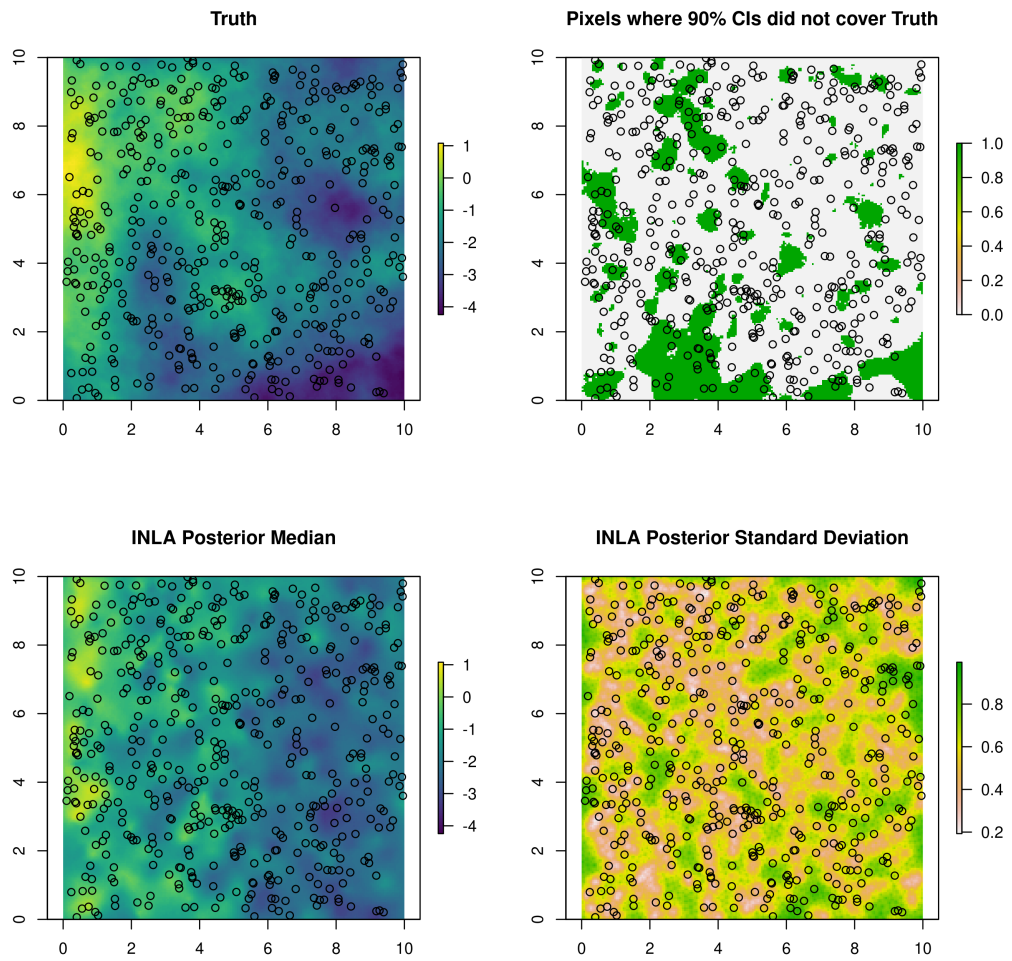


Figure E.28: Simulated GP on  $10 \times 10$  grid, posterior median and standard deviations summarized from 500 draws from the approximate INLA posterior distribution, and a binary plot indicating which pixels fell outside the 90% credible interval. Points indicate cluster locations.

### Appendix E.3. Continuous GP modeling with SPDE in TMB

```

1 ## define the TMB model using c++ template code
2 ## this is usually done in a separate file,
3 ## but it can be done all from within 1 R script
4
5 tmb_spde <-
6   /// include libraries
7 #include <TMB.hpp>
8 #include <Eigen/Sparse>
9 #include <vector>
10 using namespace density;
11 using Eigen::SparseMatrix;
12
13 // helper function for detecting NAs in the data supplied from R
14 template<class Type>
15 bool isNA(Type x){
16   return R_IsNA(asDouble(x));
17 }
18
19 // helper function to make sparse SPDE precision matrix
20 // Inputs:
21 //   logkappa: log(kappa) parameter value
22 //   logtau: log(tau) parameter value
23 //   M0, M1, M2: these sparse matrices are output from:
24 //     R::INLA::inla.spde2.matern()$param.inla$M*
25 template<class Type>
26 SparseMatrix<Type> spde_Q(Type logkappa, Type logtau, SparseMatrix<Type> M0,
27                           SparseMatrix<Type> M1, SparseMatrix<Type> M2) {
28   SparseMatrix<Type> Q;
29   Type kappa2 = exp(2. * logkappa);
30   Type kappa4 = kappa2*kappa2;
31   Q = pow(exp(logtau), 2.) * (kappa4*M0 + Type(2.0)*kappa2*M1 + M2);
32   return Q;
33 }
34
35 // helper function to use the same penalized complexity prior on
36 // matern params that is used in INLA
37
38 template<class Type>
39 Type dPCPriSPDE(Type logtau, Type logkappa,
40                   Type matern_par_a, Type matern_par_b,
41                   Type matern_par_c, Type matern_par_d,
42                   //vector<Type> matern_pri(4),
43                   int give_log=0)
44 {
45
46   // matern_pri = c(a, b, c, d): P(range < a) = b; P(sigma > c) = d
47
48   Type penalty; // prior contribution to jnll
49
50   Type d = 2.; // dimension
51   Type lambda1 = -log(matern_par_b) * pow(matern_par_a, d/2.);
52   Type lambda2 = -log(matern_par_d) / matern_par_c;
53   Type range = sqrt(8.0) / exp(logkappa);
54   Type sigma = 1.0 / sqrt(4.0 * 3.14159265359 * exp(2.0 * logtau) *
55                           exp(2.0 * logkappa));

```

```

56
57     penalty = (-d/2. - 1.) * log(range) - lambda1 * pow(range, -d/2.) -
58             lambda2 * sigma;
59 // Note: (rho, sigma) --> (x=log kappa, y=log tau) -->
60 // transforms: rho = sqrt(8)/e^x & sigma = 1/(sqrt(4pi)*e^x*e^y)
61 // --> Jacobian: |J| propto e^(-y -2x)
62 Type jacobian = - logtau - 2.0*logkappa;
63 penalty += jacobian;
64
65 if(give_log) return penalty; else return exp(penalty);
66 }
67
68 /////////////////
69 // the main function //
70 // to calculate the jnll //
71 ///////////////////
72 template<class Type>
73 Type objective_function<Type>::operator() ()
74 {
75
76 // ~~~~~-----~~~~~
77 // FIRST, we define params/values/data that will be passed in from R
78 // ~~~~~-----~~~~~
79
80 // normalization flag - used for speed-up
81 DATA_INTEGER( flag ); // flag == 0 => no data contribution added to jnll
82
83 // Indices
84 DATA_INTEGER( num_i ); // Number of data points in space
85 DATA_INTEGER( num_s ); // Number of mesh points in space mesh
86
87 // Data (all except for X_ij is a vector of length num_i)
88 DATA_VECTOR( y_i ); // obs per binomial experiment at point i (clust)
89 DATA_VECTOR( n_i ); // Trials per cluster
90 DATA_MATRIX( X_alpha ); // 'design matrix' for just int
91
92 // SPDE objects
93 DATA_SPARSE_MATRIX( M0 );
94 DATA_SPARSE_MATRIX( M1 );
95 DATA_SPARSE_MATRIX( M2 );
96 DATA_SPARSE_MATRIX( Aproj );
97
98 // Options
99 DATA_VECTOR( options );
100 // options[0] == 1 : use normalization trick
101 // options[1] == 1 : adreport transformed params
102
103 // Prior specifications
104 DATA_VECTOR( alpha_pri );
105 DATA_VECTOR( matern_pri );
106 // matern_pri = c(a, b, c, d): P(range < a) = b; P(sigma > c) = d
107 Type matern_par_a = matern_pri[0]; // range limit: rho0
108 Type matern_par_b = matern_pri[1]; // range prob: alpha_rho
109 Type matern_par_c = matern_pri[2]; // field sd limit: sigma0
110 Type matern_par_d = matern_pri[3]; // field sd prob: alpha_sigma
111
112 // Fixed effects

```

```

113  PARAMETER( alpha ); // Intercept
114  // Log of INLA tau param (precision of space covariance matrix)
115  PARAMETER( log_tau );
116  // Log of INLA kappa (related to spatial correlation and range)
117  PARAMETER( log_kappa );
118
119  // Random effects for each spatial mesh vertex
120  PARAMETER_VECTOR( Epsilon_s );
121
122  // -----
123  // SECOND, we define all other objects that we need internally
124  // -----
125
126  // objective function -- joint negative log-likelihood
127  Type jnll = 0;
128
129  // Make spatial precision matrix
130  SparseMatrix<Type> Q_ss = spde_Q(log_kappa, log_tau, M0, M1, M2);
131
132  // Transform some of our parameters
133  Type sp_range = sqrt(8.0) / exp(log_kappa);
134  Type sp_sigma = 1.0 / sqrt(4.0 * 3.14159265359 *
135      exp(2.0 * log_tau) * exp(2.0 * log_kappa));
136
137  // Define objects for derived values
138  vector<Type> fe_i(num_i); // main effect: alpha
139  // Logit estimated prob for each cluster i
140  vector<Type> latent_field_i(num_i);
141  // value of gmrf at data points
142  vector<Type> projepsilon_i(num_i);
143
144  // fixed effects is just alpha in this example
145  fe_i = X_alpha * Type(alpha); // initialize
146
147  // Project GP approx from mesh points to data points
148  projepsilon_i = Aproj * Epsilon_s.matrix();
149
150  // -----
151  // THIRD, we calculate the contribution to the likelihood from:
152  // 1) priors
153  // 2) GP field
154  // 3) data
155  // -----
156
157  //////////
158  // (1) //
159  //////////
160  // the random effects. we do this first so to do the
161  // normalization outside of every optimization step
162  // NOTE: likelihoods from namespace 'density' already return NEGATIVE
163  // log-lik's so we add other likelihoods return positive log-lik's
164  if(options[0] == 1){
165      // then we are not calculating the normalizing constant in the inner opt
166      // that norm constant means taking an expensive determinant of Q_ss
167      jnll += GMRF(Q_ss, false)(Epsilon_s);
168      // return without data ll contrib to avoid unnecessary log(det(Q)) calcs
169      if (flag == 0) return jnll;

```

```

170     }else{
171         jnll += GMRF(Q_ss)(Epsilon_s);
172     }
173
174     //////////////
175     // (2) //
176     //////////////
177     // Prior contributions to joint likelihood (if options[1]==1)
178
179     // add in priors for spde gp
180     jnll -= dPCPriSPDE(log_tau, log_kappa,
181                         matern_par_a, matern_par_b, matern_par_c, matern_par_d,
182                         true);
183
184     // prior for intercept
185     jnll -= dnorm(alpha, alpha_pri[0], alpha_pri[1], true); // N(mean, sd)
186
187     //////////////
188     // (3) //
189     //////////////
190     // jnll contribution from each datapoint i
191
192     for (int i = 0; i < num_i; i++){
193
194         // latent field estimate at each obs
195         latent_field_i(i) = fe_i(i) + projepsilon_i(i);
196
197         // and add data contribution to jnll
198         if(!isNA(y_i(i))){
199
200             // Uses the dbinom_robust function, which takes the logit probability
201             jnll -= dbinom_robust( y_i(i), n_i(i), latent_field_i(i), true );
202
203         } // !isNA
204     } // for( i )
205
206
207
208     // ~~~~~
209     // ADREPORT: used to return estimates and cov for transforms?
210     // ~~~~~
211     if(options[1]==1){
212         ADREPORT(sp_range);
213         ADREPORT(sp_sigma);
214     }
215
216     return jnll;
217
218 }
219
220 ## write model to file, compile, and load it into R
221 dir.create('TMB_spde_example')
222 write(tmb_spde,file="TMB_spde_example/tmb_spde.cpp")
223 compile( "TMB_spde_example/tmb_spde.cpp")
224 dyn.load( dynlib("TMB_spde_example/tmb_spde") )
225
226 ## prep inputs for TMB

```

```

227 data_full <- list(num_i = nrow(dat), # Total number of observations
228     num_s = mesh.s[['n']], # num. of vertices in SPDE mesh
229     y_i = dat[, obs],# num. of pos. obs in the cluster
230     n_i = dat[, n], # num. of exposures in the cluster
231     X_alpha = matrix(1, nrow = nrow(dat), ncol = 1),# des.mat
232     M0 = spde[['param.inla']][['M0']], # SPDE sparse matrix
233     M1 = spde[['param.inla']][['M1']], # SPDE sparse matrix
234     M2 = spde[['param.inla']][['M2']], # SPDE sparse matrix
235     Aproj = A.proj, # Projection matrix
236     options = c(1, ## if 1, use normalization trick
237                 1), ## if 1, run adreport
238     # normalization flag.
239     flag = 1,
240     alpha_pri = alpha.pri, ## normal
241     matern_pri = matern.pri
242 )
243
244 ## Specify starting values for TMB params
245 tmb_params <- list(alpha = 0.0, # intercept
246                         log_tau = 0, # Log inverse of tau (Epsilon)
247                         log_kappa = 0, # Matern range parameter
248                         Epsilon_s = rep(0, mesh.s[['n']]) # RE on mesh vertices
249 )
250
251 ## make a list of things that are random effects
252 rand_effs <- c('Epsilon_s')
253
254 ## make the autodiff generated likelihood func & gradient
255 obj <- MakeADFun(data=data_full,
256                     parameters=tmb_params,
257                     random=rand_effs,
258                     hessian=TRUE,
259                     DLL='tmb_spde')
260
261 ## we can normalize the GMRF outside of the nested optimization,
262 ## avoiding unnecessary and expensive cholesky operations.
263 obj <- normalize(obj, flag="flag", value = 0)
264
265 ## run TMB
266 opt0 <- nlminb(start      = obj[['par']],
267                  objective   = obj[['fn']],
268                  gradient    = obj[['gr']],
269                  lower       = rep(-10, length(obj[['par']])),
270                  upper       = rep( 10, length(obj[['par']])),
271                  control     = list(trace=1))
272
273 ## Get standard errors
274 SDO <- TMB::sdreport(obj, getJointPrecision=TRUE,
275                         bias.correct = TRUE,
276                         bias.correct.control = list(sd = TRUE))
277 ## summary(SDO, 'report')
278
279 ## take samples from fitted model
280 mu <- c(SDO$par.fixed, SDO$par.random)
281
282 ## simulate draws
283 rmvnorm_prec <- function(mu, chol_prec, n.sims) {

```

```

284 z <- matrix(rnorm(length(mu) * n.sims), ncol=n.sims)
285 L <- chol_prec #Cholesky(prec, super=TRUE)
286 z <- Matrix::solve(L, z, system = "Lt") ## z = Lt^-1 %*% z
287 z <- Matrix::solve(L, z, system = "Pt") ## z = Pt      %*% z
288 z <- as.matrix(z)
289 mu + z
290 }
291
292 L <- Cholesky(SDO[["jointPrecision"]], super = T)
293 t.draws <- rmvnorm_prec(mu = mu , chol_prec = L, n.sims = 500)
294
295 ## summarize the draws
296 parnames <- c(names(SDO[["par.fixed"]]), names(SDO[["par.random"]]))
297 epsilon_tmb_draws <- t.draws[parnames == 'Epsilon_s',]
298 alpha_tmb_draws <- matrix(t.draws[parnames == 'alpha'], nrow = 1)
299
300 # project from mesh to raster, add intercept
301 pred_tmb <- as.matrix(A.pred %*% epsilon_tmb_draws)
302 pred_tmb <- sweep(pred_tmb, 2, alpha_tmb_draws, '+')
303
304 ## find the median and sd across draws, as well as 90% intervals
305 summ_tmb <- cbind(median = (apply(pred_tmb, 1, median)),
306                      sd      = (apply(pred_tmb, 1, sd)),
307                      lower   = (apply(pred_tmb, 1, quantile, .05)),
308                      upper   = (apply(pred_tmb, 1, quantile, .95)))
309
310 ## make summary rasters
311 ras_med_tmb <- ras_sdv_tmb <- ras_lower_tmb <-
312 ras_upper_tmb <- ras_inInt_tmb <- gp.rast
313 values(ras_med_tmb) <- summ_tmb[, 1]
314 values(ras_sdv_tmb) <- summ_tmb[, 2]
315 values(ras_lower_tmb) <- summ_tmb[, 3]
316 values(ras_upper_tmb) <- summ_tmb[, 4]
317 values(ras_inInt_tmb) <- 0
318 ras_inInt_tmb[gp.rast < ras_lower_tmb | ras_upper_tmb < gp.rast] <- 1
319
320 ## plot truth, pixels falling within/without the 90% interval,
321 ## post. median, and post sd
322
323 # set the range for the truth and median
324 rast.zrange <- range(c(values(gp.rast), values(ras_med_tmb)), na.rm = T)
325
326 # plot tmb
327 png(file='figures/example_tmb.png', width=9, height=9, units='in', res=300)
328 par(mfrow = c(2, 2))
329 plot(gp.rast, main = 'Truth', zlim = rast.zrange, col = (viridis(100)))
330 points(dat[, .(x, y)])
331 plot(ras_inInt_tmb, main = 'Pixels where 90% CIs did not cover Truth')
332 points(dat[, .(x, y)])
333 plot(ras_med_tmb, main = 'TMB Posterior Median',
334       zlim = rast.zrange, col = (viridis(100)))
335 points(dat[, .(x, y)])
336 plot(ras_sdv_tmb, main='TMB Posterior Standard Deviation')
337 points(dat[, .(x, y)])
338 dev.off()
339
340

```

```

341 ## compare INLA and TMB meds and stdevs
342 med.zrange <- range(c(values(ras_med_tmb), values(ras_med_inla)), na.rm = T)
343 sdv.zrange <- range(c(values(ras_sdv_tmb), values(ras_sdv_inla)), na.rm = T)
344
345 png(file='figures/example_tmb_v_inla.png', width=9, height=9, units='in',
       res=300)
346 par(mfrow = c(2, 2))
347 plot(ras_med_inla, main = 'INLA Posterior Median',
       zlim = med.zrange, col = (viridis(100)))
348 points(dat[, .(x, y)])
349 plot(ras_sdv_inla, main = 'INLA Posterior Standard Deviation',
       zlim = sdv.zrange)
350 points(dat[, .(x, y)])
351 plot(ras_med_tmb, main = 'TMB Posterior Median',
       zlim = med.zrange, col = (viridis(100)))
352 points(dat[, .(x, y)])
353 plot(ras_sdv_tmb, main = 'TMB Posterior Standard Deviation',
       zlim = sdv.zrange)
354 points(dat[, .(x, y)])
355 dev.off()

```

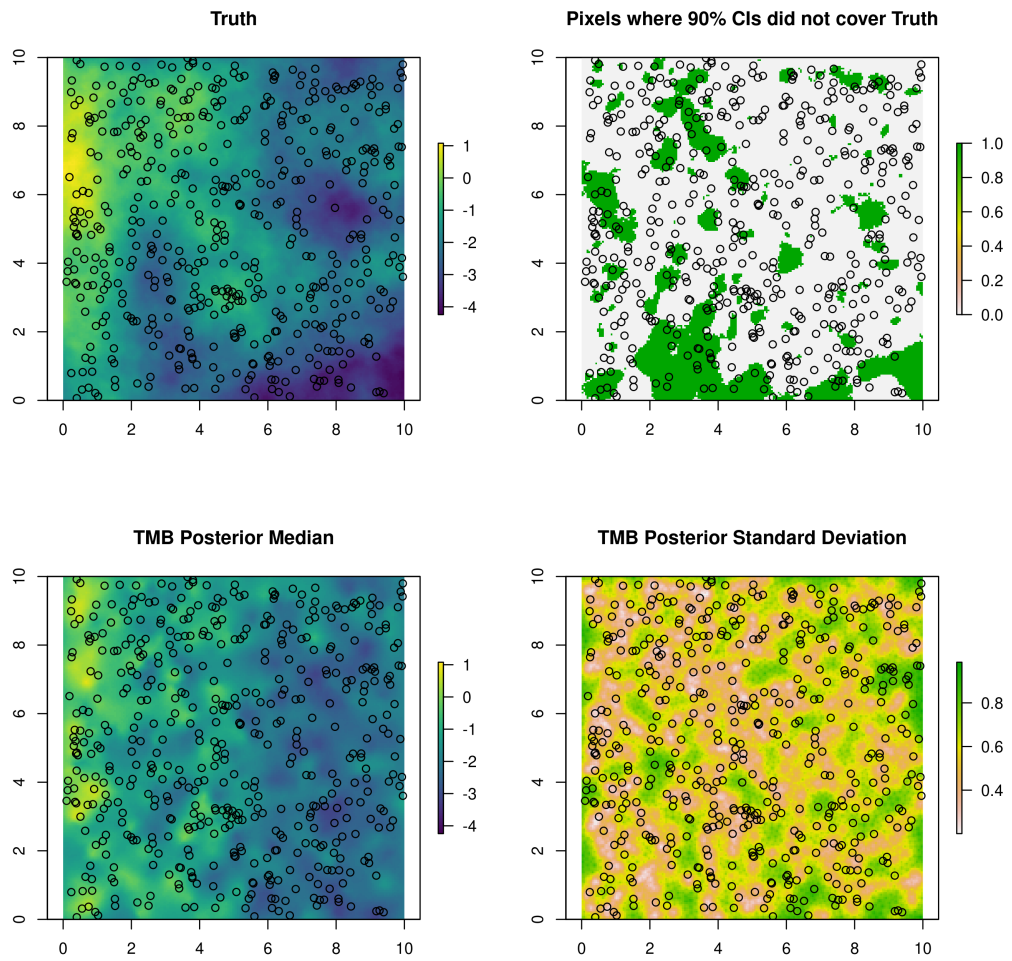


Figure E.29: Simulated GP on  $10 \times 10$  grid, posterior median and standard deviations summarized from 500 draws from the approximate TMB posterior distribution, and a binary plot indicating which pixels fell outside the 90% credible interval. Points indicate cluster locations.

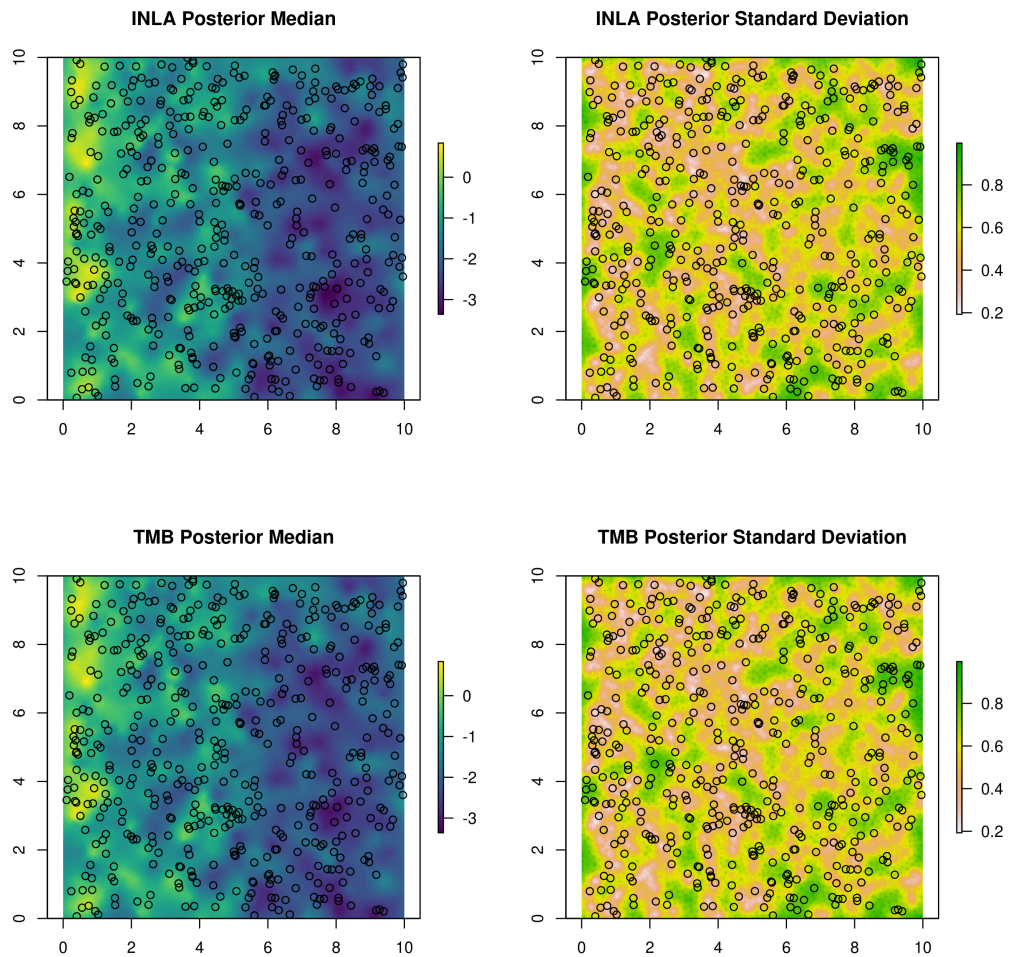


Figure E.30: Comparison of the posterior median and standard deviations from the example R-INLA and TMB code. Points indicate cluster locations.

## Appendix F. Software and hardware details

The large scale continuous simulations of Section 6.1 were run on a large computing cluster containing a variety of hardware types. The jobs were randomly placed onto different machines as space became available and the effects of the various hardware were averaged over in producing all results, including the serial timing results in Figure B.22. A singularity image was used to ensure consistent software versions across the nodes. Specifically, these simulations were run on:

- R 3.6.1,
- R-INLA 20.01.29.9000,
- TMB 1.7.16.

All other work was performed on a laptop with an Intel Core i7-8550U CPU (4 cores, 8 threads @ 1.8GHz) and 16Gb of RAM. This machine used the following software versions:

- R 4.0.4,
- R-INLA 21.02.23, with PARDISO solver enabled,
- TMB 1.7.18, with METIS reordering enabled.